Graph-theoretic Methods for the Analysis and Synthesis of Networked Dynamic Systems

Daniel Zelazo

A dissertation submitted in partial fulfillment of
the requirements for the degree of

Doctor of Philosophy

University of Washington

2009

Program Authorized to Offer Degree: Aeronautics & Astronautics

University of Washington
Graduate School

This is to certify that I have examined this copy of a doctoral dissertation by

Daniel Zelazo

and have found that it is complete and satisfactory in all respects,
and that any and all revisions required by the final
examining committee have been made.

Chair of the Supervisory Committee:

Mehran Mesbahi

Reading Committee:

Mehran Mesbahi

Uy-Loi Ly

Kristi A. Morgansen

Kristi Morgansen

Date: September 4, 2009

Signature

Date September 4, 2009

University of Washington

Abstract

Graph-theoretic Methods for the Analysis and Synthesis of Networked Dynamic Systems

Daniel Zelazo

Chair of the Supervisory Committee:
Professor Mehran Mesbahi
Aeronautics & Astronautics

This dissertation aims to develop a graph-centric framework for the analysis and synthesis of certain classes of large-scale systems, namely, those with linear dynamic subsystems that interact with other subsystems via an interconnection topology. Four canonical models for networked dynamic systems (NDS) are derived as the analytic foundation for this work. The role of heterogeneity of the agent dynamics comprising the system is also made explicit. An essential construct used to describe these systems is a new algebraic representation for a graph that we term the *edge Laplacian*. Equipped with models that explicitly describe the role of the underlying connection topology, we consider the controllability, observability, and performance of the NDS models in terms of the structural properties of the connection graph. Motivated by the analysis results, we also provide various synthesis procedures, including optimal topology design, local inner-loop control for each agent in an NDS, and decentralized control laws for the entire NDS.

TABLE OF CONTENTS

LIST OF FIGURES

Figure Number Page

ACKNOWLEDGMENTS

When I decided to return to academia after a few years working in the real world, I had visions of ivory towers, corduroy jackets with elbow patches, and the unconstrained intellectual freedom university life is supposed to provide. These idealist visions were at the same time put in check by more realist view of life; I was not going to fool myself into believing that the pillars of hard work and perseverance could be brushed aside en route to a doctorate. With this perspective I naturally hoped for a happy balance between the two. My first year at the University of Washington, however, gave me a glimpse of both extremes. Unfortunately, the notion of averaging in mathematics does not translate to graduate life, making for a tumultuous first year. The Gothic beauty of UW's campus seemed to mock me as I wrestled with fluid dynamics and homework after years without.

It was during my second year that I joined the Distributed Space Systems Laboratory under the supervision of Mehran Mesbahi. From that moment my idealist visions of graduate school returned with a vigor as my interactions with Prof. Mesbahi increased. As a teacher, he revitalized my passion for research in controls through mathematical elegance, philosophical pondering, and teaching excellence. As an advisor, he always left his door open with no constraints on discussion topics or time. For these reasons and more, I consider myself extremely fortunate and grateful to have worked with him. In this regard, I would like to thank him for all his contributions to my growth as a student, researcher, and person.

I would also like to thank the members of my reading and doctoral committee, Uy-loi Ly, Kristi Morgansen, Mark Damborg, and Paul Tseng. Their insightful comments were very useful, especially in initiating my own assessment of the scope of my research. In particular, I would like to thank Prof. Ly for my time as his teaching assistant over three quarters. His passion for teaching is contagious, and working with him taught me how consuming and rewarding teaching can be.

Finally, I must also acknowledge and thank my entire family for their love and support. I only need to observe my parents to understand where my passion for learning comes from; a passion that continues indefinitely. To my brother and sister, grandparents, uncles and aunts, cousins and friends, thank-you.

DEDICATION

to my family

Chapter 1

INTRODUCTION

The analysis and synthesis of large-scale systems poses a range of challenges due to the number of their subsystems and the complexity of their interactions. In the meantime, the importance of these systems has become increasingly prevalent in science and engineering, especially in the realm of multi-agent systems such as the coordination of autonomous vehicles, as well as localization and sensor fusion, energy networks, and distributed computation [2, 3, 11, 13, 21, 26, 55, 57]. One aspect of the complexity of large-scale systems is that their subsystems, which we occasionally refer to as 'agents,' may not be described by the same set of input-output dynamics. The difference between the dynamics of distinct subsystems may be the result of manufacturing inconsistencies or intentional differences due to varying requirements for each subsystem in the ensemble. An important component to the analysis of these systems, therefore, is to understand how heterogeneity in the subsystem dynamics affects the behavior and performance of the entire system. Another facet of this complexity relates to the interconnections of the different subsystems. The underlying interconnection topology of a large-scale system may be determined by the governing dynamic equations of each subsystem, e.g., when the interconnection is a function of some state of each subsystem, or it may be designed as part of the engineering process. In both cases, the interconnection topology has a profound impact on the overall system in terms of its stability, controllability, observability, and performance. Hence, it becomes crucial to understand and explicitly parameterize the role of the interconnection topology for both the analysis and synthesis of large-scale systems.

As a result of this research, a graph-theoretic approach has been identified as a promising way to study this class of systems. Graph theory is a mature branch of mathematics used to study, in a rigorous manner, the relations between objects from a certain collection [22, 32]. The main advantages of graph theory in a dynamical system setting are the various algebraic representations that graphs admit. Matrix representations of graphs can easily, if not elegantly, be incorporated into a dynamical system as an additional parameter to describe interactions between agents.

For linear and time-invariant (LTI) multi-agent systems, it may seem natural to embed the connection topology into the quadruple of system matrices (A, B, C, D) using the aforementioned representations for graphs. Such a representation of a multi-agent system can be used to study systems-theoretic properties in the traditional way. However, a more enlightening approach is to make the connection topology, which we denote as $\mathcal{G}$, explicit in the system description. This refinement leads us to consider the quintuple $(A, B, C, D, \mathcal{G})$, and consequently all systems theoretic properties should be described based on this representation. This approach can lead to a graph-based intuition on such systems.

Perhaps the most studied illustration of this approach is the Laplacian Dynamics, also known as the consensus or agreement protocol [54, 59, 65]. In consensus problems, it is the goal of a network of dynamic systems to reach agreement on a certain quantity of interest (for example, the heading of a team of UAVs). This model has proven useful in a broad range of fields including social networks, flocking, formation control, and distributed computation [13, 64, 77, 78]. In its simplest form, the consensus problem assumes a finite group of dynamic units, each connected to a fixed number of other units in the ensemble. The interconnection of these units can be represented using a graph, and the dynamics of each agent is assumed to be of the single integrator type. Each unit's control is then assumed to be the sum of differences between its own state and its neighbors state, as defined by the connection graph. The dynamic evolution of the entire system can be aptly captured by the autonomous system

$$\dot{x}(t) = -L(\mathcal{G})x(t), \tag{1.1}$$

where $L(\mathcal{G})$ represents the graph Laplacian matrix for the connection graph [32]. The power of this model is in its simplicity, allowing for the development of strong connections between classical systems properties, such as the rate of convergence, with spectral properties of the graph. The implications of this model have been explored under more sophisticated scenarios, including switching topologies, random graphs, and state-dependant graphs, to mention a few [35, 38, 53, 59].

While the main thrust of research related to consensus type problems has been the stability and convergence properties of the system, there has been some important work relating other system theoretic properties to the connection graph. The work in [26] relates classic notions from Nyquist stability theory to the connection graph when consensus is used as a feedback mechanism for a group of homogeneous agents. In [63], the consensus model was augmented to include a control input, and the notion of controllability was related to symmetry properties of the graph. A graph-centric observability analysis for a consensus based distributed estimation algorithm was presented in [40].

Although the consensus protocol has garnered much attention in the community, it does not represent the breadth of networked dynamic systems. Another important class of systems are relative sensing networks (RSN), such as those used for formation keeping [14, 48]. A compelling application of this class of systems is in the arena of space exploration. Spacecraft constellations for studying, for example, the structure of the heliopause, stereographic imaging and tomography for space physics, and space borne optical interferometry for probing the origins of the cosmos and identifying Earth-like planets (e.g., TPF, MAXIM), must rely on relative sensing to achieve their mission objectives [21, 29, 48]. The work in [73, 74] uses an incidence matrix representation of a graph to describe a relative formation in the context of formation control, but the connection between systems theory and graph theory could be pushed further. A more formal connection between concepts in graph theory and RSN was given in [70], specifically relating controller reconfiguration to spanning trees in the connection topology.

Sensor fusion and localization is yet another example of an NDS. An important component of sensor fusion is the ability to decide the communication structure for each sensing node in a distributed array. The work presented in [43] highlighted the importance of certain graph structures, such as k-regular graphs, for the design of sensor networks. A significant contribution related to RSNs and estimation over these networks was presented in [10]. Graph-theoretic concepts such as graph lattices and resistances were explicitly related to the corresponding estimation problem.

There is a wealth of research related to the aforementioned problems in addition to other applications and system models [8, 9, 13, 20, 46]. However, one common lacking theme is a true notion of system performance, as understood in systems theory, with the properties of the connection topology. The maturation of this field of research depends on the ability to analyze these systems beyond the notions of just stability and convergence. A theory that explicitly characterizes precise performance metrics (such as $\mathcal{H}_2$ or $\mathcal{H}_\infty$ performance) in terms of the connection graph would lead to a richer intuition between these fields. Additionally, synthesis of these networks would be permitted to be designed with strict requirements on their performance, rather than constructed from heuristics.

In another direction, optimization theory is a branch of mathematics that has become increasingly important in the context of the synthesis of controllers and estimators for dynamic systems [17, 19, 24, 68, 71]. Classical control design methods, such as root-locus or Nyquist diagrams, although providing a deep analytic connection between the notions of stability and system performance, are more of an engineering art than an exact science. The marriage of optimization theory and control design formalized the meaning of what the "best" controller should be. Although not as intuitive as the classical methods, much progress has been made in the justification of optimal control in the context of dynamical systems properties. In this venue, numerically tractable solution methods for solving these optimal control problems have been developed. For example, advances in robust control theory and $\mathcal{H}_\infty$ control are largely due to the maturation of semi-definite programming [24, 71].

Optimization theory also has a close and storied connection to graph theory. The most famous of which is the paper by Leonhard Euler on the Seven Bridges of Könisgsberg, written in 1736 (Figure 1.1). The city of Könisgsberg, once part of Prussia, is located on the Pregel River, and had two islands that were connected to each other and the mainland by a network of seven bridges. The problem Euler solved was to determine if it was possible to walk a route that used every bridge exactly once. The answer is decidedly no, and the solution methods provided the foundations of many graph theoretical concepts; see, for example, [66].

The marriage of graph theory and optimization theory is fully realized in the broad area of network and combinatorial optimization [47, 66]. Classic problems such as max-

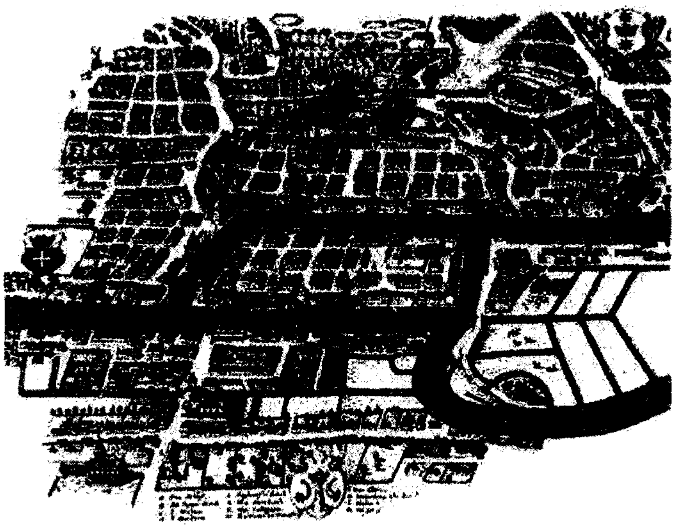

Figure 1.1: The seven bridges of Könisgsberg; deciding if a path exists that uses each bridge once is an example of optimization over graphs [1].

flow/min-cut, shortest path, and matching problems represent an elegant connection between concepts in optimization and graph theory. One unique feature of these problems is the ability to interpret mathematical concepts such as duality and feasibility in the context of graphical objects.

In the literature related to NDS, optimization has taken only a secondary role. As mentioned earlier, much of the prior work has concentrated on properties of stability and convergence of networked systems. The *algebraic connectivity* of a graph [28], for example, is related to the second smallest eigenvalue of the graph Laplacian. Semi-definite characterizations for the optimization of this value were derived in [16], and applied in various applications related to consensus and formation keeping [45, 55, 80]. In many instances, heuristic methods are used to avoid the computational difficulties of combinatorial optimization. For example, the work in [31] provides guidelines for adding a set of edges to produce the greatest impact in the algebraic connectivity. However, the lack of a strong analytic connection between concepts in graph theory and systems theory has resulted in a corresponding void in applying results from combinatorial optimization in this setting. There is a large untapped resource in combinatorial optimization that provide various use-

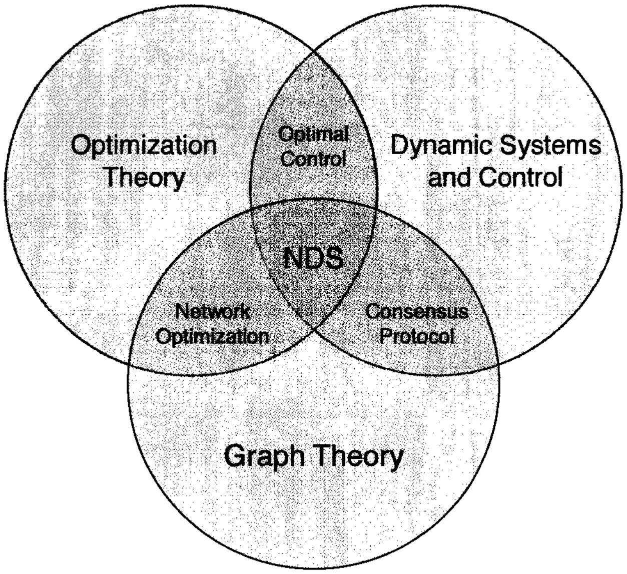

Figure 1.2: NDS is at the intersection of three broad subjects.

ful semi-definite approximation algorithms for certain graph theoretic properties [72]. For example, a semi-definite relaxation for finding the maximal stable set of a graph, which is a $\mathcal{NP}$ hard problem, is given in [50, 51].

It seems natural, therefore, that the broad areas of dynamical systems and control, optimization theory, and graph theory, should all intersect and define a new class of problems. It is precisely this intersection where networked dynamic systems lie, as shown in Figure 1.2, that defines the focus of this research. This intersection addresses both the problems of analysis of NDS and synthesis of controllers and estimators for such systems. This research aims to address these issues, and its fundamental contributions are:

1. Development of canonical models for studying networked dynamic systems.

2. A Graph-centric characterization of system-theoretic properties (e.g., observability, performance).

3. Synthesis techniques for topology and controller design.

The organization of this work is as follows. Chapter §2 reviews some fundamental concepts and notations in systems theory, graph theory, and optimization. In §3, a new algebraic representation of a graph, which we term the *edge Laplacian*, will be presented. The edge Laplacian turns out to be a central tool for the description of certain NDS models, which we fully develop in §4. This section describes in detail four canonical models for networked dynamic systems. It also introduces the notion of heterogeneity in the description of the dynamics of each agent in the ensemble. The analysis of the different NDS models, including discussions on observability, controllability, and system performance, is presented in §5. These results motivate synthesis procedures for topology design, inner-loop control design, as well as decentralized outer-loop control, all of which are presented in §6. Finally, §7 offers some concluding remarks in addition to potential extensions of this work.

Chapter 2

PRELIMINARIES

This chapter introduces notational conventions and a brief review of relevant concepts in the areas of dynamical systems and control theory, graph theory, and optimization theory. The set of real numbers is denoted by $\mathbb{R}$, whereas $\mathbb{R}^{n\times m}$ denotes the space of $n \times m$ real matrices. Similarly, $\mathbb{C}$ is the set of complex numbers. The matrix-theoretic notation used in the work is as follows: for a matrix A, $\mathcal{R}(A)$ and $\mathcal{N}(A)$ denote, respectively, its range space and null space. The eigenvalues of a square matrix A are denoted $\lambda_i(A)$, whereas the singular values of an arbitrary sized matrix are denoted $\sigma_i(A)$. Diagonal matrices will be written as $D = \mathbf{diag}\{d_1, \ldots, d_n\}$, with d_i denoting the i-th entry on the diagonal; this notation is also used for describing block-diagonal matrices, as in $\mathbf{A} = \mathbf{diag}\{A_1, \ldots, A_n\}$. The notation $[A]_{ij}$ refers to the ij-th entry of A. A matrix and/or a vector that consists of all zero entries will be denoted by $\mathbf{0}$; whereas, '0' will simply denote the scalar zero. Similarly, the vector $\mathbb{1}$ denotes the vector of all ones, and $\mathbf{J} = \mathbb{1}\mathbb{1}^T$. The i-th element of a vector x is denoted x_i. The element-wise absolute value of a vector x and, respectively, a matrix A, is denoted $|x|$ and $|A|$. The transpose of a vector, and respectively, a matrix is denoted x^T and A^T; the complex conjugate of x and A is written x^* and A^*. The Euclidean norm of a vector $x \in \mathbb{R}^n$ is denoted as $\|x\|$; the p-norm of x is defined as

$$\|x\|_p = \left(\sum_{i=1}^{n} |x_i|^p \right)^{\frac{1}{p}}; \tag{2.1}$$

for $p = \infty$, $\|x\|_\infty = \max_i \{|x_i|\}$. The p-norm of a matrix is induced by the equivalent vector p-norm,

$$\|A\|_p = \max_{\|x\|_p \leq 1} \|Ax\|_p; \tag{2.2}$$

for $p = 2$, $\|A\| = \max_i \{\sigma_i(A)\}$[1]. The Frobenius norm of a matrix is defined as

$$\|A\|_F \;=\; (\mathbf{trace}\{A^T A\})^{1/2}. \tag{2.3}$$

A symmetric matrix $A \in \mathbb{R}^{n \times n}$ has the property $A = A^T$. It is called *positive-definite* (*positive semi-definite*) if all its eigenvalues are positive (non-negative); this is notated as $A > 0$ ($A \geq 0$). Equivalently, the matrix A is positive-definite if $x^T A x > 0$ for all x. The notation $A > B$ ($A \geq B$) means the matrix $(A - B)$ is positive-definite (positive semi-definite). The notation $g(n) = O(f(n))$ signifies that the function $g(n)$ is bounded from above by some constant multiple of $f(n)$ for large enough values of n. The cardinality of a set of discrete elements $\mathcal{I} = \{i_1, \ldots, i_n\}$ is denoted $|\mathcal{I}| = n$.

We also make use of normed infinite-dimensional spaces. In particular, the space $\mathcal{L}_2^n(0, \infty)$ consists of all n-dimensional functions such that

$$\left(\int_0^\infty u(t)^* u(t) dt\right)^{1/2} \;<\; \infty.$$

We will at times abbreviate this space as simply $\mathcal{L}_2$. The normed spaces are induced by an inner-product, which we define for $\mathcal{L}_2$ as

$$\langle x(t), y(t) \rangle \;=\; \int_0^\infty x(t)^* y(t) dt. \tag{2.4}$$

The norms of signals in $\mathcal{L}_2$ are therefore written as $\|x(t)\|_{\mathcal{L}_2} = (\langle x(t), x(t) \rangle)^{1/2}$. The Fourier transform of a function maps a signal in $u(t) \in \mathcal{L}_2$ to the frequency domain $\hat{\mathcal{L}}_2(j\mathbb{R})$, and is defined as

$$\hat{u}(j\omega) \;=\; \int_{-\infty}^\infty u(t) e^{-j\omega t} dt. \tag{2.5}$$

Plancherel's theorem is an important result showing equality between the inner-products on $\mathcal{L}_2$ and $\hat{\mathcal{L}}_2(j\mathbb{R})$ [24]. This leads to the following statement on the norms, known as Parseval's theorem,

$$\begin{aligned} \|\hat{u}(j\omega)\|_{\hat{\mathcal{L}}_2} &= \left(\int_{-\infty}^\infty u(j\omega)^* u(j\omega) d\omega\right)^{1/2} \\ &= \|u(t)\|_{\mathcal{L}_2}. \end{aligned} \tag{2.6}$$

[1] The subscript '2' is dropped in the case of the matrix and vector 2-norms.

2.1 Dynamic Systems and Control

This section offers a short summary of some relevant results from dynamic systems and control theory [4, 19, 24, 42]. We consider a linear and time-invariant (LTI) system with states $x(t) \in \mathbb{R}^n$, controls $u(t) \in \mathbb{R}^{m_u}$, exogenous disturbances $w(t) \in \mathbb{R}^{m_w}$, performance outputs $z(t) \in \mathbb{R}^{p_z}$, measured outputs $y(t) \in \mathbb{R}^{p_y}$, and initial conditions $x(t_0) \in \mathbb{R}^n$. The LTI system, which we denote by the operator Σ, has the following state-space realization:

$$\Sigma : \begin{cases} \dot{x}(t) &= Ax(t) &+ & Bu(t) &+ & \Gamma w(t) \\ z(t) &= C^z x(t) &+ & D^{zu}u(t) &+ & D^{zw}w(t) \\ y(t) &= C^y x(t) &+ & D^{yu}u(t), &+ & D^{yw}w(t) \\ x(t_0) &= x_0 \end{cases} \tag{2.7}$$

The linear system (2.7) is *asymptotically stable* if all the eigenvalues of A, also referred to as the *poles* of Σ, are in the open left-half plane of $\mathbb{C}^2$. Equivalently, we say that Σ is stable if the state-matrix A is *Hurwitz*.

The system Σ also has an input-output representation referred to as the *transfer-function* and denoted as $\hat{\Sigma}$. The transfer-function of (2.7) is given as

$$\hat{\Sigma} : \begin{bmatrix} H^{uz}(s) & H^{wz}(s) \\ H^{uy}(s) & H^{wy}(s) \end{bmatrix}, \tag{2.8}$$

where, $H^{uz}(s) = C^z(sI - A)^{-1}B + D^{zu}$ (the other elements of (2.8) are similarly defined).

The transfer-function of Σ represents a *minimal* description of the system[2]; that is $\hat{\Sigma}$ is the input-output map for a completely *controllable* and *observable* system. The controllability and observability properties of a stable system can be studied using the gramians of the system,

$$X_c = \int_0^\infty e^{At}BB^Te^{A^Tt}dt \tag{2.9}$$

$$Y_o = \int_0^\infty e^{A^Tt}(C^y)^TC^ye^{At}dt \tag{2.10}$$

[2] After all pole-zero cancelations.

The gramian can also be computed by solving a set of linear equations, through the following Lyapunov equations, as

$$AX_c + X_cA^T + BB^T = 0, \tag{2.11}$$

$$A^TY_o + Y_oA + (C^y)^TC^y = 0. \tag{2.12}$$

In both cases, the gramians are symmetric positive semi-definite matrices. When the gramian X_c (Y_o) is positive definite, the system is controllable (observable). If this condition is not met, then each 0 eigenvalue of the gramian X_c (Y_o) corresponds to an uncontrollable (unobservable) mode in the system.

In the case where the state matrix is not stable, there are other tests, such as the PHB test, that can be used to determine if the system is controllable or observable [42]. The advantage of the gramian is the ability to infer the relative degree of controllability or observability of the different modes in the system. This is accomplished by comparing the singular values of the gramian using the singular value decomposition (SVD) [36],

$$X_c = V\Sigma_cV^T, \quad Y_o = U\Sigma_oU^T. \tag{2.13}$$

We denote, respectively, the largest and smallest singular values of X_c (Y_o) as $\overline{\sigma}(X_c)$ and $\underline{\sigma}(X_c)$ ($\overline{\sigma}(Y_o)$ and $\underline{\sigma}(Y_o)$). For example, a quantitative way to compare the relative observability of different modes in the system can be inferred from the SVD of the observability gramian as

$$\|y(t)\|_{\mathcal{L}_2} = \|Y_o^{1/2}x(t_0)\|.$$

Of primary interest is the design of a feedback control law of the form

$$u(t) = Ky(t), \tag{2.14}$$

where K is itself a dynamic system that has the following state-space realization:

$$K \ : \ \begin{cases} \dot{x}_k(t) = A_kx_k(t) + B_ky(t) \\ u(t) = C_kx_k(t) + D_ky(t) \end{cases}, \tag{2.15}$$

where $x_k(t) \in \mathbb{R}^{n_k}$ is the internal state of the controller, and $y(t)$ and $u(t)$ are respectively, the output and input of the system Σ. The interconnection between the system Σ and the

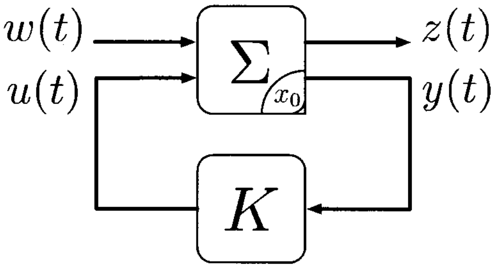

Figure 2.1: A controlled dynamic system.

controller K can be described with a block diagram, as in Figure 2.1. We sometimes use the short-hand notation for a state-space realization of a system as

$$K \;:=\; \left[\begin{array}{c|c} A_k & B_k \\ \hline C_k & D_k \end{array}\right].$$

The controller should be designed such that the system in Figure 2.1 is internally stable and a certain level of performance is achieved. The notion of performance can be quantified in numerous ways, and we will generally consider performance metrics that take the following form:

$$J = \|T^{w \mapsto z}\|_p, \tag{2.16}$$

where $T^{w \mapsto z}$ represents the closed-loop map from the exogenous input $w(t)$ to the performance output $z(t)$, and $\| \bullet \|_p$ denotes the system p-norm of the argument.

As an example, when $p = 2$, minimization of the performance metric (2.16) is the $\mathcal{H}_2$ optimal control problem (which is equivalent to the classic Linear Quadratic Gaussian problem). Similarly, when $p = \infty$, the problem becomes an $\mathcal{H}_\infty$ optimal control problem. It should be noted that additional performance metrics, such as robustness and regional pole placement, can be formulated in the same way through appropriate modification of the plant.

The $\mathcal{H}_2$-norm of a system can be calculated using the controllability and observability gramians of the system. For example, the $\mathcal{H}_2$ norm of Σ from the input channel $w(t)$ to the output channel $y(t)$ is written as

$$\|\Sigma\|_2 = \sqrt{\mathbf{trace}(\Gamma^T Y_o \Gamma)} \tag{2.17}$$

$$= \sqrt{\mathbf{trace}(C^y X_c (C^y)^T)}. \tag{2.18}$$

The $\mathcal{H}_\infty$-norm of a system is an induced $\mathcal{L}_2$ norm, and is defined as

$$\|\hat{\Sigma}(j\omega)\|_\infty = \sup_{\|U(j\omega)\|_{\hat{\mathcal{L}}_2=1}} \|\hat{\Sigma}(j\omega)U(j\omega)\|_{\hat{\mathcal{L}}_2}; \tag{2.19}$$

this description allows us to state the sub-multiplicative property of the $\mathcal{H}_\infty$ norm,

$$\|H(j\omega)P(j\omega)\|_\infty \leq \|H(j\omega)\|_\infty \|P(j\omega)\|_\infty.$$

Alternatively, the norm can be computed from the frequency dependant singular values of $\hat{\Sigma}$ as

$$\|\Sigma\|_\infty = \sup_\omega \bar{\sigma}(\hat{\Sigma}(j\omega)). \tag{2.20}$$

2.2 Graph Theory

A review of relevant concepts from graph theory is presented here [15, 32]. An undirected (simple) graph $\mathcal{G}$ is specified by a vertex set $\mathcal{V} = \{1, 2, \dots, n\}$ and an edge set $\mathcal{E}$ whose elements characterize the incidence relation between distinct pairs of $\mathcal{V}$. Two vertices i and j are called *adjacent* (or neighbors) when $\{i, j\} \in \mathcal{E}$; we denote this by writing $i \sim j$. An *orientation* of an undirected graph $\mathcal{G}$ is the assignment of directions to its edges, i.e., an edge e_k is an ordered pair (i, j) such that i and j are, respectively, the initial and the terminal nodes of e_k. Similarly, we define two edges $e_k, e_l \in \mathcal{E}$ to be positively (negatively) adjacent if they share a node and point in opposite (same) directions relative to this shared node. We denote the positive and negative adjacency of edges as $e_k \sim^+ e_l$ and $e_k \sim^- e_l$, respectively. By convention, an edge is not considered adjacent to itself. A *subgraph* of $\mathcal{G}$ is a graph whose vertex and edge sets are subsets of those of $\mathcal{G}$.

Graphs admit a set of convenient matrix representations. For example, the $|\mathcal{V}| \times |\mathcal{E}|$ incidence matrix, $E(\mathcal{G})$, for an oriented graph $\mathcal{G}$ is a $\{0, \pm 1\}$-matrix with rows and columns

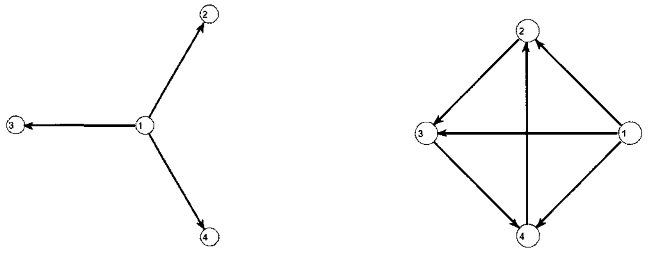

(a) $\mathcal{G}_1$ (b) $\mathcal{G}_2$

Figure 2.2: Two directed graphs on 4 nodes.

indexed by vertices and edges of $\mathcal{G}$, respectively, such that

$$[E(\mathcal{G})]_{ik} = \begin{cases} +1 & \text{if } i \text{ is the initial node of edge } e_k \\ -1 & \text{if } i \text{ is the terminal node of edge } e_k \\ 0 & \text{otherwise} \end{cases} .$$

Figure 2.2 depicts an example of two oriented graphs and their respective incidence matrices are given as

$$E(\mathcal{G}_1) = \begin{bmatrix} 1 & 1 & 1 \\ -1 & 0 & 0 \\ 0 & -1 & 0 \\ 0 & 0 & -1 \end{bmatrix}, \quad E(\mathcal{G}_2) = \begin{bmatrix} 1 & 1 & 1 & 0 & 0 & 0 \\ -1 & 0 & 0 & 1 & -1 & 0 \\ 0 & -1 & 0 & -1 & 0 & 1 \\ 0 & 0 & -1 & 0 & 1 & -1 \end{bmatrix}. \tag{2.21}$$

From the definition of the incidence matrix it follows that the null space of its transpose, $\mathcal{N}(E(\mathcal{G})^T)$, contains **span** $\{\mathbb{1}\}$.

The rank of the incidence matrix depends only on $|\mathcal{V}|$ and the number of its connected components.

Theorem 2.2.1 ([32]). *Let $\mathcal{G} = (\mathcal{V}, \mathcal{E})$ be a graph with c connected components. Then* **rank** $E(\mathcal{G}) = |\mathcal{V}| - c$.

The degree of a vertex i, denoted d_i, is the cardinality of the set of vertices adjacent to it. The degree matrix of $\mathcal{G}$, $\Delta(\mathcal{G})$, is a diagonal matrix with the degree of vertex i at its (i, i)

position. The adjacency matrix of $\mathcal{G}$ is a symmetric $\mid \mathcal{V} \mid \times \mid \mathcal{V} \mid$ matrix defined as,

$$[A(\mathcal{G})]_{ij} := \begin{cases} 1 & \text{if} \quad \{i,j\} \in \mathcal{E} \\ 0 & \text{otherwise.} \end{cases}$$

A sequence of $r+1$ distinct and consecutively adjacent vertices, starting from vertex i and ending at vertex j, is called a path of length r (form i to j); when $i = j$, we call this path a *cycle*. We call a graph *connected* if there exists a path between any pair of vertices. A connected graph without cycles is referred to as a *tree*. Equivalently, a tree is a connected graph on $\mid \mathcal{V} \mid$ vertices with $\mid \mathcal{V} \mid - 1$ edges.

A connected graph $\mathcal{G}$ can be written as the union of two edge-disjoint subgraphs on the same vertex set as $\mathcal{G} = \mathcal{G}_\tau \cup \mathcal{G}_c$, where $\mathcal{G}_\tau$ is a spanning tree subgraph and $\mathcal{G}_c$ contains the remaining edges that necessarily complete the cycles in $\mathcal{G}$. Similarly, the columns of the incidence matrix for the graph $\mathcal{G}$ can always be permuted such that $E(\mathcal{G})$ is written as

$$E(\mathcal{G}) \quad = \quad \begin{bmatrix} E(\mathcal{G}_\tau) & E(\mathcal{G}_c) \end{bmatrix}. \tag{2.22}$$

For the duration of this work we assume the incidence matrix to always be partitioned according to (2.22).

The cycle edges can be constructed from linear combinations of the tree edges via a linear transformation [66, 70], as

$$E(\mathcal{G}_\tau)T_\tau^c(\mathcal{G}) \quad = \quad E(\mathcal{G}_c), \tag{2.23}$$

where

$$T_\tau^c(\mathcal{G}) \quad = \quad \left(E(\mathcal{G}_\tau)^T E(\mathcal{G}_\tau)\right)^{-1} E(\mathcal{G}_\tau)^T E(\mathcal{G}_c). \tag{2.24}$$

Using (2.23) we obtain the following alternative representation of the incidence matrix of the graph

$$E(\mathcal{G}) \quad = \quad E(\mathcal{G}_\tau)\begin{bmatrix} I & T_\tau^c(\mathcal{G}) \end{bmatrix} \quad = \quad E(\mathcal{G}_\tau)R(\mathcal{G}); \tag{2.25}$$

the rows of the matrix

$$R(\mathcal{G}) = \begin{bmatrix} I & T_\tau^c(\mathcal{G}) \end{bmatrix} \tag{2.26}$$

are viewed as the basis for the *cut space* of $\mathcal{G}$ [32]. The matrix $\begin{bmatrix} -T_\tau^c(\mathcal{G}) & I \end{bmatrix}^T$, on the other hand, forms a basis for the *flow space.*

The matrix $R(\mathcal{G})$ has a close connection with a number of structural properties of the underlying network. For example, the number of spanning trees in a graph, $\tau(\mathcal{G})$, can be determined from the cut space basis [32], as

$$\tau(\mathcal{G}) \quad = \quad \det\left[R(\mathcal{G})R(\mathcal{G})^T\right]. \tag{2.27}$$

The null space of the incidence matrix can be characterized in terms of the independent cycles of the graph. We elaborate on this connection between graphical and algebraic properties of a graph with the following definitions and theorem.

Definition 2.2.1. *Given an incidence matrix $E(\mathcal{G})$ for a directed graph, a* signed path vector *is a vector $z \in \mathbb{R}^{|\mathcal{E}|}$ corresponding to a path such that the ith element of z takes the value '+1' if edge i is traversed positively, '-1' if traversed negatively, and '0' if the edge is not used in the path.*

Lemma 2.2.2. *Given a path with distinct initial and terminal nodes described by a signed path vector z in a graph $\mathcal{G}$, the vector $y \in \mathbb{R}^{|\mathcal{V}|}$ is defined as $y = E(\mathcal{G})z$ and the ith element of y takes the value '+1' if node i is the initial node of the path, '-1' if it is the terminal node of the path, and '0' otherwise.*

Proof. We can rewrite $E(\mathcal{G})z$ as $E(\mathcal{G})\,\mathbf{diag}(z)\,\mathbb{1}$. The ij-th entry of the matrix $E(\mathcal{G})\,\mathbf{diag}(z)$ will be -1 if edge j is used by the path to leave node i, $+1$ if edge j is used by the path to enter node i, and zero otherwise. If node i is an intermediate node in the path (neither the initial nor the terminal node), then the path must enter and leave the node an equal number of times, resulting in the i-th row-sum of $E(\mathcal{G})\,\mathbf{diag}(z)$ to be zero. On the other hand, if node i is the initial node, the path must eventually leave the node without ever returning to it, resulting in the i-th row-sum to be equal to 1. Similarly, if i is the terminal node, the path must eventually enter the node without ever leaving it, resulting in the i-th row-sum to be equal to -1.

□

Theorem 2.2.3 ([32]). *Given a connected graph $\mathcal{G}$ with arbitrary orientation assigned, the null space of $E(\mathcal{G})$ is spanned by all the linearly independent signed path vectors corresponding to the cycles in $E(\mathcal{G})$.*

Proof. For any node used in a cycle, the path must enter and exit that node an equal number of times. Using the same argument as in the proof of Lemma 2.2.2, it follows that $E(\mathcal{G})z = \mathbf{0}$ when z is the signed path vector for a cycle.

□

The graph Laplacian of an oriented graph is defined as

$$L(\mathcal{G}) := E(\mathcal{G})\, E(\mathcal{G})^T; \tag{2.28}$$

however, the graph Laplacian is independent of a particular orientation of the graph as

$$L(\mathcal{G}) = \Delta(\mathcal{G}) - A(\mathcal{G}). \tag{2.29}$$

The graph Laplacian of $\mathcal{G}$ is a rank deficient positive semi-definite matrix. The real spectrum of $L(\mathcal{G})$ can thereby be ordered as

$$0 = \lambda_1(L(\mathcal{G})) \leq \lambda_2(L(\mathcal{G})) \leq \ldots \leq \lambda_{|\mathcal{V}|}(L(\mathcal{G})).$$

We will use the shorthand notation $\lambda_i(\mathcal{G})$ to refer to the i-th ordered eigenvalue of $L(\mathcal{G})$. A direct consequence of Theorem 2.2.1 is that the multiplicity of the zero eigenvalue of the graph Laplacian is equal to the number of connected components of the graph [32]. Moreover, the second smallest eigenvalue of $L(\mathcal{G})$, $\lambda_2(\mathcal{G})$, also known as algebraic connectivity, turns out to be a judicious measure of graph connectivity [27].

Two graphs, $\mathcal{G}_1$ and $\mathcal{G}_2$, are said to be *cospectral* if the spectrum of $A(\mathcal{G}_1)$ is the same as the spectrum of $A(\mathcal{G}_2)$. Similarly, two graphs, $\mathcal{G}_1$ and $\mathcal{G}_2$, are said to be *cospectral with respect to the graph Laplacian* if the spectrum of $L(\mathcal{G}_1)$ is the same as the spectrum of $L(\mathcal{G}_2)$. Note that two graphs that are isomorphic are always cospectral with respect to the graph Laplacian, but the converse is not true. That is, two graphs that are cospectral with respect to the Laplacian need not be isomorphic.

In order to apply the framework developed in this work to specific graphs, we will work with the complete graph and its generalization in terms of k-regular graphs, which

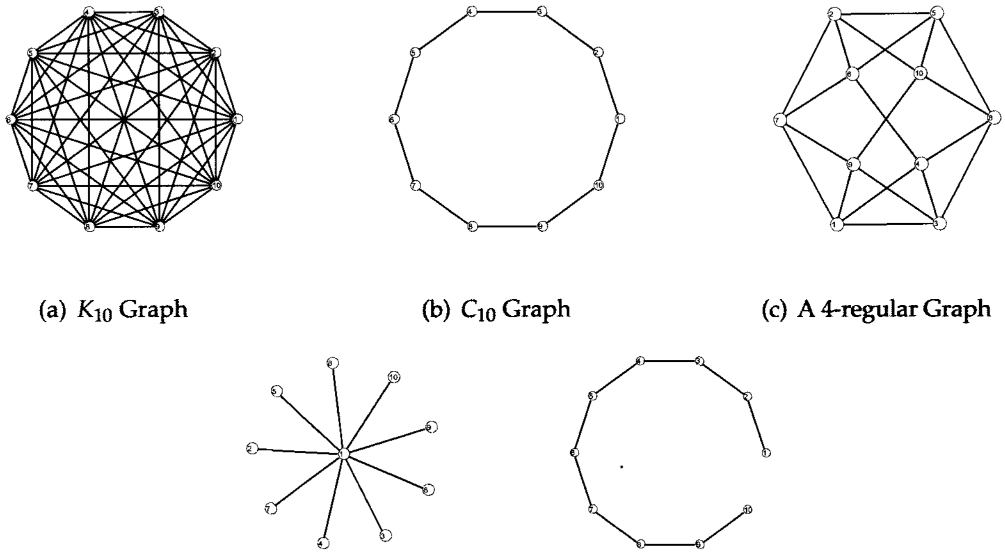

(a) K_{10} Graph

(b) C_{10} Graph

(c) A 4-regular Graph

(d) S_{10} Graph

(e) P_{10} Graph

Figure 2.3: Example of regular graphs and trees.

are defined as follows. The *complete graph* on n nodes, K_n, is the graph where all possible pairs of vertices are adjacent, or equivalently, if the degree of all vertices is $n-1$. Figure 2.3(a) depicts K_{10}, the complete graph on 10 nodes. When every node in a graph with n nodes has the same degree $k \leq n-1$, it is called a k-regular graph. The k-regular graph on n nodes for $k=2$ is called the *cycle graph*, C_n. Figures 2.3(b) and 2.3(c) show, respectively, the cycle graph C_{10} and a 4-regular graph. The *star graph*, S_n, is a tree graph with one node having degree $n-1$ and all others have degree 1, as in Figure 2.3(d). Similarly, the *path graph*, P_n, is a tree with two nodes of degree 1, and the other $n-2$ nodes with degree 2, shown in Figure 2.3(e).

The line graph of $\mathcal{G}$, denoted as $\mathscr{L}(\mathcal{G})$, is the graph where the edges of $\mathcal{G}$ correspond to the nodes of $\mathscr{L}(\mathcal{G})$, and two edges in $\mathscr{L}(\mathcal{G})$ are adjacent if they share a node in $\mathcal{G}$. Figure 2.4 shows an example of a graph and its undirected line graph.

For the duration of this work, we will make explicit the dependance of the various algebraic representations on the underlying graph $\mathcal{G}$. However, in instances where the context is clear, we will drop the explicit dependence to reduce notational clutter (e.g., $R(\mathcal{G})$ will be replaced simply by R).

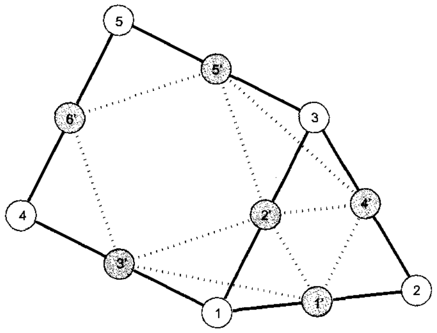

Figure 2.4: A graph on the vertex set $\{1,2,3,4,5\}$ and its undirected line graph on the set $\{1',2',3',4',5',6'\}$.

2.3 Optimization Theory

We make use of concepts from convex optimization, with an emphasis on semi-definite programming (SDP) [18, 66]. A real-valued function $f : \mathbb{R}^n \mapsto \mathbb{R}$ is called *convex*, if for any two points $x, y \in \mathbb{R}^n$ and any $0 \leq \lambda \leq 1$, one has

$$f(\lambda x + (1-\lambda)y) \;\; \leq \;\; \lambda f(x) + (1-\lambda)f(y). \tag{2.30}$$

If f and g are convex functions, then so is their sum.

SDPs are concerned with the optimization of a linear objective function over the space of positive semi-definite matrices. The general form of an SDP is written as

$$\min_{x} \quad c^T x \tag{2.31}$$

$$\text{subject to} \quad F(x) = F_o + \sum_{i=1}^{m} x_i F_i \geq 0, \tag{2.32}$$

where $x \in \mathbb{R}^m$ is the optimization variable, $c \in \mathbb{R}^m$, and $F(x)$ is an affine map from $\mathbb{R}^m$ to the space of symmetric $n \times n$ matrices. Recall the notation $F(x) \geq 0$ means that $F(x)$ is a positive semi-definite matrix. The constraint (2.32) is referred to as a *linear matrix inequality* (LMI). An attractive feature of SDPs are the efficient polynomial-time algorithms used to solve them, such as interior-point methods [18].

The $\mathcal{H}_2$ optimal state-feedback controller for the system Σ (2.7) can be formulated as an

SDP [24] as

$$\begin{aligned}
\min_{W,X,Z} \quad & \textbf{trace}[W] && (2.33)\\
\text{s.t.} \quad & \begin{bmatrix} A & B \end{bmatrix}\begin{bmatrix} X \\ Z \end{bmatrix} + \begin{bmatrix} X & Z^T \end{bmatrix}\begin{bmatrix} A^T \\ B^T \end{bmatrix} + \Gamma\Gamma^T < 0 \\
& \begin{bmatrix} X & (C^z X + D^{zu} Z)^T \\ (C^z X + D^{zu} Z) & W \end{bmatrix} > 0\,;
\end{aligned}$$

the control can be reconstructed as $K = ZX^{-1}$.

At times we also consider a *mixed-integer SDP* (MISDP), which is a variation of (2.31) that has an additional constraint $x_i \in \{0,1\}$ [51, 72]. MISDPs arise in many combinatorial optimization problems. These problems pose a computational challenge due to the loss of convexity of the constraint set. A common solution is to consider the *convex relaxation* of the integer constraint, $0 \le x_i \le 1$. Alternatively, efficient algorithms can be found for special instances of these problems, which we discuss later in §6.1 [47, 51].

2.4 Matrix Kronecker and Hadamard Products

We make extensive use of the matrix Kronecker product. The Kronecker product of matrices $A \in \mathbb{R}^{n\times m}$ and $B \in \mathbb{R}^{p\times q}$ is given as

$$A \otimes B = \begin{bmatrix} a_{11}B & \cdots & a_{1m}B \\ \vdots & \ddots & \vdots \\ a_{n1}B & \cdots & a_{nm}B \end{bmatrix}, \qquad (2.34)$$

where a_{ij} denotes the ij-th entry of the matrix A.

Theorem 2.4.1 ([37]). *Let $A \in \mathbb{R}^{m\times n}$ and $B \in \mathbb{R}^{p\times q}$ each have a singular value decomposition of $A = U_A \Sigma_A V_A^T$ and $B = U_B \Sigma_B V_B^T$. The singular value decomposition of the Kronecker product of A and B is*

$$A \otimes B = (U_A \otimes U_B)(\Sigma_A \otimes \Sigma_B)(V_A^T \otimes V_B^T). \qquad (2.35)$$

An immediate consequence of Theorem 2.4.1 is the following result on the matrix 2-norm,

$$\|A \otimes B\| = \|A\| \, \|B\|. \tag{2.36}$$

We also make extensive use of the following Kronecker product matrix multiplication property,

$$(A \otimes B)(C \otimes D) = (AC \otimes BD), \tag{2.37}$$

where the matrices are all of commensurate dimension.

The Hadamard product of two matrices $A, B \in \mathbb{R}^{n \times m}$ is given as

$$A \circ B = \begin{bmatrix} a_{11}b_{11} & \cdots & a_{1m}b_{1m} \\ \vdots & \ddots & \vdots \\ a_{n1}b_{n1} & \cdots & a_{nm}b_{nm} \end{bmatrix}. \tag{2.38}$$

Listed below are some useful properties of the Hadamard product.

Theorem 2.4.2 (Schur's Theorems [41]). *Given matrices A and B of commensurate dimension,*

1. *If A and B are positive semidefinite, then $A \circ B$ is positive semidefinite.*

2. *If A and B are positive semidefinite, then*

$$\left(\min_i a_{ii}\right) \lambda_{min}(B) \leq \lambda_{min}(A \circ B) \leq \lambda_{max}(A \circ B) \leq \left(\max_i a_{ii}\right) \lambda_{max}(B). \tag{2.39}$$

3. *If B is positive definite and if A is positive semidefinite with all its main diagonal entries positive, then $A \circ B$ is positive definite.*

4. *If A is positive semidefinite, then $\|A \circ B\| \leq (\max_i a_{ii}) \, \|B\|$.*

5. $\|A \circ B\| \leq \|A\| \|B\|$.

Chapter 3

THE EDGE LAPLACIAN

An important contribution of this work is the development of a new algebraic representation for graphs that we term the *Edge Laplacian* [83, 87]. The edge Laplacian can be considered as an edge variant of the graph Laplacian (2.28). It is worth mentioning that edge interpretations of certain algebraic graph structures have been discussed in the literature. For example, the notion of edge adjacency in the context of the structure of molecular graphs was presented in [25]. Other edge-variants, including the one presented here, has also been implicitly realized in the literature relating to formation control and sensor fusion [23, 56, 75]. One goal of this chapter, therefore, is to formalize and define the edge Laplacian in a strictly graph-theoretic context. As we will show in this chapter, the edge Laplacian leads to a more explicit characterization of the role that certain sub-graphs play in relation to its algebraic properties.

The *edge Laplacian* is defined as

$$L_e(\mathcal{G}) \quad := \quad E(\mathcal{G})^T E(\mathcal{G}). \tag{3.1}$$

The structure of the edge Laplacian is closely related to the adjacency matrix of the undirected *line* graph of $\mathcal{G}$, $\mathscr{L}(\mathcal{G})$, as

$$A(\mathscr{L}(\mathcal{G})) \quad = \quad |\, L_e(\mathcal{G}) - 2I \,|. \tag{3.2}$$

Theorem 3.0.3. *Let $L_e(\mathcal{G})$ and $E(\mathcal{G})$ denote, respectively, the edge Laplacian and the incidence matrix of the graph $\mathcal{G}$. Then*

$$\mathcal{N}(L_e(\mathcal{G})) = \mathcal{N}(E(\mathcal{G})). \tag{3.3}$$

Proof. Let $x \in \mathcal{N}(E)$; then $L_e(\mathcal{G})x = E(\mathcal{G})^T E(\mathcal{G})x = \mathbf{0}$ and it follows that $\mathcal{N}(E(\mathcal{G})) \subseteq \mathcal{N}(L_e)$. On the other hand when $x \in \mathcal{N}(L_e(\mathcal{G}))$, $E(\mathcal{G})^T E(\mathcal{G})x = \mathbf{0}$ and $x^T E(\mathcal{G})^T E(\mathcal{G})x = \|E(\mathcal{G})x\|^2 = 0$. Thus $x \in \mathcal{N}(E(\mathcal{G}))$.

□

We can alternatively define the edge Laplacian in an analogous way to the graph Laplacian identity (2.29). In this venue, let us define the edge adjacency matrix as,

$$[A_e(\mathcal{G})]_{kl} := \begin{cases} +1 & e_k \sim^{+} e_l \\ -1 & e_k \sim^{-} e_l \\ 0 & \text{otherwise.} \end{cases}$$

The edge degree matrix, $\Delta_e(\mathcal{G})$, is a diagonal matrix with the number of nodes connected to each edge. As we do not allow self-loops, we have that $\Delta_e(\mathcal{G}) = 2I$. Thus, the edge Laplacian can be equivalently defined as

$$L_e(\mathcal{G}) := 2I - A_e(\mathcal{G}). \tag{3.4}$$

This alternative definition can be used to further deepen the connection between the edge Laplacian of $\mathcal{G}$ and its line graph $\mathscr{L}(\mathcal{G})$. We note that the (i,i) element of $A_e^2(\mathcal{G})$ corresponds to the degree of each node in the line graph of $\mathcal{G}$.

For a disconnected graph with c components the edge Laplacian can be partitioned into a block diagonal matrix.

Lemma 3.0.4. *Consider a graph with c connected components $\mathcal{G}_i$ for $i = 1, \ldots, c$ such that $\mathcal{G} = \mathcal{G}_1 \cup \cdots \cup \mathcal{G}_c$. The edge Laplacian for $\mathcal{G}$ can be written as*

$$L_e(\mathcal{G}) = \begin{bmatrix} L_e(\mathcal{G}_1) & & \\ & \ddots & \\ & & L_e(\mathcal{G}_c) \end{bmatrix}. \tag{3.5}$$

Proof. The incidence matrix for $\mathcal{G}$ can be partitioned as $E(\mathcal{G}) = \begin{bmatrix} E(\mathcal{G}_1) & \cdots & E(\mathcal{G}_c) \end{bmatrix}$. The result then follows from (3.1). □

3.1 *Similarity between the Graph and Edge Laplacians*

The connection between the edge and graph Laplacians can be made explicit through the introduction of an appropriate similarity transformation. Furthermore, we find similarity transformations that relate the Laplacians for connected graphs with cycles to graphs on spanning trees.

Theorem 3.1.1. *The graph Laplacian for a connected graph $L(\mathcal{G})$ containing cycles is similar to*

$$\begin{bmatrix} L_e(\mathcal{G}_\tau)R(\mathcal{G})R(\mathcal{G})^T & 0 \\ 0 & 0 \end{bmatrix},$$

where $\mathcal{G}_\tau$ is a spanning tree subgraph of $\mathcal{G}$ and the matrix $R(\mathcal{G})$ is defined via (2.25).

Proof. We define the transformation

$$S_v(\mathcal{G}) = \begin{bmatrix} E(\mathcal{G}_\tau)(E(\mathcal{G}_\tau)^T E(\mathcal{G}_\tau))^{-1} & \mathbb{1} \end{bmatrix}, \quad S_v(\mathcal{G})^{-1} = \begin{bmatrix} E(\mathcal{G}_\tau)^T \\ (1/|\mathcal{V}|)\,\mathbb{1}^T \end{bmatrix}, \tag{3.6}$$

where $E(\mathcal{G}_\tau)$ is the incidence matrix of $\mathcal{G}_\tau$. Applying the transformation as

$$\begin{aligned} S_v(\mathcal{G})^{-1}L(\mathcal{G})S_v(\mathcal{G}) &= \begin{bmatrix} E(\mathcal{G}_\tau)^T E(\mathcal{G}_\tau) \\ 0 \end{bmatrix} R(\mathcal{G})R(\mathcal{G})^T \begin{bmatrix} I & 0 \end{bmatrix} \\ &= \begin{bmatrix} L_e(\mathcal{G}_\tau)R(\mathcal{G})R(\mathcal{G})^T & 0 \\ 0 & 0 \end{bmatrix}, \end{aligned} \tag{3.7}$$

leads to the desired result. □

The transformation (3.7) provides a transparent way to separate the zero eigenvalue of the Laplacian for a connected graph while preserving algebraic properties of the graph via the edge Laplacian. When the graph has no cycles Theorem 3.6 shows that the non-zero eigenvalues of the graph Laplacian are identical to the eigenvalues of the edge Laplacian. It is also worth mentioning that this result holds for any choice of a spanning tree subgraph $\mathcal{G}_\tau$. An important feature to note is while the graph Laplacian is a symmetric matrix, the matrix $L_e(\mathcal{G}_\tau)R(\mathcal{G})R(\mathcal{G})$ is in general not (except when there are no cycles).

Theorem 3.1.2. *The edge Laplacian for a graph with cycles, $L_e(\mathcal{G})$ is similar to the matrix*

$$\begin{bmatrix} L_e(\mathcal{G}_\tau)R(\mathcal{G})R(\mathcal{G})^T & 0 \\ 0 & \mathbf{0} \end{bmatrix},$$

where $\mathcal{G}_\tau$ is a spanning tree subgraph of $\mathcal{G}$, the matrix $R(\mathcal{G})$ is defined via (2.25), and the block-matrix of zeros is square with dimension equal to the number of independent cycles in the graph.

Proof. Define the transformation matrix

$$S_e(\mathcal{G}) = \begin{bmatrix} R(\mathcal{G})^T & V_e(\mathcal{G}) \end{bmatrix}, \quad S_e(\mathcal{G})^{-1} = \begin{bmatrix} (R(\mathcal{G})R(\mathcal{G})^T)^{-1}R(\mathcal{G}) \\ V_e(\mathcal{G})^T \end{bmatrix}, \tag{3.8}$$

where the matrix $V_e(\mathcal{G})$ is the matrix representation of the orthonormal basis for the null space of $L_e(\mathcal{G})$. As shown by Theorem 2.2.3, the columns of $V_e(\mathcal{G})$ span the cycle space of the underlying graph. Applying the transformation matrix $S_e(\mathcal{G})$ as

$$\begin{aligned} S_e(\mathcal{G})^{-1}L_e(\mathcal{G})S_e(\mathcal{G}) &= S_e(\mathcal{G})^{-1}R(\mathcal{G})^T L_e(\mathcal{G}_\tau)R(\mathcal{G})S_e(\mathcal{G}) \\ &= \begin{bmatrix} L_e(\mathcal{G}_\tau)R(\mathcal{G})R(\mathcal{G})^T & 0 \\ 0 & \mathbf{0} \end{bmatrix}, \end{aligned}$$

leads to the desired result. □

Theorem 3.1.2 shows that the eigenvalues of $L_e(\mathcal{G}_\tau)R(\mathcal{G})R(\mathcal{G})^T$ corresponds to the non-zero eigenvalues of $L_e(\mathcal{G})$. We also note that the block matrix of zeros is square of size equal to the dimension of the kernel of $L_e(\mathcal{G})$, providing an additional proof for Theorem 2.2.3. The above results can now be combined to characterize a similarity transformation between the graph and edge Laplacians.

Theorem 3.1.3. *The edge Laplacian for a graph, $L_e(\mathcal{G})$, is similar to the bordered graph Laplacian*

$$\begin{bmatrix} L(\mathcal{G}) & 0 \\ 0 & \mathbf{0} \end{bmatrix},$$

where the block-matrix of zeros is square with dimension equal to the number of independent cycles in the graph minus one.

Proof. We define the transformation

$$S(\mathcal{G}) = S_e(\mathcal{G})\bar{S_v}(\mathcal{G})^{-1}, \tag{3.9}$$

where

$$\bar{S_v}(\mathcal{G}) = \begin{bmatrix} S_v(\mathcal{G}) & 0 \\ 0 & I \end{bmatrix},$$

and I is the identity matrix of the size of dimension of $\mathcal{N}(L_e(\mathcal{G}))$ minus one. □

$$\begin{tikzcd}
 & L_e(\mathcal{G}_\tau)RR^T \arrow[dl, shift left, "S_v"] \arrow[dr, shift right, "S_e"'] & \\
L(\mathcal{G}) \arrow[ur, shift left, "S_v^{-1}"] \arrow[rr, shift left, "S"] & & L_e(\mathcal{G}) \arrow[ul, shift right, "S_e^{-1}"'] \arrow[ll, shift left, "S^{-1}"]
\end{tikzcd}$$

Figure 3.1: Transformations between the node and edge Laplacians.

Theorem 3.1.3 highlights an important transformation between the graph and edge Laplacians. In both representations, the algebraic structure of the graph is retained while emphasizing the role of spanning trees. Note that when $\mathcal{G} = \mathcal{G}_\tau$ (no cycles), then $R = I$ and we see a direct connection between the graph and edge Laplacians. Furthermore, for a spanning tree $\mathcal{G}_\tau$, the edge Laplacian is guaranteed to be invertible as all its eigenvalues are strictly positive. Figure 3.1 shows a graphical representation of the relationship between the edge and graph Laplacians.

3.2 *Star, Path, and Regular Graphs*

For certain graphs, the edge Laplacian can have special structure that will be useful for our analysis in the sequel. We present here structural properties for $L_e(\mathcal{G})$, $L_e(\mathcal{G})^{-1}$, and $R(\mathcal{G})$ for the graphs P_n, S_n, C_n, and K_n.

Proposition 3.2.1.

$$R(C_n) = \begin{bmatrix} I & -\mathbb{1} \end{bmatrix} \quad \textit{and} \quad \left(R(C_n)R(C_n)^T\right) = I + \mathbf{J} \tag{3.10}$$

Proof. For the cycle graph, the only spanning tree subgraph is the path, P_n. Without loss of generality, we assume P_n is labeled such that $e_i = (v_i, v_{i+1}) \in \mathcal{E}(P_n)$ for $i = 1, \ldots, n-1$. Then the cycle edge must have the form $e_n = (v_n, v_1)$, and $T_\tau^c(C_n) = -\mathbb{1}$. □

Proposition 3.2.2. *Consider the graph K_n with node set $\mathcal{V} = \{1, \ldots, n\}$ and the graphs $\tilde{S}_i$ on the node set $\tilde{\mathcal{V}} = \{2, \ldots, n\} \subset \mathcal{V}$ such that $\mathcal{E}(\tilde{S}_i) = \{(v_i, v_j) \, : \, v_i, v_j \in \tilde{\mathcal{V}} \textit{ and } j = i+1, \ldots, n\}$.*

$$R(K_n) = \begin{bmatrix} I & E(\tilde{S}_2) & \cdots & E(\tilde{S}_{n-1}) \end{bmatrix} \tag{3.11}$$

Proof. First, note that the graph $\tilde{S}_i$ has $i-2$ singleton nodes (i.e., nodes with no incident edges). It suffices to show that the columns of $E\left(\tilde{S}_i\right)$ are contained in the columns of $T_\tau^c(K_n)$. Without loss of generality, we chose the spanning tree subgraph to be the star S_n with center node v_1 and all edges of the form $e_i = (v_1, v_{i+1})$ for $i = 1, \ldots, l, n-1$. Define the index sets $\mathcal{I}_\tau = \{1, \ldots, n-1\}$ and $\mathcal{I}_c = \{n, \ldots, n(n-1)/2\}$. Then all the cycle edges must have the form $e_{\sigma(k)} = (v_i, v_j)$ for all $i, j \neq 1, i < j$ and $\sigma(k) \in \mathcal{I}_c$ ($\sigma(k) = k+n,\ k = 1, \ldots, n(n-3)/2+1$).

Consider the cycle edge $e = (v_i, v_j)$ for $v_i, v_j \in \tilde{\mathcal{V}}$. This edge can be written as a linear combination of the tree edges e_{i-1} and e_{j-1}; the cycle has length three and the signed path vector has value '+1' for edge e_{i-1} and edge e, and '-1' for edge e_{j-1}. In terms of the columns of $E(S_n)$, it is a linear combination of column $i-1$ and $j-1$. If we consider all cycle edges that are of the form (v_i, v_j) for $j = i+1, \ldots, n$, it follows that each edge can be constructed from the columns of corresponding to the tree edges e_{i-1} and e_{j-1}. There will be a total of $n-i$ columns, each with a value of '+1' in the i-th row and '-1' in the j-th row; corresponding precisely to the graph $\tilde{S}_i$. This procedure is employed for each node $v_i, i > 1$ to produce (3.11). □

Proposition 3.2.3. *The edge Laplacian for the path graph, P_n, is the tri-diagonal matrix*

$$L_e(P_n) = \begin{bmatrix} 2 & -1 & & & \\ -1 & 2 & -1 & & \\ & \ddots & \ddots & \ddots & \\ & & -1 & 2 & -1 \\ & & & -1 & 2 \end{bmatrix}. \tag{3.12}$$

Proof. The structure of (3.12) follows from the edge adjacency definition of the edge Laplacian (3.4). This structure also assumes an ordering of nodes and edges such that node i is always connected to node $i+1$ by edge e_i. □

Proposition 3.2.4. *The inverse of the edge Laplacian for the path graph P_n is determined by observing that*

$$\left[(L_e(P_n))^{-1}\right]_{ij} = \frac{\min(i,j)(n-\max(i,j))}{n}. \tag{3.13}$$

Proposition 3.2.5. *The edge Laplacian for the cycle graph C_n is given as*

$$L_e(C_n) = \begin{bmatrix} 2 & -1 & & & -1 \\ -1 & 2 & -1 & & \\ & \ddots & \ddots & \ddots & \\ & & -1 & 2 & -1 \\ -1 & & & -1 & 2 \end{bmatrix}, \tag{3.14}$$

where unmarked entries are taken to be zero.

Proof. The structure assumes the spanning tree subgraph to be the path, $\mathcal{G}_\tau = P_n$. The cycle edge, therefore, connects the first and last nodes together. From Proposition 3.10, $R(C_n) = \begin{bmatrix} I & -\mathbb{1} \end{bmatrix}$, and $R(C_n)^T L_e(P_n) R(C_n)$ leads to the desired result. □

The structure of $L_e(C_n)$, it turns out, is identical to the graph Laplacian, $L(C_n)$. Recall that the graph Laplacian for a connected graph (in this case, C_n) has precisely one eigenvalue at the origin. At the same time, from Theorem 2.2.3 we conclude that $L_e(C_n)$ also has one eigenvalue at the origin.

Theorem 3.2.1. *For cycle graphs C_n,*

$$L_e(C_n) = L(C_n). \tag{3.15}$$

Proof. The graph Laplacian can be written as

$$\begin{aligned} L(C_n) &= E(P_n)R(C_n)R(C_n)^T E(P_n)^T \\ &= L(P_n) + E(P_n) J E(P_n)^T = L_e(C_n). \end{aligned}$$

We have assumed the path graph to be of the form (v_i, v_{i+1}) for $i = 1, \ldots, n-1$. The remaining equalities are straightforward to verify. □

Proposition 3.2.6. *For the cycle graph C_n with $\mathcal{G}_\tau = P_n$,*

$$R(C_n)^T(R(C_n)R(C_n)^T)^{-1} = \begin{bmatrix} I - \frac{1}{n}\mathbf{J} \\ -\frac{1}{n}\mathbb{1}^T \end{bmatrix}. \tag{3.16}$$

Proof. For the cycle graph, $R(C_n) = \begin{bmatrix} I & -\mathbb{1} \end{bmatrix}$ which implies that $R(C_n)R(C_n)^T = I + \mathbf{J}$. It then follows that $(R(C_n)R(C_n)^T)^{-1} = I - (1/n)\mathbf{J}$. □

Proposition 3.2.7. *The edge Laplacian for the star graph S_n is specified as*

$$L_e(S_n) = I + \mathbf{J}. \tag{3.17}$$

Proof. The structure of (3.17) follows from the edge adjacency definition of the edge Laplacian (3.4) by noting that every edge is adjacent to each other in the star graph. This structure also assumes each edge is positively adjacent to each other edge. □

Proposition 3.2.8. *The inverse of the edge Laplacian for the path graph S_n is*

$$(L_e(S_n))^{-1} = I - \frac{1}{n}\mathbf{J}. \tag{3.18}$$

Proof. The proof follows directly from Proposition 3.2.7. □

Proposition 3.2.9. *The matrix*

$$R(C_n)^T(R(C_n)R(C_n)^T)^{-1}(L_e(P_n))^{-1}(R(C_n)R(C_n)^T)^{-1}R(C_n)$$

is similar to

$$\begin{bmatrix} (L_e(P_n)R(C_n)R(C_n)^T)^{-1} & 0 \\ 0 & 0 \end{bmatrix}. \tag{3.19}$$

Proof. Defining the transformation matrix

$$M = \begin{bmatrix} L_e(P_n)R(C_n) \\ \mathbb{1}^T \end{bmatrix}, \quad M^{-1} = \begin{bmatrix} R(C_n)^T(R(C_n)R(C_n)^T)^{-1}(L_e(P_n))^{-1} & \frac{1}{n}\mathbb{1} \end{bmatrix},$$

and applying it as

$$\begin{aligned} &MR(C_n)^T(R(C_n)R(C_n)^T)^{-1}(L_e(P_n))^{-1}(R(C_n)R(C_n)^T)^{-1}R(C_n)M^{-1} \\ &\qquad = \begin{bmatrix} (L_e(P_n)R(C_n)R(C_n)^T)^{-1} & 0 \\ 0 & 0 \end{bmatrix}, \end{aligned}$$

yields the desired result. □

We note that the eigenvalues of the matrix (3.19) is $(1/\lambda_i(C_n))$ for $i = 2, \ldots, n$, i.e., these eigenvalues are the inverse of the non-zero eigenvalues of the graph Laplacian for the cycle graph.

Chapter 4

CANONICAL MODELS OF NETWORKED DYNAMIC SYSTEMS

In this chapter we develop a set of general linear time-invariant models for networked dynamic systems with an emphasis on the means by which the underlying connection topology enters into the system [81]. As alluded to in the introduction, we develop models which explicitly highlights how the underlying connection topology interacts with each agent in the ensemble.

4.1 Homogeneous and Heterogenous Dynamic Systems

Fundamental to all NDS is the notion of a "local" and "global" dynamic system layer. The local layer corresponds to the dynamics of each individual agent in the ensemble. This layer captures both the dynamic behavior of each agent in addition to local performance criteria that may or may not be related to certain global or team objectives. For example, the formation control for a team of unmanned vehicles may require each agent to perform a local control and estimation in order to accept higher level navigation commands relating to the team objective.

In this direction, we identify two broad classes of NDS: 1) homogeneous, and 2) heterogeneous. For both cases, we will work with a group of n dynamic systems, referred to as agents, each modeled as a linear and time-invariant system of the form

$$\Sigma_i : \left\{ \begin{array}{rclclcl} \dot{x}_i(t) & = & A_i x_i(t) & + & B_i u_i(t) & + & \Gamma_i w_i(t) \\ z_i(t) & = & C_i^z x_i(t) & + & D_i^{zu} u_i(t) & + & D_i^{zw} w_i(t) \\ y_i(t) & = & C_i^y x_i(t) & + & D_i^{yw} w_i(t) & & \end{array} \right. , \tag{4.1}$$

where each agent is indexed by the sub-script i. Here, $x_i(t) \in \mathbb{R}^{n_i}$ represents the state, $u_i(t) \in \mathbb{R}^{m_i}$ the control, $w_i(t) \in \mathbb{R}^{r_i}$ an exogenous input (e.g., disturbances and noises), $z_i(t) \in \mathbb{R}^{p_i}$ the controlled variable, and $y_i(t) \in \mathbb{R}^{b_i}$ the locally measured output.

We denote the transfer-function representation of Σ_i as $\hat{\Sigma}_i$,

$$\begin{aligned} \begin{bmatrix} Z_i(s) \\ Y_i(s) \end{bmatrix} &= \begin{bmatrix} H_i^{zu}(s) & H_i^{zw}(s) \\ H_i^{yu}(s) & H_i^{yw}(s) \end{bmatrix} \begin{bmatrix} U_i(s) \\ W_i(s) \end{bmatrix} \\ &= \hat{\Sigma}_i \begin{bmatrix} U_i(s) \\ W_i(s) \end{bmatrix}, \end{aligned} \tag{4.2}$$

with

$$\begin{aligned} H_i^{zu}(s) &= C_i^z(sI - A_i)^{-1}B_i + D_i^{zu}, H_i^{zw}(s) = C_i^z(sI - A_i)^{-1}\Gamma_i + D_i^{zw}, \\ H_i^{yu}(s) &= C_i^y(sI - A_i)^{-1}B_i, H_i^{yw}(s) = C_i^y(sI - A_i)^{-1}\Gamma_i + D_i^{yw}; \end{aligned} \tag{4.3}$$

we shall assume a minimal realization for each agent with no feed-forward terms of the control to the measure outputs.

When working with homogeneous NDS, the subscript is dropped, as each agent is described by the same set of linear state-space dynamics (e.g., $\Sigma_i = \Sigma_j$ for all i, j). It should be noted that in a heterogeneous system, the dimension of each agent need not be the same; however, without loss of generality, we assume each agent to have the same dimension.

The parallel interconnection of all the agents has a state-space description

$$\mathbf{\Sigma} : \quad \begin{cases} \dot{\mathbf{x}}(t) = \mathbf{Ax}(\mathbf{t}) + \mathbf{Bu}(\mathbf{t}) + \mathbf{\Gamma w}(\mathbf{t}), \\ \mathbf{z}(t) = \mathbf{C^z x}(\mathbf{t}) + \mathbf{D^{zu} u}(\mathbf{t}) + \mathbf{D^{zw} w}(\mathbf{t}), \\ \mathbf{y}(t) = \mathbf{C^y x}(\mathbf{t}) + \mathbf{D^{yw} w}(\mathbf{t}), \end{cases} \tag{4.4}$$

with $\mathbf{x}(t)$, $\mathbf{u}(t)$, $\mathbf{w}(t)$, $\mathbf{z}(t)$, and $\mathbf{y}(t)$ denoting, respectively, the concatenated state vector, control vector, exogenous input vector, controlled vector, and output vector of all the agents in the NDS. The bold faced matrices represent the block diagonal aggregation of each agent's state-space matrices, e.g., $\mathbf{A} = \mathbf{diag}\{A_1, \ldots, A_n\}$.

Given the above model for each agent and motivated by the diverse applications of multi-agent systems, we can begin to incorporate the role of the interconnection topology $\mathcal{G}$. To begin, we first define four canonical classes of NDS models. Such a classification is useful for analysis purposes; we will also show in the sequel that under certain conditions they are, in a sense, equivalent.

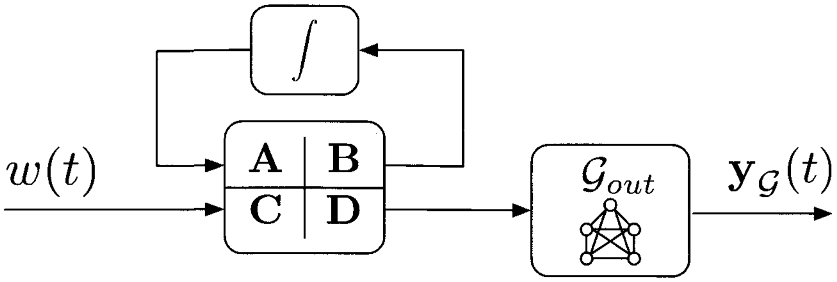

Figure 4.1: NDS coupled at the output; the feedback connection represents an upper fractional transformation [24].

4.2 NDS Coupled at the Output

In this class of NDS, the underlying network topology couples each agent through their outputs. Systems relying on relative sensing to achieve global objectives such as formation flying fall under this classification [29, 48, 73, 82, 84, 85, 86]. The block diagram in Figure 4.1 shows how the connection topology interacts with each agent. Here we have shown disturbances entering each agent and the global output of the entire system. An important feature of these types of systems is the underlying connection topology does not affect, in the open-loop, the dynamic behavior of each agent.

Motivated by applications that rely on relative sensing, we now derive a mathematical model to capture the global layer of this type of NDS. The sensed output of the system is the vector $\mathbf{y}_{\mathcal{G}}(t)$ containing relative state information of each agent and its neighbors. The incidence matrix of a graph naturally captures differences and will be the algebraic construct used to define the relative outputs. For example, the output sensed between agent i and agent j would be of the form $y_i(t) - y_j(t)$. This can be compactly written using the incidence matrix for the entire system as

$$\mathbf{y}_{\mathcal{G}}(t) = (E(\mathcal{G})^T \otimes I)\mathbf{y}(t). \tag{4.5}$$

Here, $\mathcal{G}$ is the graph the describes the connection topology; the node set is given as $\mathcal{V} = \{1, \ldots, n\}$.

When considering the analysis of the global layer, we are interested in studying the map from the agent's exogenous inputs, $\mathbf{w}(t)$, to the sensed output of the NDS, $\mathbf{y}_{\mathcal{G}}(t)$. Therefore, for the homogeneous NDS, the system $\mathbf{\Sigma}$ in (4.4) is augmented to include the sensed output

$$\mathbf{y}_{\mathcal{G}}(t) = (E(\mathcal{G})^T \otimes C^y)\mathbf{x}(t). \tag{4.6}$$

For the heterogeneous case, the sensed output is

$$\mathbf{y}_{\mathcal{G}}(t) = (E(\mathcal{G})^T \otimes I)\mathbf{C}^y\mathbf{x}(t). \tag{4.7}$$

Remark 4.2.1. *For relative sensing, the observation matrix C^y used in (4.6) and (4.7) may in fact be different from the local observation of each agent, as described in (4.1).*

In the context of NDS coupled at the output, we denote by $\Sigma_{hom}(\mathcal{G})$ the homogeneous system (4.4) with the additional sensed output (4.6). The heterogeneous system will be denoted by $\Sigma_{het}(\mathcal{G})$ and corresponds to the system (4.4) with the additional sensed output (4.7).

Similarly, the transfer function representation can be written as

$$\hat{\Sigma}_{hom}(\mathcal{G}) = \begin{bmatrix} (I_n \otimes H^{zu}(s)) & (I_n \otimes H^{zw}(s)) \\ (I_n \otimes H^{yu}(s)) & (I_n \otimes H^{yw}(s)) \\ (E(\mathcal{G})^T \otimes H^{yu}(s)) & (E(\mathcal{G})^T \otimes H^{yw}(s)) \end{bmatrix}, \tag{4.8}$$

and

$$\hat{\Sigma}_{het}(\mathcal{G}) = \begin{bmatrix} \mathbf{H}^{zu}(s) & \mathbf{H}^{zw}(s) \\ \mathbf{H}^{yu}(s) & \mathbf{H}^{yw}(s) \\ (E(\mathcal{G})^T \otimes I)\mathbf{H}^{yu}(s) & (E(\mathcal{G})^T \otimes I)\mathbf{H}^{yw}(s) \end{bmatrix}, \tag{4.9}$$

where, as in the state space model, bold faced transfer functions denotes the block diagonal aggregation of each agent's corresponding transfer function, as

$$\mathbf{H}^{zu}(s) = \mathbf{diag}\{H_1^{zu}(s), \ldots, H_n^{zu}(s)\}.$$

For notational simplicity, we denote $T_{hom}^{w \mapsto \mathcal{G}}$ and $T_{het}^{w \mapsto \mathcal{G}}$ as the map from the exogenous inputs to the NDS sensed output for homogeneous and heterogeneous systems respectively.

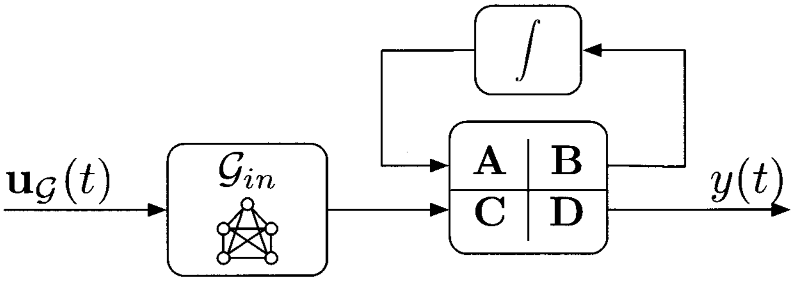

Figure 4.2: NDS coupled at the input; the feedback connection represents an upper fractional transformation [24].

4.3 NDS Coupled at the Input

In this class of NDS, the underlying network topology enters at the system input. The block diagram in Figure 4.2 shows a networked input being distributed to each agent via an interconnection topology. Large physically coupled systems where actuation affects multiple components might be modeled in this way. In fact, this class of NDS may even be considered the "dual" of the output coupled NDS presented above. The agents are therefore coupled via the inputs. To maintain a close connection with the NDS coupled at the output model, we will assume the network input, $\mathbf{u}_{\mathcal{G}}(t)$, is distributed to each agent via the incidence matrix. The control applied to each agent, therefore, is the net contribution of the control applied to all the edges incident to that agent. When the underlying graph is directed and connected, each agent's control can be written as

$$u_i(t) = \sum_{(i,j)\in\mathcal{E}} [\mathbf{u}_{\mathcal{G}}(t)]_{(i,j)} - \sum_{(j,i)\in\mathcal{E}} [\mathbf{u}_{\mathcal{G}}(t)]_{(j,i)}, \tag{4.10}$$

where $[\mathbf{u}_{\mathcal{G}}(t)]_{(i,j)}$ denotes the component of the input vector corresponding to the directed edge (i,j). This can be compactly written using the incidence matrix and Kronecker products to obtain a complete model for NDS coupled at the input.

For the homogeneous case, we have

$$\mathbf{u}(t) = (E(\mathcal{G}) \otimes B)\mathbf{u}_{\mathcal{G}}(t), \tag{4.11}$$

and for the heterogeneous case

$$\mathbf{u}(t) \;=\; \mathbf{B}(E(\mathcal{G}) \otimes I)\mathbf{u}_{\mathcal{G}}(t). \tag{4.12}$$

The parallel interconnected system (4.4) can be modified to include the network input using (4.11) and (4.12) as

$$\Sigma_{hom}(\mathcal{G}) : \left\{ \begin{array}{rclclcl} \dot{\mathbf{x}}(t) & = & (I_n \otimes A)\mathbf{x}(t) & + & (E(\mathcal{G}) \otimes B)\mathbf{u}_{\mathcal{G}}(t) & + & (I_n \otimes \Gamma)\mathbf{w}(t), \\ \mathbf{z}(t) & = & (I_n \otimes C^z)\mathbf{x}(t) & + & (I_n \otimes D^{zu})\mathbf{u}(t) & + & (I_n \otimes D^{zw})\mathbf{w}(t), \\ \mathbf{y}(t) & = & (I_n \otimes C^y)\mathbf{x}(t) & + & (I_n \otimes D^{yw})\mathbf{w}(t), & & \end{array} \right. \tag{4.13}$$

and

$$\Sigma_{het}(\mathcal{G}) : \left\{ \begin{array}{rclclcl} \dot{\mathbf{x}}(t) & = & \mathbf{A}\mathbf{x}(t) & + & \mathbf{B}(E(\mathcal{G}) \otimes I)\mathbf{u}_{\mathcal{G}}(t) & + & \Gamma\mathbf{w}(t), \\ \mathbf{z}(t) & = & \mathbf{C}^z\mathbf{x}(t) & + & \mathbf{D}^{zu}\mathbf{u}(t) & + & \mathbf{D}^{zw}\mathbf{w}(t), \\ \mathbf{y}(t) & = & \mathbf{C}^y\mathbf{x}(t) & + & \mathbf{D}^{yw}\mathbf{w}(t). & & \end{array} \right. \tag{4.14}$$

4.4 NDS Coupled at the State

This class of NDS is perhaps one of the most studied in the systems and control community. In this type of NDS, the underlying topology couples each agent at the state level, resulting in an important connection between the dynamic evolution of each agent and the underlying topology. The block diagram in Figure 4.3 shows the connection topology entering a dynamic system at the state level.

The most general way to model such systems is to simply denote the dependence of the state-matrix on the network with the notation $\mathbf{A}(\mathcal{G})$. For our purposes, however, we will focus on a special instance of this system, known as the agreement or consensus protocol [54, 58, 65]. Consequently, we will only focus on homogeneous systems for this case.

The consensus model is built upon a general setup consisting of a group of n identical single integrator units,

$$\dot{x}_i(t) \;=\; u_i(t), \quad i = 1, \ldots, n, \tag{4.15}$$

each connected to a fixed number of other units in the ensemble, determined by the interconnection topology $\mathcal{G}$. The interaction or coupling between units' dynamics is realized

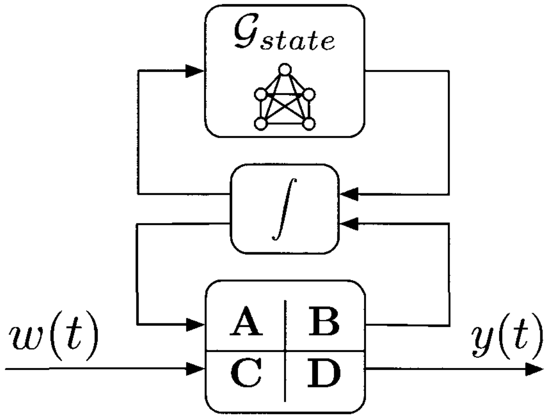

Figure 4.3: NDS coupled at the state; the feedback connection between the plant matrices and the integrator represents an upper fractional transformation [24], whereas the feedback connection between the integrator and the graph represents a relation such as (1.1).

through the control input $u_i(t)$ in (4.15), assumed to be the sum of the differences between states of an agent and its neighbors, i.e.,

$$u_i(t) = \sum_{i \sim j}(x_j(t) - x_i(t)). \tag{4.16}$$

Expressing the dynamic evolution of the resulting system in a compact matrix form one has

$$\dot{\mathbf{x}}(t) = -L(\mathcal{G})\,\mathbf{x}(t), \tag{4.17}$$

where $L(\mathcal{G})$ is the graph Laplacian. This model can be extended to include exogenous inputs and controlled variables, which will be discussed in the sequel. Variations of this model have been extensively treated, including random networks [35, 76], switching topologies [49], noisy networks [80], and non-linear extensions [39].

4.4.1 Edge Agreement

In this section we derive an edge variant of the agreement protocol (4.17) using the edge Laplacian introduced in §3 [83, 87, 88]. One of the goals of this section is to develop an input-output description of the consensus protocol in order to derive the $\mathcal{H}_2$ and $\mathcal{H}_\infty$ performance of the system which we will delve into in §5. In this direction, we first revisit the traditional agreement protocol with the addition of noises entering both the process and measurement stages of the model. We then describe a transformation of the system into the edge domain.

In consensus problems, the agreement set $\mathcal{A} \subseteq \mathbb{R}^n$, defined in [60], is the subspace $\mathbf{span}\{\mathbb{1}\}$. Let us also define $\delta(t)$ as the projection of states $x(t)$ onto the subspace orthogonal to the agreement subspace. This subspace will be denoted by $\mathbb{1}^\perp$; in [60] it is referred to as the *disagreement* subspace. In then follows that $\delta(t) = x(t) - \alpha\mathbb{1}$, where $\alpha = (1/n)\sum_i x_i(0)$.

Proposition 4.4.1 ([60]). *The Laplacian dynamics (4.17) converges to the agreement subspace from an arbitrary initial condition if and only if the underlying graph is connected.*

We now consider a general scenario where noise is introduced at both the process and measurement levels of the consensus protocol. The single integrator dynamics are modified to include the process noise for each agent as

$$x_i(t) \quad = \quad u_i(t) + w_i(t); \tag{4.18}$$

we assume that $w_i(t)$ is a zero-mean Gaussian noise with covariance $\mathbf{E}[w(t)w(t)^T] = \sigma_w^2 I$. Similarly, the measurement is assumed to be corrupted by noise as

$$y(t) \quad = \quad E(\mathcal{G})^T x(t) + v(t); \tag{4.19}$$

here, $v(t) \in \mathbb{R}^{|\mathcal{E}|}$ is also a zero-mean Gaussian noise with covariance $\mathbf{E}[v(t)v(t)^T] = \sigma_v^2 I$.

Equations (4.18) and (4.19) can be considered as the *open-loop consensus model*. We denote this open-loop system as

$$\Sigma_{ol} \;:\; \left\{ \begin{array}{rcccl} \dot{x}(t) & = & u(t) & + & w(t) \\ y(t) & = & E(\mathcal{G})^T x(t) & + & v(t) \end{array} \right. . \tag{4.20}$$

When the output-feedback control $u(t) = -E(\mathcal{G})y(t)$ is applied, the system leads to a generalized consensus protocol with noise. The noisy consensus model will be referred to

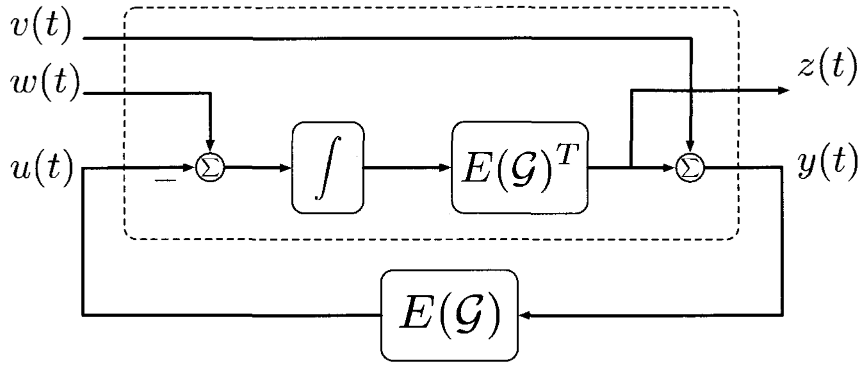

Figure 4.4: Open-loop consensus system with output feedback.

as the Σ model specified by

$$\Sigma \;:\; \begin{cases} \dot{x}(t) = -L(\mathcal{G})x(t) + \begin{bmatrix} I & -E(\mathcal{G}) \end{bmatrix} \begin{bmatrix} w(t) \\ v(t) \end{bmatrix} \\ z(t) = E(\mathcal{G})^T x(t) \end{cases} . \tag{4.21}$$

In (4.21), the variable $z(t)$ is introduced as a monitored performance signal. The open-loop system is shown in Figure 4.4 with the consensus output-feedback law.

Remark 4.4.1. *The derivation of the open-loop consensus model (4.20) assumes that relative measurements are* sensed. *Applications utilizing such a model includes formation flying where relative position is sensed via a camera system or proximity type sensors. An alternative model description might consider the state information being communicated rather than sensed. The measurement noise would consequently be associated with each state, rather than the difference between states. With an appropriate normalization of the noise signals in this scenario, the original model (4.21) can thereby be recovered.*

This problem has a natural "edge interpretation" that we now examine. In this direction, we introduce the coordinate transformation $S_v x_e(t) = x(t)$, where S_v is defined in (3.6). Applying this transformation to the consensus system with noise (4.21) yields

$$\Sigma_e : \begin{cases} \dot{x}_e(t) = \begin{bmatrix} -L_e(\mathcal{G}_\tau)R(\mathcal{G})R(\mathcal{G})^T & 0 \\ 0 & 0 \end{bmatrix} x_e(t) + \begin{bmatrix} E(\mathcal{G}_\tau)^T & -L_e(\mathcal{G}_\tau)R(\mathcal{G}) \\ \frac{1}{n}\mathbb{1}^T & 0 \end{bmatrix} \begin{bmatrix} w(t) \\ v(t) \end{bmatrix} \\ z(t) = \begin{bmatrix} R(\mathcal{G})^T & 0 \end{bmatrix} x_e(t) \end{cases}$$

The benefit of such a transformation is in view of the preservation of the algebraic structure of the underlying connection topology through the edge Laplacian. Furthermore, we note that the new state $x_e(t)$ can be partitioned as $x_e^T(t) = \left[\begin{array}{cc} x_\tau^T(t) & x_{\mathbb{1}}^T(t) \end{array} \right]^T$, where $x_\tau(t)$ represents the relative state information across the edges of a spanning tree of $\mathcal{G}$, and $x_{\mathbb{1}}(t)$ is the mode in the $\mathbb{1}$ subspace; the $x_{\mathbb{1}}(t)$ mode can be interpreted as the "inertial state" for the entire formation. In fact, we note that this transformation separates the system into its controllable and observable parts; that is, the $x_{\mathbb{1}}(t)$ mode is an unobservable mode of the system.

We can now consider a minimal realization of the system containing only the states $x_\tau(t)$ for analysis. We refer to this as the Σ_τ system specified by,

$$\Sigma_\tau : \begin{cases} \dot{x}_\tau(t) &= -L_e(\mathcal{G}_\tau)R(\mathcal{G})R(\mathcal{G})^T x_\tau(t) + \sigma_w E(\mathcal{G}_\tau)^T \hat{w}(t) - \sigma_v L_e(\mathcal{G}_\tau)R(\mathcal{G})\hat{v}(t) \\ z(t) &= R(\mathcal{G})^T x_\tau(t) \end{cases} \tag{4.22}$$

The signals $\hat{w}(t)$ and $\hat{v}(t)$ are the normalized process and measurement noise signals. The performance variable, $z(t)$, contains information on the tree states in addition to the cycle states. Here we recall that the cycle states are linear combinations of the tree states and we note that $z(t)$ actually contains redundant information. This is highlighted by recognizing that the tree states converging to the origin forces the cycle states to do the same. Consequently, we will consider the system with cycles as well as a system containing only the tree states at the output, which we denote as $\tilde{\Sigma}_\tau$,

$$\tilde{\Sigma}_\tau : \begin{cases} \dot{x}(t) &= -L_e(\mathcal{G}_\tau)R(\mathcal{G})R(\mathcal{G})^T x_\tau(t) + \sigma_w E(\mathcal{G}_\tau)^T \hat{w}(t) - \sigma_v L_e(\mathcal{G}_\tau)R(\mathcal{G})\hat{v}(t) \\ z(t) &= x_\tau(t) \end{cases} \tag{4.23}$$

This distinction will subsequently be employed to quantify the effect of cycles on the system performance. In the noise-free case, (4.22) reduces to the edge variant of the autonomous system,

$$\Sigma_\tau \; : \; \begin{cases} \dot{x}_\tau(t) &= -L_e(\mathcal{G}_\tau)R(\mathcal{G})R(\mathcal{G})^T x_\tau(t) \\ z(t) &= R(\mathcal{G})^T x_\tau(t) \end{cases} ; \tag{4.24}$$

both systems (4.22) and (4.24)) are referred to as the *edge agreement protocol.*

The first simple, yet important observation, relates to the meaning of agreement in the context of the edge states, leading to an edge interpretation of Proposition 4.4.1.

Proposition 4.4.2. *The edge agreement problem (4.24) converges to the origin for arbitrary graphs.*

Proof. If the graph $\mathcal{G}$ is connected, then we note that the agreement state is equivalent to having $x_\tau(t) = \mathbf{0}$, as $x_e(t) = S_v^{-1}x(t)$ for $x(t) \in \mathcal{A}$. In the edge setting, the agreement set $\mathcal{A}_e$, maps to the *origin*. The projection of the edge states onto this set, denoted as $\delta_e(t)$, is consequently the norm of the edge states; it also satisfies $\|\delta_e(t)\|_{\mathcal{L}_2} = \|x_\tau(t)\|_{\mathcal{L}_2} \leq \|E(\mathcal{G})\|\|\delta(t)\|_{\mathcal{L}_2}$ with respect to the distance to the agreement subspace.

For a disconnected graph $\mathcal{G}$ with c connected components, we can conclude using the results of Lemma 3.0.4 and §3.1 that each component of the edge agreement system will converge to the origin. □

From Proposition 4.4.1, the node dynamics over a connected graph converges to the agreement subspace, which implies that the corresponding edge dynamics converges to the origin. An important consequence of this result is edge agreement will not always correspond to the node agreement; having all the relative states converge to the origin will not guarantee that each node state has the same value. This merely emphasizes the need to work with connected graphs. Analogous to the node agreement, in the edge agreement setting, the evolution of an edge state depends on its current state and the states of its adjacent edges, i.e., those that share a node with it.

Much of the literature related to consensus problems focuses on the convergence rate of the system; a property dictated by the second smallest eigenvalue of the graph Laplacian. The input-output description of the consensus problem developed in this section allows for a more general notion of performance for these systems.

4.4.2 *Edge Laplacian and Nonlinear Agreement*

In this section, we explore a non-linear variation of the agreement protocol based on the edge perspective. This includes viewing the protocol in the context of Lyapunov theory- as opposed to the machinery of LaSalle's invariance [44]. We then proceed to examine the nonlinear extensions of the agreement problem via the passivity framework [5]. Our contribution in this section is to streamline the analysis of the nonlinear consensus-type problems using the edge Laplacian. To begin our analysis, consider the noise-free version

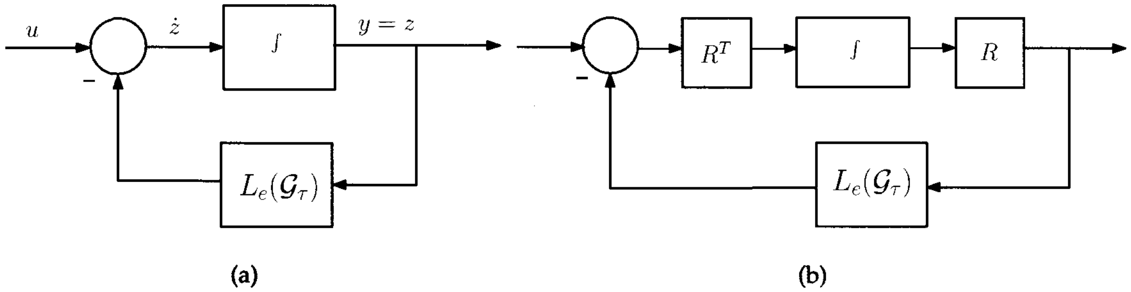

u
$\dot{z}$
$\int$
$y = z$
$-$
$L_e(\mathcal{G}_\mathcal{T})$
(a)
$-$
R^T
$\int$
R
$L_e(\mathcal{G}_\mathcal{T})$
(b)

Figure 4.5: Viewing edge agreement over a spanning tree as a strictly output passive system.

of the edge agreement problem (4.22),

$$\Sigma_\mathcal{T} \ : \ \begin{cases} \dot{x}_\mathcal{T}(t) &= -L_e(\mathcal{G}_\mathcal{T})R(\mathcal{G})R(\mathcal{G})^T x_\mathcal{T}(t) \\ z(t) &= R(\mathcal{G})^T x_\mathcal{T}(t) \end{cases} . \tag{4.25}$$

Of course, an underlying assumption of this edge variant of the consensus problem is the linearity of the interaction rule. A natural generalization of this model is to introduce non-linear passive elements in the general setup. As we move from a linear to non-linear model, we explore how passivity theory, in conjunction with the edge Laplacian, can be used to analyze this extension. First, we recall that passivity pertains to nonlinear system of the form

$$\dot{z}(t) = f(z(t), u(t)), \quad y(t) = z(t), \tag{4.26}$$

where f is locally Lipschitz and $f(0,0) = 0$; then (4.26) is passive if there exists a continuously differentiable positive semidefinite function V, referred to as the storage function, such that

$$u(t)^T y(t) \geq \dot{V}(t) \tag{4.27}$$

for all t. If $\dot{V}$ in (4.27) can be replaced by $\dot{V} + \psi(z)$ for some positive definite function ψ, then we call the system strictly passive; in our case, since the output of the system is its state, (4.26) could also be referred to as output strictly passive.

Theorem 4.4.2 ([44]). *Suppose that (4.26) is output strictly passive with a radially unbounded storage function. Then the origin is globally asymptotically stable.*

To demonstrate the utility of this passivity theorem in the context of agreement protocol, consider the interconnection of Figure 4.5(a), with an integrator in the forward path and the edge Laplacian of a spanning tree, in the feedback path, depicting the edge agreement (4.25). Note that $z(t)$ in this case denotes the vector of edge states $x_\tau(t)$. Then, with respect to the quadratic storage function $V(x) = (1/2)x(t)^T x(t)$, one has

$$\begin{aligned} u(t)^T y(t) &= u(t)^T z(t) = -z(t)^T L_e(\mathcal{G}_\tau) z(t) + u(t)^T z(t) + z(t)^T L_e(\mathcal{G}_\tau) z(t) \\ &= \dot{V} + z(t)^T L_e(\mathcal{G}_\tau) z(t), \end{aligned}$$

implying that the system is strictly (output) passive with a storage function that is radially unbounded. This observation, in turn, makes the convergence analysis for the edge agreement over a spanning tree fall in the range of applicability of Theorem 4.4.2. Hence, $z(t) \rightarrow 0$ as $t \rightarrow \infty$ and convergence to the agreement subspace of the "node" states follows, providing an alternative proof for Proposition 4.4.2.

The connection between the agreement protocol and Theorem 4.4.2 can be used to extend the basic setup of the agreement protocol in various directions, one of which is the following.

Corollary 4.4.3. *Suppose that for a network of interconnected agents the edge states evolve according to $\dot{x}_\tau(t) = -f(\mathcal{G}, x_\tau(t))$ where $f : \mathcal{G} \times \mathbb{R}^m \rightarrow \mathbb{R}^m$ for which $x_\tau(t)^T f(\mathcal{G}, x_\tau(t)) > 0$ for all $x_\tau(t) \neq 0$ when $\mathcal{G}$ is connected. Then the corresponding node states converge to the agreement subspace.*

The above corollary suggests that many passivity-type results from nonlinear systems theory can now be applied to the agreement protocol in its edge context.

Corollary 4.4.4. *Consider the feedback connection shown in Fig. 4.6, where the time-invariant passive system $G_1 : \dot{z}(t) = f(z(t), u_1(t)), y_1(t) = z(t)$ has a storage function V and the time invariant memory-less function G_2 is such that $u_2^T(t) y_2(t) \geq u_2^T(t)\phi(u_2(t))$ for some function ϕ. Then the origin of the closed loop system (with $u(t) = 0$) is asymptotically stable if $v^T(t)\phi(v(t)) > 0$ for all $v(t) \neq 0$.*

To illustrate the ramification of Corollary 4.4.4, suppose that following the integrator block in Figure 4.5, there exists a nonlinear operator ψ such that for some positive-definite

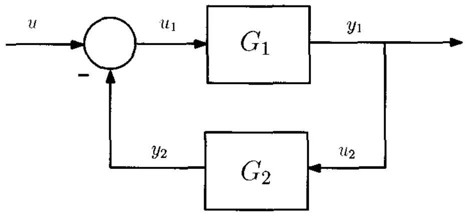

Figure 4.6: The feedback configuration for Theorem 4.4.4.

functional $V(z)$, one has $\psi(z) = \nabla V(z)$. Then

$$\dot{V}(t) = \nabla V^T \dot{z}(t) = \psi(z)^T \dot{z}(t), \tag{4.28}$$

implying that the forward path of the feedback configuration shown in Figure 4.7(a) is passive with a storage function V and the function $\phi(v)$ in Theorem 4.4.4 can be chosen as $\lambda_2(\mathcal{G})v$. Hence, the asymptotic stability of the origin with respect to the edge states $x_\tau(t)$ can be implied by invoking Theorem 4.4.4. The more general case of this result for a connected network is also immediate using Theorem 3.1.2, by observing that that

$$L_e(\mathcal{G}) \quad \text{is similar to} \quad \begin{bmatrix} L_e(\mathcal{G}_\tau)R(\mathcal{G})R(\mathcal{G})^T & 0 \\ 0 & \mathbf{0} \end{bmatrix},$$

where $\mathcal{G}$ is an arbitrary connected graph. This relationship suggests the loop transformation depicted in Fig. 4.7, keeping in mind that passivity of the forward path does not change under post- and pre-multiplication by matrices $R(\mathcal{G})^T$ and $R(\mathcal{G})$, and the linearity of the integrator operator allows an operator reordering; Theorem 4.4.4 can now be invoked under this more general setting.

An example that demonstrates the utility of the above observation for multi-agent systems pertains to the Kuramoto model of n-coupled oscillators interacting over the network $\mathcal{G}$ as [39]

$$\dot{\theta}_i(t) = k \sum_{j \sim i} \sin(\theta_j(t) - \theta_i(t)), \quad i = 1, 2, \ldots, n. \tag{4.29}$$

In (4.29) the constant k denotes the coupling strength between the oscillators, which for the purpose of this section is assumed to be non-negative. The nonlinear interaction rule (4.29) can compactly be represented as

$$\dot{\theta}(t) = -\frac{k}{n} E(\mathcal{G}) \sin\left(E(\mathcal{G})^T \theta(t)\right), \tag{4.30}$$

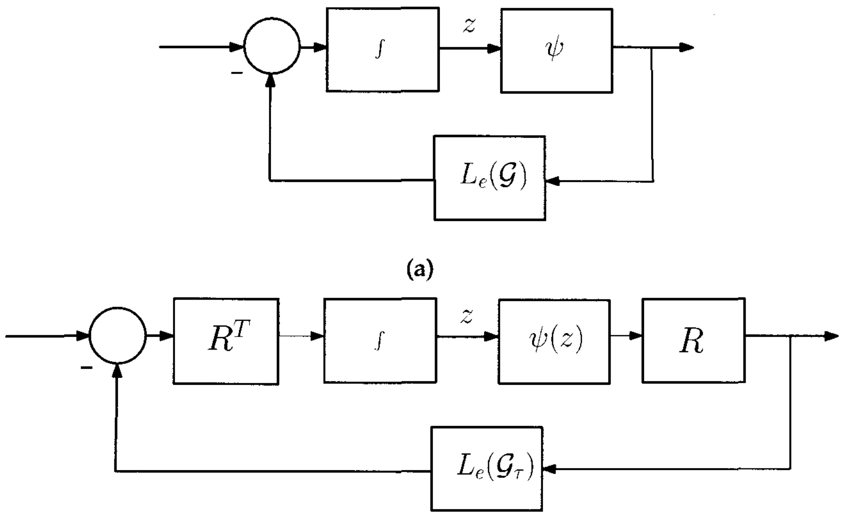

(a)

(b)

Figure 4.7: Loop transformation between feedback connection with edge Laplacian over arbitrary connected graphs shown in (a) to one over spanning trees, shown in (b).

where $\theta(t) := [\,\theta_1(t), \theta_2(t), \ldots, \theta_n(t)\,]^T$. As in §4.4.1, we can apply the state-transformation $S\theta_e(t) = \theta(t)$, where S is defined in (3.6), leading to

$$\dot{\theta}_e(t) \;=\; -\frac{k}{n}\begin{bmatrix} L_e(\mathcal{G}_\tau)R(\mathcal{G}) \\ 0 \end{bmatrix} \sin\left(\begin{bmatrix} R(\mathcal{G})^T & 0 \end{bmatrix}\theta_e(t)\right), \tag{4.31}$$

which monitors the relative phases between the oscillators. Recall that the transformed state can be expressed as $\theta_e(t) = \begin{bmatrix} \theta_\tau(t)^T & \theta_{\mathbf{1}}^T \end{bmatrix}$, where $\theta_\tau(t)$ represents the relative phase between each oscillator over a spanning tree, and $\theta_{\mathbf{1}}(t)$ is the phase in the "inertial" mode. The zeros introduced by the transformation results in a reduced model,

$$\dot{\theta}_\tau(t) \;=\; -\frac{k}{n}L_e(\mathcal{G}_\tau)R(\mathcal{G})\sin\left(R(\mathcal{G})^T\theta_\tau(t)\right).$$

Now, when the difference between the angles of the neighboring oscillators is in the interval $[-\pi/2, \pi/2]$, one can consider $V(\theta_\tau(t)) = 1 - \cos(R(\mathcal{G})^T\theta_\tau(t))$ as a candidate storage function for the Kuramoto model. In this case, $V(\theta_\tau(t)) > 0$ when $\theta_\tau(t) \in [-\pi/2, \pi/2]\backslash\{0\}$, $V(0) = 0$, and $\psi(\theta_\tau(t)) = \sin(R^T\theta_\tau(t))$. Since when $\theta(t_1) \in [-\pi/2, \pi/2]$ for some t_1, it follows that $\theta(t) \in [-\pi/2, \pi/2]$ for all $t \geq t_1$, we conclude that for the Kuramoto model over a connected graph, the synchronization state is asymptotically stable.[1]

[1] By synchronization we refer to the case when $\theta_1 = \theta_2 = \cdots = \theta_n \bmod 2\pi$.

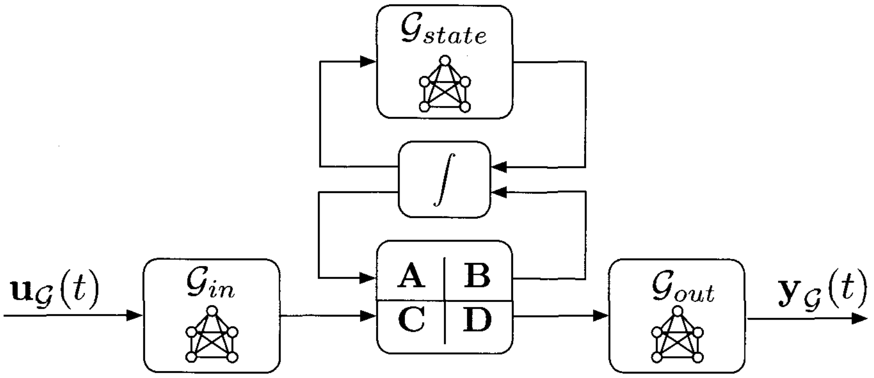

Figure 4.8: NDS coupled at the state, input, and output; the feedback connection between the plant matrices and the integrator represents an upper fractional transformation [24], whereas the feedback connection between the integrator and the graph represents a relation such as (1.1).

4.5 NDS Coupled by Combinations of State, Input, and Output

A natural extension of the above models is to consider systems that have a network coupling the agents at all component levels. Figure 4.8 shows a dynamic system where there are different connection topologies at the input, output, and state level. Clearly, this type of model represents the most complex and intricate connection between the dynamic properties and interconnection topology of a system. It is worth noting that although this type of system can be exhaustively studied on its own, we only present it here for completeness and as a vehicle to illustrate how each of the previous types can be interrelated.

Chapter 5
ANALYSIS AND GRAPH-THEORETIC PERFORMANCE BOUNDS

The development of the NDS models in §4 allows us to examine systems-theoretic properties and performance bounds for networked system from a graph-theoretic perspective. The objective of this chapter, therefore, is to develop explicit connections between control-theoretic concepts such as observability, controllability, and performance in terms of the underlying interconnection graph. We first discuss the observability properties of NDS coupled at the output, and then proceed to highlight how duality streamlines the controllability analysis of NDS coupled at the input. We then focus on characterizing the $\mathcal{H}_2$ and $\mathcal{H}_\infty$ performance of NDS coupled at the output and at the state via constructs from algebraic graph theory.

5.1 Observability and Controllability of NDS

Studying the observability and controllability properties of a linear system can provide qualitative as well as quantitative insights into the design of the corresponding controllers and estimators. In the context of NDS, we also consider how the underlying topology affects these properties in addition to examining the effects of homogeneity and heterogeneity of the agent dynamics comprising the NDS [81, 82]. In this direction, we consider simplified versions of the models presented in §4.

For the observability analysis, we consider the following simplified model of an NDS coupled at the output,

$$\left\{ \begin{array}{rcl} \dot{\mathbf{x}}(t) & = & \mathbf{A}\mathbf{x}(t) \\ \mathbf{y}_{\mathcal{G}}(t) & = & (E(\mathcal{G})^T \otimes I)\mathbf{C}^y\mathbf{x}(t) \end{array} \right. . \tag{5.1}$$

Analogously, the following simplified model for an NDS coupled at the input will be used to study the controllability properties,

$$\dot{\mathbf{x}}(t) \quad = \quad \mathbf{A}\mathbf{x}(t) + \mathbf{B}(E(\mathcal{G}) \otimes I)\mathbf{u}_{\mathcal{G}}(t); \tag{5.2}$$

for both systems, we will examine the homogeneous and heterogeneous realizations.

Our observability and controllability analysis relies on observability and controllability gramians for networked systems, as presented in §2.1. For this analysis, we will assume that each agent is stable, e.g., A_i is Hurwitz, the pair (A_i, C_i^y) is observable, and (A_i, B_i) is a controllable pair.

5.1.1 *Observability of NDS Coupled at the Output*

A natural question for this analysis is whether *the initial condition of each agent in an NDS coupled at the output can be inferred from their relative states.* The answer to this question can have profound implications for the design of estimators for such systems.

Homogeneous Case

For homogeneous NDSs, the observability gramian can be written as

$$\mathbf{Y}_o \;=\; L(\mathcal{G}) \otimes \int_0^{\infty} e^{A^T t}(C^y)^T C^y e^{At} dt \;=\; L(\mathcal{G}) \otimes Y_o, \tag{5.3}$$

where Y_o is the gramian for an individual agent in the NDS.

Theorem 5.1.1. *The homogeneous NDS coupled at the output in (5.1) is unobservable.*

Proof. Using the gramian expression in (5.3) and Theorem 2.4.1 we conclude that $\mathbf{Y}_o$ has precisely n eigenvalues at the origin, leading to an unobservable system. □

The unobservable modes of (5.1), in fact, correspond to the inertial position of the entire formation; these modes lie in the subspace $\mathbf{span}\{\mathbb{1} \otimes I\}$. This can be shown explicitly by considering the state transformation $(S_v \otimes I)\tilde{\mathbf{x}}(t) = \mathbf{x}(t)$, where S_v is defined in (3.6);

$$\left\{\begin{array}{rcl} \dot{\tilde{\mathbf{x}}}(t) & = & (I \otimes A)\tilde{\mathbf{x}}(t) \\ \mathbf{y}_{\mathcal{G}}(t) & = & \left(\begin{bmatrix} R(\mathcal{G})^T & 0 \end{bmatrix} \otimes C^y\right)\tilde{\mathbf{x}}(t) \\ & = & \begin{bmatrix} (R(\mathcal{G})^T \otimes C^y) & 0 \end{bmatrix}\tilde{\mathbf{x}}(t) \end{array}\right. . \tag{5.4}$$

The system in (5.4) is obtained using the identity (2.37) and recalling for homogeneous NDS, $\mathbf{A} = I \otimes A$ and $\mathbf{C}^y = I \otimes C^y$.

The importance of this result is that when each agent has identical dynamics, relative measurements alone are insufficient to reconstruct their inertial states. If in addition to the relative output, an additional inertial measurement is available, say one that corresponds to the inertial position of a single agent, then the observability of the system can be recovered.

An interesting consequence of this result highlights how the underlying connection topology influences the relative degree of observability of the observable modes. We denote and index each singular value of Y_o as σ_i, and using the results of Theorem 2.4.1 we can express the non-zero singular values of $\mathbf{Y}_o$ as $\lambda_j(\mathcal{G})\sigma_i$ for $j = 2, \ldots, n$ and all i. The eigenvalues of the graph Laplacian, therefore, can amplify or attenuate the relative degree of observability of the system. For example, the complete graph as in Figure 2.3(a), has $\lambda_i(\mathcal{G}) = \lambda_j(\mathcal{G}) = n$ for $i, j \geq 2$. In this case, the connection topology does not favor any particular modes of the system as each is scaled by the same amount. Conversely, when the graph is disconnected with two connected components, then $\lambda_2(\mathcal{G}) = 0$ and n additional unobservable modes are introduced into the system.

Heterogeneous Case

In the heterogeneous case, the observability gramian of (5.1) has a non-trivial form. We define the observability operator for an individual agent as $\Psi_i(x) = C_i^y e^{A_i t} x$, and its adjoint as $\Psi_i^*(y(t)) = \int_0^\infty e^{A_i^T t}(C_i^y)^T y(t)dt$ [24]. The observability gramian of (5.1) can be written as

$$\mathbf{Y}_o \;=\; \mathbf{diag}\{\mathbf{\Psi}^*\}(L(\mathcal{G}) \otimes I)\mathbf{diag}\{\mathbf{\Psi}\} \;=\; (L(\mathcal{G}) \otimes I) \circ \mathbf{\Psi}^*\mathbf{\Psi}, \tag{5.5}$$

where $\mathbf{\Psi} = \begin{bmatrix} \Psi_1 & \cdots & \Psi_n \end{bmatrix}$.

This expression is derived by first noting that

$$\mathbf{C}^y e^{\mathbf{A}t} \;=\; \sum_{i=1}^{n}(e_i e_i^T \otimes C_i^y e^{A_i t}),$$

where $e_i \in \mathbb{R}^n$ is the i-th unit coordinate basis vector for $\mathbb{R}^n$. It can also be verified that

$$L(\mathcal{G}) \;=\; \sum_{i=1}^{n}\sum_{j=1}^{n} e_i e_i^T L(\mathcal{G}) e_j e_j^T.$$

Using these results, the expression for the observability gramian can be further simplified to

$$\mathbf{Y}_o = \sum_{i=1}^{n}\sum_{j=1}^{n}\int_0^{\infty} e_ie_i^T L(\mathcal{G})e_je_j^T \otimes \left(e^{A_i^Tt}\left(C_i^y\right)^T C_j^y e^{A_jt}\right) dt.$$

Each agent is assumed to be stable and minimal, so we have that $\Psi_i : \mathbb{R}^n \mapsto \mathcal{L}_2^m[0,\infty)$ and the adjoint $\Psi_i^* : \mathcal{L}_2^m[0,\infty) \mapsto \mathbb{R}^n$. We also note that the composition of Ψ_i^* with its adjoint, as in $\Psi_i^*\Psi_i$, is precisely equal to the observability gramian of agent i, Y_o^i. More generally, $Y_{ij} = \Psi_i^*\Psi_j$ can be calculated by solving the Sylvester equation

$$A_i^T Y_{ij} + Y_{ij}A_j + \left(C_i^y\right)^T C_j^y = 0. \tag{5.6}$$

Theorem 5.1.2. *The heterogeneous NDS coupled at the output in (5.1) is unobservable if and only if the following conditions are met:*

1. *there exists an eigenvalue, μ^*, of $\mathbf{A}$ that is common to each A_i, and*

2. *one has $C_i^y q_i = C_j^y q_j$ for all i, j with $A_iq_i = \mu^* q_i$ for all i.*

Proof. For the necessary condition, recall that a linear system with state matrix A and observation matrix C is unobservable if and only if there exists a non-zero vector q such that $Aq = \lambda q$ and $Cq = 0$ (known as the PHB test [42]). For the system in (5.1), the PHB test can be used to conclude that unobservability implies that conditions 1 and 2 must be satisfied. For sufficiency, assume that there exists μ^* that is an eigenvalue for each A_i. We can then construct an eigenvector for $\mathbf{A}$ as $q = \left[\begin{array}{ccc} q_1^T & \cdots & q_n^T \end{array}\right]^T$, with $A_iq_i = \mu^* q_i$. By condition 2, we have that $\mathbf{C}q = \mathbb{1} \otimes r$, where $r = C_iq_i \neq 0$ for all i. Using properties of the Kronecker product we then have

$$(E(\mathcal{G})^T \otimes I)\mathbf{C}^y q = (E(\mathcal{G})^T \otimes I)(\mathbb{1} \otimes r) = (E(\mathcal{G})^T\mathbb{1} \otimes r) = 0. \tag{5.7}$$

This shows the system is unobservable with q the corresponding unobservable mode. □

Theorem 5.1.2 shows that a heterogeneous NDS becomes unobservable only when the outputs of each agent associated with a certain initial condition direction becomes indistinguishable. For general heterogeneous NDS- therefore- the system is 'expected' to be observable. This is a rather non-trivial result, as it suggests that the inertial position of each agent can be reconstructed solely from relative measurements.

As in the homogeneous case, the underlying connection topology can have a profound affect on the relative degree of observability of the system. The form of (5.5) is appealing in how it separates the role of the network from each agent, although a precise characterization of the eigenvalues of (5.5) is non-trivial. Using the results of Theorem 2.4.2, bounds on those values can obtained.

Corollary 5.1.3. *The smallest and largest eigenvalues of the observability gramian (5.5) are bounded as*

$$\underline{d}\,\underline{\sigma}(\mathbf{\Upsilon}^*\mathbf{\Upsilon}) \leq \underline{\sigma}(\mathbf{Y}_o) \leq \overline{\sigma}(\mathbf{Y}_o) \leq \overline{d}\,\overline{\sigma}(\mathbf{\Upsilon}^*\mathbf{\Upsilon}), \tag{5.8}$$

where $\underline{\sigma}(\mathbf{Y}_o)$ and $\overline{\sigma}(\mathbf{Y}_o)$ correspond, respectively, to the smallest and largest singular values of $\mathbf{Y}_o$, and

$$\underline{d} = \min_i\,[L(\mathcal{G}) \otimes J_n]_{ii}, \quad \overline{d} = \max_i\,[L(\mathcal{G}) \otimes J_n]_{ii};$$

the quantities $\underline{d}$ and $\overline{d}$ correspond, respectively, to the minimum and maximum degree vertices of the underlying graph.

We note that the bounds (5.8) become tight when the agents have homogeneous dynamics. Such observations point to interesting connections between the degree of each agent in the ensemble and the relative observability of the modes of the system. This theme will be revisited when we study the $\mathcal{H}_2$ performance of heterogeneous NDS coupled at the output.

The gramian expression (5.5) can alternatively be represented as a *node weighted* Laplacian. Consider scalar weights q_i on each node collected together into a vector q and the diagonal matrix $Q = \mathbf{diag}\{q_1, \ldots, q_n\}$. The *node weighted* Laplacian can be defined as

$$\hat{L}(\mathcal{G}) \;=\; QL(\mathcal{G})Q \;=\; L(\mathcal{G}) \circ qq^T. \tag{5.9}$$

This can be generalized to $n \times n$-block matrix weights, Q_i, and (5.9) can be equivalently written as

$$L_n(\mathcal{G}) = \mathbf{Q}(L(\mathcal{G}) \otimes I)\mathbf{Q}^T, \tag{5.10}$$

where $\mathbf{Q} = \mathbf{diag}\{Q_1, \ldots, Q_n\}$.

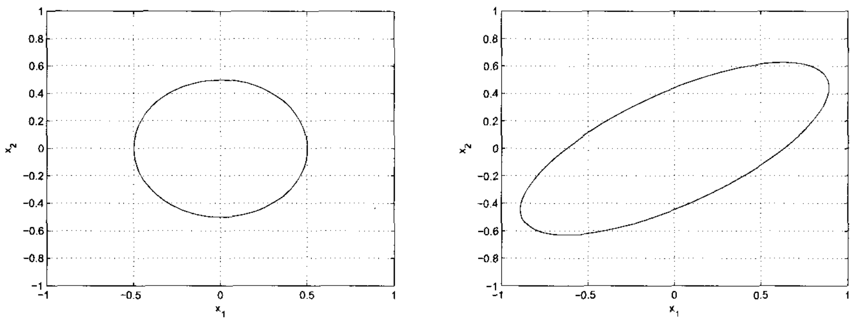

(a) Symmetric Ellipsoid

(b) Stretched Ellipsoid

Figure 5.1: Visualization of observability gramian ellipsoids for a "symmetric" system and "stretched" system.

Using (5.10) leads to a new interpretation of the expression in (5.5). Each node in the graph is weighted by the observability operator of the agent assigned to that node.

$$\mathbf{Y}_o = \mathbf{diag}\{\Upsilon^*\}(L(\mathcal{G}) \otimes I)\mathbf{diag}\{\Upsilon\}. \tag{5.11}$$

Index of Homogeneity and Heterogeneity

The previous section only provides a "yes" or "no" answer to the question of observability in a NDS coupled at the output. As discussed in §2.1, the singular values of the observability gramian can be used to give a quantitative comparison of the relative observability between different modes of the system. In the context of a single agent, the symmetry of the observability ellipsoid could be considered as a description of the homogeneity of that agents' initial condition to output map. As an example, the ellipsoid in Figure 5.1(a) is symmetric, which corresponds to the output energy being independent of the direction of the initial condition of the system. On the other hand, the ellipsoid in Figure 5.1(b) shows the output energy is strongly dependent on the direction of the initial condition. The shape of the ellipsoid, of course, corresponds to the relative magnitude of the singular values of the observability gramian.

This notion can be extended for NDS coupled at the output to answer the following questions:

1. How does the structure of the underlying network topology affect the relative observability of the NDS?

2. How does the placement of agents in the network affect the relative observability of the NDS?

More fundamentally, these questions suggest that certain topologies in a homogeneous system might be "more homogeneous" then others. Similarly, placing heterogeneous agents in different locations in the connection graph might also result in a "more heterogeneous" NDS. This would correspond to a symmetry, or lack thereof, of the observability ellipsoid of the NDS.

This section aims to develop an *index of homogeneity* for the homogeneous case, and an *index of heterogeneity* for the heterogeneous case that can be used to answer these questions. It is natural that these measures should relate to the observability gramian of the NDS.

In the homogeneous case, as indicated by (5.3), we recognize that the network topology has a direct affect on the observability gramian. Furthermore, the statement of Theorem 2.4.1 shows that the eigenvalues of $\mathbf{Y_o}$ are the eigenvalues of Y_o scaled by the eigenvalues of the graph Laplacian, $L(\mathcal{G})$. The index of homogeneity should capture the affect of the network on the overall observability properties. Using the symmetry analogy developed earlier, a more homogeneous NDS should correspond to a more symmetric observability gramian.

This leads us to the following definition for the index of homogeneity, denoted as $\rho(\Sigma_{hom}(\mathcal{G}))$.

Proposition 5.1.1. *Let*

$$\rho(\Sigma_{hom}(\mathcal{G})) = \left(\frac{\lambda_2(\mathcal{G})}{\lambda_n(\mathcal{G})}\right)\frac{\underline{\sigma}(Y_o)}{\overline{\sigma}(Y_o)}. \tag{5.12}$$

Using this index for characterizing the relative observability properties of the homogeneous NDS leads to some interesting observations. First, note that whenever the graph is disconnected, $\rho(\Sigma_{hom}(\mathcal{G})) = 0$. This corresponds to the intuitive result that a disconnected

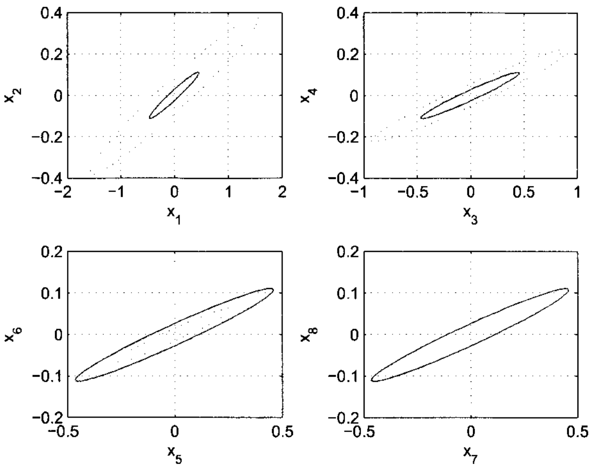

Figure 5.2: Visualization of observability gramian ellipsoids for an NDS.

graph should somehow be "less homogeneous" than a connected one. In terms of this specific index, the homogeneity of the NDS is lower bounded by 0, and is indistinguishable from any disconnected graph on n nodes.

This index is also upper-bounded by $\underline{\sigma}(Y_o)/\overline{\sigma}(Y_o)$. This upper-bound is achieved whenever the underlying graph is complete. The complete graph is the only graph where $\lambda_2(\mathcal{G}) = \lambda_n(\mathcal{G})$. We also note the set of graphs that are cospectral with respect to the graph Laplacian will all result in the same index of homogeneity. This property could prove to be useful if reconfiguration of the connection topology is required.

The motivation for choosing such a function has a more intuitive explanation relating to the symmetry arguments of the observability gramian. The term containing the ratio of the smallest and largest singular values of Y_o corresponds loosely to a measure of the eccentricity of the gramian ellipsoid. The closer this ratio is to the value 1, the more symmetric the ellipsoid is. Conversely, as this ratio approaches 0, the ellipsoid becomes more elongated (along one plane). As we have assumed a minimal realization for the system dynamics, we are guaranteed that this ratio will always be strictly positive.

In this direction, consider the observability gramian of the parallel interconnection of n homogeneous agents, as in (4.4). The gramian can be written as $\tilde{Y}_o = I_n \otimes Y_o$. In the n agent case, the ellipsoid of agent i is oriented orthogonally to the ellipsoid of agent j.

As an example, consider the gramian for a 4-agent homogeneous system, each with 2 states. The gramian for each agent is the same, and its 2-d projection is plotted for each pair of state variables in Figure 5.2. When the system is coupled by a network, say a path graph, the ellipsoid becomes scaled and rotated. This is visualized by the dotted lines in Figure 5.2. We immediately notice that one ellipsoid is scaled by the 0 eigenvalue of graph Laplacian. Using Theorem 2.4.1, we see that $\underline{\sigma}(\mathbf{Y}_o) = \lambda_2(\mathcal{G})\,\underline{\sigma}(Y_o)$ and $\overline{\sigma}(\mathbf{Y}_o) = \lambda_n(\mathcal{G})\,\overline{\sigma}(Y_o)$ are respectively, the minimum and maximum non-zero singular values of $\mathbf{Y}_o$. We thus have the following relationship:

$$0 < \lambda_2(\mathcal{G})\,\underline{\sigma}(Y_o) \leq \lambda_n(\mathcal{G})\,\overline{\sigma}(Y_o). \tag{5.13}$$

In the homogeneous case, Y_o represents a fixed property of the system, determined by the agent dynamics. Thus, in terms of the symmetry argument, a more homogeneous NDS should preserve as closely as possible the shape of the gramian. Scaling the eigenvalues of $\mathbf{Y}_o$ by $\lambda_n(\mathcal{G})\overline{\sigma}(Y_o)$ is effectively normalizing the observability gramian singular values to 1.

In the heterogeneous case, we wish not only to characterize how the topology affects the observability properties, but also how the placement of agents within that topology affects the observability of the NDS as well. Contrary to the homogeneous case, the interplay between the graph Laplacian eigenvalues and the eigenvalues of the NDS gramian is less straightforward. A nice property of the index of homogeneity is that it can be computed by studying- independently- the spectral properties of the graph and the observability properties of the homogeneous agents. Finding an analogous approach for the index of heterogeneity reduces to understanding the spectral properties of (5.5) or (5.11).

An index of heterogeneity can be developed using the numerical evaluation of the gramian. The index of heterogeneity will be denoted as $\rho(\Sigma_{het}(\mathcal{G}))$. One choice for this index is

$$\rho(\Sigma_{het}(\mathcal{G})) = \left(\min_{\sigma_i(\mathbf{Y}_o)\neq 0} \sigma_i(\mathbf{Y}_o)\right)^{-1} \overline{\sigma}(\mathbf{Y}_o), \tag{5.14}$$

where $\mathbf{Y}_o$ is given in (5.11).

Although not as transparent as the index of homogeneity, some useful observations can be made about this choice of index. It can be seen that the index is upper-bounded by 1,

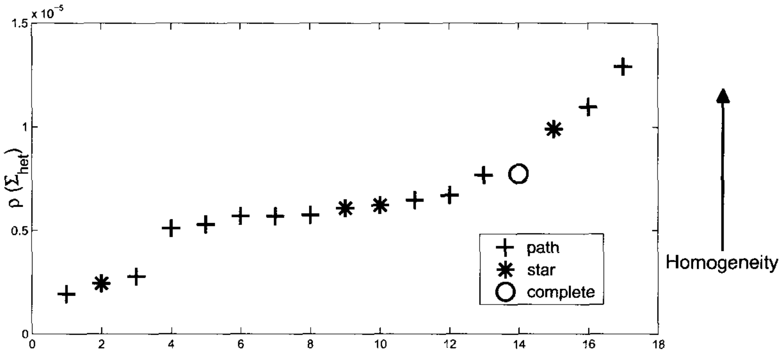

Figure 5.3: Index of Heterogeneity

which corresponds to an upper-bound on the homogeneity of the NDS. It is interesting to note that this upper-bound can be achieved by a homogeneous NDS with a complete graph topology, and with the agent gramian ellipsoid being completely symmetric.

In fact, if all the agents in the NDS are homogeneous, then the index of heterogeneity reduces to (5.12). It might be natural to assume that the observed properties of (5.12) also apply to the heterogeneous case. Unfortunately, this is not the case, and is best illustrated with a simple example.

We consider a heterogeneous NDS with 4 agents and three different topologies; the star graph S_4, the path graph P_4, and the complete graph K_4. Note that there are only four unique node assignments for the star graph, twelve unique assignments for the path graph, and one for the complete graph. For each permutation of the agent's position, the index of heterogeneity was calculated and plotted in Figure 5.3. As indicated in the above discussion, larger values of $\rho\left(\Sigma_{het}(\mathcal{G})\right)$ correspond to the NDS being "more homogeneous". The important point to notice in the figure is that the topology alone is not sufficient to determine which systems are more homogeneous. Furthermore, it can be seen that the complete graph does not correspond to the most homogeneous system.

5.1.2 Controllability of NDS Coupled at the Input

In this section, we consider whether *from any initial condition, each agent can be driven to an arbitrary final state when the input is distributed to each agent through a network.*

Homogeneous Case

For homogeneous NDS, the controllability gramian can be written by inspection as

$$\mathbf{X}_c = L(\mathcal{G}) \otimes \int_0^{\infty} e^{At}BB^Te^{A^Tt}dt = L(\mathcal{G}) \otimes X_c, \tag{5.15}$$

where X_c is the controllability gramian for an individual agent in the NDS.

Theorem 5.1.4. *The homogeneous NDS coupled at the input (5.2) is uncontrollable.*

Proof. The gramian (5.15) has precisely n eigenvalues at the origin, leading to an uncontrollable system. □

Here, the dual nature of the NDS coupled at the output and input becomes immediately apparent. As in the former case, the uncontrollable mode corresponds to the inertial position of the entire ensemble, lying in the subspace $\mathbf{span}\{\mathbb{1} \otimes I\}$. We also note that the relative degree of controllability can be inferred from the gramian, but this analysis is omitted as it mirrors that of the observability analysis for NDS coupled at the output.

Heterogeneous Case

For the heterogeneous case, we arrive at the following result.

Theorem 5.1.5. *The heterogeneous NDS coupled at the input (5.2) is uncontrollable if and only if the following conditions are met:*

1. *there exists an eigenvalue, μ^*, of $\mathbf{A}$ that is common to each A_i, and*

2. *one has $q_i^TB_i = q_j^TB_j$ for all i, j with $q_i^TA_i = \mu^*q_i^T$ for all i.*

The proof of Theorem 5.1.5 follows the same procedure as for Theorem 5.1.4, and is omitted. The conclusion, as expected, shows that heterogeneity in the dynamics of each agent can lead to a fully controllable system.

The dual structure between the NDS coupled at the input and coupled at the output should now be clear. A simple exercise will show that the controllability gramian for (5.2) has a similar form to the observability gramian (5.5), with the role of Ψ^* replaced with the controllability operator. It becomes apparent that the degree of each agent in the ensemble can have a profound affect on the overall controllability properties of the system.

5.2 *Graph-Theoretic Bounds on NDS Performance*

In this section we explore a graph-theoretic characterization of the $\mathcal{H}_2$ and $\mathcal{H}_\infty$ performance of the different NDS models [83, 84, 85, 86]. The main goal is to again make explicit the role of the underlying connection topology on the system performance norms. We will assume throughout this section that the underlying connection graph $\mathcal{G}$ is connected. For analysis, we also assume each agent is stable.

5.2.1 *Performance of NDS Coupled at the Output*

For NDS coupled at the output, it is important to consider how disturbances entering the dynamics of each agent propagates through the network to the sensed output. In this analysis, we assume that each agent is driven by an external disturbance.A simplified version of the agent dynamics is given as

$$\Sigma_i : \left\{ \begin{array}{rcll} \dot{x}_i(t) & = & A_i x_i(t) & + \; \Gamma_i w_i(t) \\ y_i(t) & = & C_i^y x_i(t). & \end{array} \right. \tag{5.16}$$

The corresponding model for the NDS coupled at the output takes the form

$$\Sigma_{het}(\mathcal{G}) : \left\{ \begin{array}{rcll} \dot{\mathbf{x}}(t) & = & \mathbf{A}\mathbf{x}(t) & + \; \mathbf{\Gamma}\mathbf{w}(t) \\ \mathbf{y}(t) & = & \mathbf{C}^y\mathbf{x}(t) & \\ \mathbf{y}_{\mathcal{G}}(t) & = & (E(\mathcal{G})^T \otimes I)\mathbf{C}^y\mathbf{x}(t). & \end{array} \right. \tag{5.17}$$

$\mathcal{H}_2$ *Performance*

The sensed output of an NDS coupled at the output can be used to achieve a variety of objectives, including localization- for which the observability results of §5.1 apply- and formation control. It is important, therefore, to examine how noise entering the dynamics of each agent in the NDS propagates through the network to the sensed output. A natural measure for quantifying this property is the $\mathcal{H}_2$ system norm. This section, therefore, aims to explicitly characterize the affect of the network on the $\mathcal{H}_2$ performance of the system. For this analysis we assume the external disturbances to be a white Gaussian noise.

Theorem 5.2.1. *The $\mathcal{H}_2$ norm of the homogeneous NDS coupled at the output (5.17) is given by*

$$\left\| T_{hom}^{w \mapsto \mathcal{G}} \right\|_2 = \|E(\mathcal{G})\|_F \|\Sigma\|_2. \tag{5.18}$$

Proof. The $\mathcal{H}_2$ norm can be written directly from (5.3) as

$$\left\| T_{hom}^{w \mapsto \mathcal{G}} \right\|_2 = \sqrt{\mathbf{trace}((I_n \otimes \Gamma)^T (L(\mathcal{G}) \otimes Y_o)(I_n \otimes \Gamma))}.$$

Using the properties of the Kronecker product defined in §2 and the definition of the Frobenius norm (2.3), leads to the expression in (5.18). □

The expression in (5.18) gives an explicit characterization of how the network affects the system performance. For homogeneous systems, we find that the $\mathcal{H}_2$ performance changes with the addition or removal of an edge. Recall that the Frobenius norm of a matrix can be expressed in terms of the 2-norm of each column, as

$$\|M\|_F = \left(\sum_{i=1}^{n} \|m_i\|^2 \right)^{1/2},$$

where m_i is the ith column of the matrix M. As each column of $E(\mathcal{G})$ represents an edge in $\mathcal{G}$, the Frobenius norm can be expressed in terms of the number of edges in the graph, $|\mathcal{E}|$, as

$$\|E(\mathcal{G})\|_F = (2|\mathcal{E}|)^{1/2}. \tag{5.19}$$

This highlights the importance of *the number of edges* as opposed to the actual structure of the graph (e.g., a star graph or k-regular graph). This makes intuitive sense, as more edges would correspond to additional amplification of the disturbances entering the system.

If we consider only connected graphs, we arrive at the following corollaries providing lower and upper bounds on the $\mathcal{H}_2$ norm of the system.

Corollary 5.2.2. *The $\mathcal{H}_2$ norm of the homogeneous NDS coupled at the output (5.17) for an arbitrary connected graph $\mathcal{G}$ is lower bounded by an NDS where $\mathcal{G}$ is a spanning tree, as*

$$\left\| T_{hom}^{w \mapsto \mathcal{G}} \right\|_2^2 \geq 2 \|\Sigma\|_2^2 \, (n-1); \tag{5.20}$$

the lower bound is attained with equality whenever the underlying graph is a spanning tree.

It is clear from the definition of the Frobenius norm that the choice of tree is irrelevant (e.g., a star or a path).

Corollary 5.2.3. *The $\mathcal{H}_2$ norm of the homogeneous NDS coupled at the output (5.17) for an arbitrary connected graph $\mathcal{G}$ is upper bounded by an NDS where $\mathcal{G} = K_n$, the complete graph, as*

$$\left\| T_{hom}^{w \mapsto \mathcal{G}} \right\|_2^2 \leq 2 \left\| \Sigma \right\|_2^2 n \; (n-1); \tag{5.21}$$

the upper bound is attained with equality whenever the underlying graph is complete.

For the heterogeneous case we rely on (2.18) to derive the $\mathcal{H}_2$ norm. The connection topology only couples agents at the output leading to a block diagonal description for the controllability gramian, with each block corresponding to each agent's controllability gramian.

Theorem 5.2.4. *The $\mathcal{H}_2$ norm of the heterogeneous NDS coupled at the output (5.17) is given as*

$$\left\| T_{het}^{w \mapsto \mathcal{G}} \right\|_2 = \left(\sum_i d_i \left\| \Sigma_i \right\|_2^2 \right)^{1/2}, \tag{5.22}$$

where d_i is the degree of the i-th agent in the graph.

Proof. The norm expression in (5.22) can be derived using (2.18) as,

$$\left\| T_{het}^{w \mapsto \mathcal{G}} \right\|_2 = \left(\mathbf{trace}\left\{ (E(\mathcal{G})^T \otimes I) \mathbf{C}^y \mathbf{X}_c (\mathbf{C}^y)^T (E(\mathcal{G}) \otimes I) \right\} \right)^{1/2}, \tag{5.23}$$

where $\mathbf{X}_c$ denotes the block diagonal aggregation of each agent's controllability gramian. First, we make the following observation,

$$\mathbf{trace}\left\{ \mathbf{C}^y \mathbf{X}_c (\mathbf{C}^y)^T \right\} = \sum_{i=1}^{n} \left\| \Sigma_i \right\|_2^2.$$

Using the cyclic property of the trace operator [89] and exploiting the block diagonal structure of the argument leads to the following identity simplification,

$$\begin{aligned} \mathbf{trace}\left\{ \mathbf{C}^y \mathbf{X}_c (\mathbf{C}^y)^T ((\Delta(\mathcal{G}) - A(\mathcal{G})) \otimes I) \right\} &= \sum_i \mathbf{trace}\left\{ C_i^y X_c^i (C_i^y)^T (d_i \otimes I) \right\} \\ &= \sum_i d_i \left\| \Sigma_i \right\|_2^2 . \end{aligned} \tag{5.24}$$

This leads to the desired result. □

A further examination of (5.22) reveals that it can be written as the Frobenius norm of a node-weighted incidence matrix,

$$\left\| T_{het}^{w \mapsto \mathcal{G}} \right\|_2 = \| QE(\mathcal{G}) \|_F , \tag{5.25}$$

where $Q = \mathbf{diag}\{\|\Sigma_1\|_2, \ldots, \|\Sigma_n\|_2\}$.

When each agent has the same dynamics, (5.25) reduces to the expression in (5.18). This characterization paints a clear picture of how the placement of an agent within a certain topology affects the overall system gain. In order to minimize the gain, it is beneficial to keep systems with high norm in locations with minimum degree.

For certain graph structures, a more explicit characterization of the $\mathcal{H}_2$ performance can be derived, leading to the following corollaries.

Corollary 5.2.5. *The $\mathcal{H}_2$ norm of the heterogeneous NDS coupled at the output (5.17) when the underlying connection graph is k-regular is*

$$\left\| T_{het}^{w \mapsto \mathcal{G}} \right\|_2 = \left(k \sum_i \|\Sigma_i\|_2^2 \right)^{1/2} , \tag{5.26}$$

where every node has degree k.

Note that having regularity in the connection topology introduces homogeneity into the heterogeneous NDS. As in the homogeneous case, the placement of an agent in the network will not affect the overall performance. The system norm for this topology becomes a scaled version of the parallel connection of the n sub-systems.

$\mathcal{H}_\infty$ Performance

Given the transfer function representation of the homogenous NDS in (4.8), we can write the map from the disturbances to the networked output as

$$\mathbf{Y}_{\mathcal{G}}(s) = \left(E(\mathcal{G})^T \otimes H^{yw} \right) \mathbf{U}(s). \tag{5.27}$$

Theorem 5.2.6. *The $\mathcal{H}_\infty$ norm of the homogeneous RSN (4.13) is given as*

$$\left\| T_{hom}^{w \mapsto \mathcal{G}} \right\|_\infty = \|E(\mathcal{G})\| \|H^{yw}\|_\infty . \tag{5.28}$$

Proof. The norm expression follows directly from the definition in (2.20) and (2.36). □

The expression in (5.28) gives an explicit characterization of how the network affects the overall $\mathcal{L}_2$ gain of the system. In fact, we see that it is proportional to the matrix 2-norm of the incidence matrix. Examining the singular values of $E(\mathcal{G})$, therefore, can lead to an understanding of how the topology affects the system norm. First, we note that $\|E(\mathcal{G})\| = \sqrt{\|L(\mathcal{G})\|} = \lambda_n^{1/2}$. Therefore, we can examine the largest eigenvalue of the graph Laplacian.

An important observation is that certain graph structures will naturally lead to a smaller $\mathcal{H}_\infty$ norm. If we restrict our topology to spanning trees we can state stronger results.

Corollary 5.2.7. *When the underlying topology is a spanning tree, the path graph is the topology resulting in the smallest $\mathcal{H}_\infty$ norm for (4.13).*

Proof. In [62] it was shown that the path graph has the smallest spectral norm for the graph Laplacian among all spanning trees. □

Corollary 5.2.8. *When the underlying topology is a spanning tree, the star graph is the topology resulting in the largest $\mathcal{H}_\infty$ norm for (4.13).*

Proof. In [34] it was shown that the star graph has the largest spectral norm for the graph Laplacian among all spanning trees. □

Contrary to the results of §5.2.1, we find that the structure of the graph plays a significant role in the system performance. Recall that the $\mathcal{H}_2$ norm for homogeneous RSN reduced to a property related to the number of edges in the graph. In the $\mathcal{H}_\infty$ case, the spectral norm of the graph Laplacian becomes the central quantity.

We follow a similar procedure for the heterogeneous case. Using the transfer function representation of the heterogeneous RSN in (4.9) we can write the map from the disturbances to the networked output as

$$\mathbf{Y}_{\mathcal{G}}(s) = \left(E(\mathcal{G})^T \otimes I\right) \mathbf{H}^{yw}(s)\mathbf{U}(s). \tag{5.29}$$

Calculating the $\mathcal{H}_\infty$ norm involves finding the singular values of the transfer function

$$T_{het}^{w \mapsto \mathcal{G}} = \left(E(\mathcal{G})^T \otimes I\right) \mathbf{H}^{yw}(s). \tag{5.30}$$

In general, an analytic expression for the singular values of the system in (5.30) is difficult to obtain. However, it is possible to generate bounds on the system-norm, leading to the following result.

Theorem 5.2.9. *The $\mathcal{H}_\infty$ norm of the homogeneous RSN (4.14) is bounded as*

$$\|T_{het}^{w\mapsto\mathcal{G}}\|_\infty \;\leq\; \|E(\mathcal{G})^TQ\| \;\leq\; \left\|E(\mathcal{G})^T\right\| \max_i \|H_i^{yw}\|_\infty, \tag{5.31}$$

where $Q = \mathbf{diag}\{\|H_1^{yw}\|_\infty, \dots, \|H_n^{yw}\|_\infty\}$.

Proof. The upper-bound immediately arises from the sub-multiplicative property of the matrix 2-norm as $\|E(\mathcal{G})^TQ\| \leq \|E(\mathcal{G})^T\|\|Q\|$. Since Q is a diagonal matrix we conclude that $\|Q\| = \max_i \|H_i^{yw}\|_\infty$. To show the lower-bound we follow the following chain of inequalities as

$$\begin{aligned}
\|T_{het}^{w\mapsto\mathcal{G}}\|_\infty^2 &= \sup_{\|U(j\omega)\|_{\mathcal{L}_2}=1} \left\|(E(\mathcal{G})^T \otimes I)\mathbf{H}^{yw}(j\omega)U(j\omega)\right\|_{\mathcal{L}_2}^2 \\
&= \sup_{\|U(j\omega)\|_{\mathcal{L}_2}=1} \left\langle U(j\omega), (E(\mathcal{G})^T \otimes I)\mathbf{H}^{yw}(j\omega)\mathbf{H}^{yw}(j\omega)^*(E(\mathcal{G}) \otimes I)U(j\omega)\right\rangle \\
&\leq \sup_{\|U(j\omega)\|_{\mathcal{L}_2}=1} \left\langle U(j\omega), (E(\mathcal{G})^TQ^2E(\mathcal{G}) \otimes I)U(j\omega)\right\rangle = \|QE(\mathcal{G})\|,
\end{aligned} \tag{5.32}$$

where the last inequality follows from the property that the positive-definite ordering $\mathbf{H}^{yw}(j\omega)\mathbf{H}^{yw}(j\omega)^* \leq Q^2 \otimes I$ holds for all ω.[1] □

Corollary 5.2.10. *When each agent in (4.14) is a single-input single-output (SISO) system, the norm bound in (5.31) is tight.*

An interesting implication of the norm bounds developed in the proof relates the $\mathcal{L}_2$ gain of a heterogeneous RSN to that of a homogeneous RSN. Consider an ordering of each agent in a heterogeneous RSN by the value of the $\mathcal{H}_\infty$ norm of each agent,

$$\|H_{k(1)}^{yw}\|_\infty \leq \cdots \leq \|H_{k(n)}^{yw}\|_\infty, \tag{5.33}$$

[1] We also invoke the property that for a linear operator Σ with state-space realization $(0,0,0,D)$, $\|\Sigma\|_\infty = \|D\|$.

where $k : \{1, \ldots, n\} \mapsto \{1, \ldots, n\}$ maps the old index to the norm-ordered index. The $\mathcal{H}_\infty$ norm of the heterogeneous system $T_{het}^{w \mapsto \mathcal{G}}$ can be bounded from above and below by homogeneous systems as

$$\|E(\mathcal{G})\| \|H_{k(1)}^{yw}\|_\infty \leq \|T_{het}^{w \mapsto \mathcal{G}}\|_\infty \leq \|E(\mathcal{G})\| \|H_{k(n)}^{yw}\|_\infty.$$

This inequality suggests that in addition to the structure of the underlying topology, one can consider the dynamic difference between agents as an important factor in the performance of the system.

5.2.2 *Performance of NDS Coupled at the State*

In this section we consider the performance of the edge agreement protocol derived in §4.4.1. Examining the $\mathcal{H}_2$ and $\mathcal{H}_\infty$ performance of the edge agreement can be employed to reason how disturbances entering the edges of the network result in asymptotic deviation of each node's state from the consensus state.

$\mathcal{H}_2$ Performance

For this analysis we consider the models (4.22) and (4.23). The $\mathcal{H}_2$ norm of Σ_τ and $\tilde{\Sigma}_\tau$ can be calculated using the controllability gramian as,

$$\|\Sigma_\tau\|_2^2 = \mathbf{trace}[R^T X^* R], \quad \text{and} \quad \|\tilde{\Sigma}_\tau\|_2^2 = \mathbf{trace}[X^*], \tag{5.34}$$

where R is defined in (2.26) and X^* is the positive-definite solution to the Lyapunov equation

$$-L_e(\mathcal{G}_\tau)RR^T X - XRR^T L_e(\mathcal{G}_\tau) + \sigma_w^2 L_e(\mathcal{G}_\tau) + \sigma_v^2 L_e(\mathcal{G}_\tau)RR^T L_e(\mathcal{G}_\tau) = 0. \tag{5.35}$$

The structure of (5.35) suggests that the solution will be dependent on certain properties of the graph. In fact, the solution can found by inspection by first noting that

$$\sigma_w^2 L_e(\mathcal{G}_\tau) + \sigma_v^2 L_e(\mathcal{G}_\tau)RR^T L_e(\mathcal{G}_\tau) = L_e(\mathcal{G}_\tau)\left(\sigma_w^2 (L_e(\mathcal{G}_\tau))^{-1} + \sigma_v^2 RR^T\right) L_e(\mathcal{G}_\tau).$$

The solution to (5.35) is therefore

$$X^* = \frac{1}{2}\left(\sigma_w^2 (RR^T)^{-1} + \sigma_v^2 L_e(\mathcal{G}_\tau)\right), \tag{5.36}$$

and we arrive at the following result.

Theorem 5.2.11. *The $\mathcal{H}_2$ norm of the system Σ_τ (4.22) is*

$$\|\Sigma_\tau\|_2^2 \;=\; \frac{\sigma_w^2}{2}(n-1)+\sigma_v^2|\mathcal{E}|. \tag{5.37}$$

On the other hand, the $\mathcal{H}_2$ norm of the $\hat{\Sigma}_\tau$ system (4.23) is

$$\|\hat{\Sigma}_\tau\|_2^2 \;=\; \frac{\sigma_w^2}{2}\,\mathbf{trace}[(RR^T)^{-1}]+\sigma_v^2(n-1). \tag{5.38}$$

Proof. The proof follows from (5.36) and noting that $\mathbf{trace}[L_e(\mathcal{G}_\tau)] = 2(n-1)$, or twice the number of edges in a spanning tree. □

We observe that $\|\Sigma_\tau\|_2^2$ is a linear function of the number of edges in the graph. This has a clear practical relevance, as it indicates that the addition of each edge corresponds to an amplification of the noise in the consensus-type network. Let us consider the implications of the graph-theoretic characterization of the $\mathcal{H}_2$ norm for two classes of graphs.

(a) **Spanning Trees:** The first case resulting in a simplification of (5.37) arises when $\mathcal{G}$ is a spanning tree. In this case $R = I$ and (5.38) simplifies to

$$\|\hat{\Sigma}_\tau\|_2^2 \;=\; (n-1)\left(\frac{\sigma_w^2}{2}+\sigma_v^2\right). \tag{5.39}$$

A direct consequence of this result is that *all* spanning trees result in the same $\mathcal{H}_2$ system performance. That is, the choice of spanning tree (e.g., a path or a star) does not affect this performance metric. As expected, in this scenario $\|\Sigma_\tau\|_2^2 = \|\hat{\Sigma}_\tau\|_2^2$.

(b) *k*-**Regular Graphs:** Regular graphs also lead to a simplification of (5.38). In general, any connected k-regular graph will contain cycles resulting in a non-trivial expression for matrix product RR^T. The $\mathcal{H}_2$ norm is therefore intimately related to the cut space of the graph.

Denote the eigenvalues of RR^T by μ_i and note that

$$\mathbf{trace}\left[(RR^T)^{-1}\right] \;=\; \sum_{i=1}^{n-1}\frac{1}{\mu_i}=\frac{1}{\tau(\mathcal{G})}\sum_{i=1}^{n-1}\prod_{j\neq i}^{n-1}\mu_j, \tag{5.40}$$

where $\tau(\mathcal{G})$ is the number of spanning trees in $\mathcal{G}$, defined in (2.27). The quantity $\prod_{j \neq i}^{n-1} \mu_j$ is recognized as a first minor of the matrix RR^T.

Corollary 5.2.12. *The cycle graph C_n has n spanning trees and hence*

$$\textbf{trace}\left[(R(C_n)R(C_n)^T)^{-1}\right] = \frac{(n-1)^2}{n}. \tag{5.41}$$

Thereby, the $\mathcal{H}_2$ norm of the $\tilde{\Sigma}_\tau$ system when the underlying graph is the cycle graph C_n is given as

$$\|\tilde{\Sigma}_\tau\|_2^2 = (n-1)\left(\frac{\sigma_w^2(n-1)}{n} + \sigma_v^2\right). \tag{5.42}$$

Proof. From Proposition 3.2.1 it is straightforward to verify (5.41). Combined with (5.37) yields the desired result. □

Corollary 5.2.13. *The complete graph K_n has n^{n-2} spanning trees, and therefore*

$$\textbf{trace}\left[\left(R(K_n)R(K_n)^T\right)^{-1}\right] = \frac{2(n-1)n^{n-3}}{n^{n-2}} = \frac{2(n-1)}{n}. \tag{5.43}$$

Thereby, the $\mathcal{H}_2$ norm of the $\tilde{\Sigma}_\tau$ system when the underlying graph is the complete graph K_n is given as

$$\|\tilde{\Sigma}_\tau\|_2^2 = (n-1)\left(\frac{\sigma_w^2}{n} + \sigma_v^2\right). \tag{5.44}$$

Proof. From Proposition 3.2.2 it is straightforward to verify (5.43). Combined with (5.37) yields the desired result. □

Figure 5.4 depicts the sorted values of $\textbf{trace}\left[(RR^T)^{-1}\right]$ for 500 randomly generated regular graphs of degree five. As this figure shows, although the degree of each node remains constant, the actual cycle structure of each graph instance varies, effecting the resulting $\mathcal{H}_2$ norm of the corresponding consensus-type input-output system.

Using the above analysis, we now proceed to characterize how the cycle structure of the graph effects the $\mathcal{H}_2$ performance for the corresponding consensus-type system. In fact, examining the ratio

$$\frac{\|\Sigma_\tau(\mathcal{G})\|_2^2}{\|\Sigma_\tau(\mathcal{G}_\tau)\|_2^2}$$

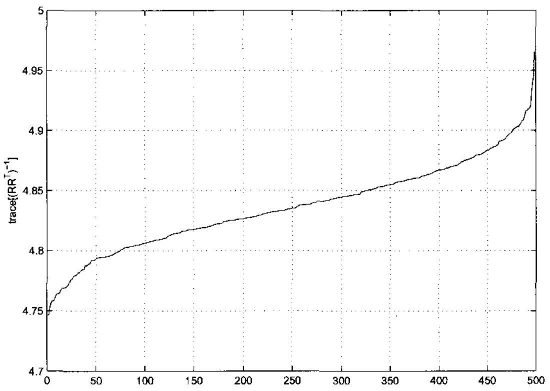

Figure 5.4: Plot of **trace**$[(R(\mathcal{G})R(\mathcal{G})^T)^{-1}]$ for random 5-regular graphs, sorted by increasing magnitude.

provides an indication of how the cycles increase the $\mathcal{H}_2$ norm; recall that $\mathcal{G}$ is in general a graph containing cycles and $\mathcal{G}_\tau \subseteq \mathcal{G}$ is the spanning tree subgraph.

For example, consider the cycle graph C_n and assume unit covariance for both the process and measurement noise. Then, as the number of nodes increase, the ratio of the two $\mathcal{H}_2$ norms behaves as

$$\lim_{n\to\infty} \frac{\|\Sigma_\tau(C_n)\|_2^2}{\|\Sigma_\tau(P_n)\|_2^2} = \lim_{n\to\infty} \frac{3n-1}{3(n-1)} = \frac{1}{3}, \tag{5.45}$$

indicating that for large cycles, the $\mathcal{H}_2$ performance is a constant fraction of the $\mathcal{H}_2$ performance for the path graph P_n.

In the meantime, for the complete graph K_n we have

$$\frac{\|\Sigma_\tau(K_n)\|_2^2}{\|\Sigma_\tau(\mathcal{G}_\tau)\|_2^2} = \frac{n+1}{3} = O(n); \tag{5.46}$$

in this case, we see that the norm is amplified linearly as a function of the number of vertices in the graph. It is worth mentioning here that typical performance measures for consensus problems, such as $\lambda_2(\mathcal{G})$, would favor the complete graph over the cycle graph. However, in terms of the $\mathcal{H}_2$ performance, we see that there is a penalty to be paid for faster convergence offered by the complete graph due to its cycle structure.

Alternatively, insight is also gained by considering the ratio

$$\frac{\|\Sigma_\tau(\mathcal{G})\|_2^2}{\|\tilde{\Sigma}_\tau(\mathcal{G})\|_2^2},$$

which highlights the effects of including cycles in the performance variable $z(t)$. For the cycle graph we have

$$\lim_{n\to\infty}\frac{\|\Sigma_\tau(C_n)\|_2^2}{\|\tilde{\Sigma}_\tau(C_n)\|_2^2} = \lim_{n\to\infty}\frac{n(3n-1)}{2(n-1)(2n-1)} = \frac{3}{4}, \tag{5.47}$$

suggesting that the effect of including the cycle for performance does not vary significantly with the size of the graph.

For the complete graph, on the other hand, one has

$$\frac{\|\Sigma_\tau(K_n)\|_2^2}{\|\tilde{\Sigma}_\tau(K_n)\|_2^2} = \frac{n}{2} = O(n), \tag{5.48}$$

suggesting that the inclusion of cycles results in $\mathcal{H}_2$ performance that increases linearly as a function of vertices in the graph.

$\mathcal{H}_\infty$ Performance

We first recall that the $\mathcal{H}_\infty$ norm for a dynamic system captures how a measurable signal with finite energy, i.e., a signal in $\mathcal{L}_2$, is amplified at the monitored output of the system. Moreover this norm, has implications for robustness, disturbance rejection, and uncertainty management for dynamic systems. In the context of the agreement protocol, therefore, *the $\mathcal{H}_\infty$ system norm can be used to capture how disturbances and finite energy exogenous signals, including reference signals, result in the asymptotic deviation of each node state from consensus.* In this section, in view of (4.22), we proceed to examine the $\mathcal{H}_\infty$-norm for the agreement protocol using an edge perspective.

To begin this analysis, we first write the transfer-function representation of (4.22) as

$$\Sigma_\tau(s) = R^T\left(sI + L_e(\mathcal{G}_\tau)RR^T\right)^{-1}\begin{bmatrix}\sigma_w E(\mathcal{G}_\tau)^T & -\sigma_v L_e(\mathcal{G}_\tau)R\end{bmatrix}. \tag{5.49}$$

The transfer-function representation for $\tilde{\Sigma}_\tau(s)$ is similarly defined from its state-space representation. Before we begin our analysis of the transfer-function matrix (5.49), let us provide a useful result on the ordering properties of the eigenvalues of congruent Hermitian matrices.

Theorem 5.2.14 ([36]). *Let A be a Hermitian matrix and S a nonsingular square matrix. Let the eigenvalues of A and SS^* be arranged in an increasing order. Then, for each $k = 1, \dots, n$, there exists a positive real number θ_k such that $\lambda_1(SS^*) \leq \theta_k \leq \lambda_n(SS^*)$ and*

$$\lambda_k(SAS^*) = \theta_k \lambda_k(A). \tag{5.50}$$

Recall now that the state matrix $-L_e(\mathcal{G}_\tau)RR^T$ in (4.22) arises from a similarity transformation with the graph Laplacian, as shown in Theorem 3.6. This allows us to infer that the eigenvalues of $L_e(\mathcal{G}_\tau)RR^T$ are all positive and real, and the state matrix is diagonalizable. Therefore, we can diagonalize the system using a modal decomposition with transformation matrix S to obtain

$$\left\{ \begin{array}{lcl} \dot{\hat{x}}_\tau(t) & = & -\Lambda(\mathcal{G})\hat{x}_\tau(t) \quad + \quad S^{-1}\left[\begin{array}{cc} \sigma_w E(\mathcal{G}_\tau)^T & -\sigma_v L_e(\mathcal{G}_\tau)R(\mathcal{G}) \end{array} \right] \left[\begin{array}{c} \hat{w}(t) \\ \hat{v}(t) \end{array} \right] \\ z(t) & = & R(\mathcal{G})^T S \hat{x}_\tau(t) \end{array} \right. , \tag{5.51}$$

where $\Lambda(\mathcal{G}) = \mathbf{diag}\{\lambda_2(\mathcal{G}), \dots, \lambda_n(\mathcal{G})\}$.

Consider first a variation of (5.51) where the output equation is simplified to $z(t) = \hat{x}_\tau(t)$. The modified system has a transfer matrix representation

$$H(s) = (sI + \Lambda(\mathcal{G}))^{-1}B, \tag{5.52}$$

where for notational simplicity we have defined

$$B := S^{-1}\left[\begin{array}{cc} \sigma_w E(\mathcal{G}_\tau)^T & -\sigma_v L_e(\mathcal{G}_\tau)R \end{array} \right],$$

noting that $\Sigma_\tau(s) = R^T S H(s)$.

Proposition 5.2.1. *For the system matrix $H(s)$ (5.52), one has*

$$\|H(s)\|_\infty \quad = \quad \bar{\sigma}(H(0)). \tag{5.53}$$

Proof. From (2.20), we must find the singular values of $H(j\omega)$. This is facilitated by examining the eigenvalues of $H(j\omega)H^*(j\omega)$,

$$\begin{array}{rcl} H(j\omega)H^*(j\omega) & = & (j\omega I + \Lambda(\mathcal{G}))^{-1}BB^T(-j\omega I + \Lambda(\mathcal{G}))^{-1} \\ & = & (j\omega\Lambda(\mathcal{G})^{-1} + I)^{-1}\Lambda(\mathcal{G})^{-1}BB^T\Lambda(\mathcal{G})^{-1}(-j\omega\Lambda(\mathcal{G})^{-1} + I)^{-1}. \end{array} \tag{5.54}$$

Let $Q = \Lambda(\mathcal{G})^{-1}BB^T\Lambda(\mathcal{G})^{-1}$ and $V(\omega) = (j\omega\Lambda(\mathcal{G})^{-1} + I)^{-1}$; then (5.54) simplifies to

$$H(j\omega)H^*(j\omega) \quad = \quad V(\omega)QV^*(\omega).$$

We note that the last identity describes $H(j\omega)H^*(j\omega)$ as a congruence transformation of the matrix Q, which is in the form required to use Theorem 5.2.14. The matrix $V(\omega)V^*(\omega)$ has the form

$$V(\omega)V^*(\omega) \quad = \quad \mathbf{diag}\left\{\frac{\lambda_2(\mathcal{G})^2}{\omega^2 + \lambda_2(\mathcal{G})^2}, \ldots, \frac{\lambda_n(\mathcal{G})^2}{\omega^2 + \lambda_n(\mathcal{G})^2}\right\} \tag{5.55}$$

Denote the eigenvalues of $V(\omega)V^*(\omega)$ as $\mu_i(\omega) = \lambda_{i+1}(\mathcal{G})^2/(\omega^2 + \lambda_{i+1}(\mathcal{G})^2)$ to highlight their dependency on the frequency ω. It is now verified that for any fixed frequency ω, we have $\mu_1(\omega) \leq \mu_2(\omega) \leq \ldots \leq \mu_n(\omega)$. Furthermore, for any $\omega > 0$, we have $\mu_i(\omega) < 1$ for $i = 1, 2, \ldots, n-1$. We thereby invoke Theorem 5.2.14 to conclude that $\theta_k(\omega) < 1$ for $k = 1, 2, \ldots, n-1$ for all $\omega > 0$. At $\omega = 0$, $H(j\omega)H^*(j\omega) = Q$ and hence the singular values of $H(j\omega)$ are a strictly decreasing function of ω. Therefore, the maximum singular value must occur at $\omega = 0$ which corresponds to $\overline{\sigma}(H(0))$, concluding the proof. □

It remains to show that introducing the output equation $z(t) = R^TS\hat{x}_\tau(t)$ does not change the frequency at which the supremum in (2.20) occurs.

Proposition 5.2.2. *The $\mathcal{H}_\infty$-norm for the system (5.51) corresponds to the maximum singular value of its transfer matrix at $\omega = 0$.*

Proof. It suffices to show that $\|R^TSH(s)\|_\infty = \overline{\sigma}(R^TSH(0))$, where $H(s)$ is defined in (5.52). The system $H(s)$ has a singular value decomposition $H(s) = U\Sigma(s)V^*$, with $U \in \mathbb{R}^{n-1\times n-1}$ and $V \in \mathbb{R}^{n+|\mathcal{E}|\times n+|\mathcal{E}|}$. Consider a pure sinusoidal input $W(j\omega)$ expressed in terms of the basis vectors in V as

$$W(j\omega) \quad = \quad \sum_{i=1}^{n+|\mathcal{E}|} \alpha_i(j\omega)v_i,$$

where v_i is the i-th column of V. We can express the output of $H(j\omega)$ to the sinusoidal input as

$$Y(j\omega) \quad = \quad H(j\omega)W(j\omega) = H(j\omega)\sum_{i=1}^{n+|\mathcal{E}|} \alpha_i(j\omega)v_i = \sum_{i=1}^{n+|\mathcal{E}|} \alpha_i(j\omega)\sigma_i(j\omega)u_i.$$

Similarly, the matrix R^TS has a singular value decomposition PMG^*, with $P \in \mathbb{R}^{n-1 \times n-1}$ and $G \in \mathbb{R}^{|\mathcal{E}| \times |\mathcal{E}|}$. As R^TS is connected in series with $H(s)$, we can express the output of the overall system as

$$\begin{aligned} Z(j\omega) &= R^TSH(j\omega)W(j\omega) \\ &= \sum_{i=1}^{n+|\mathcal{E}|} \alpha_i(j\omega)\sigma_i(j\omega)\left(\sum_{j=1}^{|\mathcal{E}|} \beta_j \mu_j p_j\right) = \sum_{i=1}^{n+|\mathcal{E}|} \alpha_i(j\omega)\sigma_i(j\omega)\xi_i, \end{aligned} \quad (5.56)$$

where we have expressed each signal as a linear combination of the appropriate basis vectors, and μ_i is the i-th singular value of R^TS.

For $\|W(j\omega)\|_{\mathcal{L}_2} = 1$, the $\mathcal{H}_\infty$ norm of $R^TSH(s)$ is equivalently characterized by finding the frequency that maximizes $\|Z(j\omega)\|_{\mathcal{L}_2}$. Using (5.56), we express the output norm at a given frequency as

$$\|Z(j\omega)\|^2_{\mathcal{L}_2} = \sum_{i=1}^{n+|\mathcal{E}|} (|\alpha_i(j\omega)\sigma_i(j\omega)|)^2 \|\xi_i\|^2,$$

where we used the property that $\xi_i^T\xi_j = 0$ for $i \neq j$.

As we are restricting the input to be on the unit ball, we have that $\sum|\alpha_i(j\omega)|^2 = 1$. From Proposition 5.2.1 we have that $|\sigma_i(j\omega)| < |\sigma_i(0)|$ for all $\omega > 0$. Therefore, it is straightforward to verify that the coefficients $|\alpha_i(j\omega)\sigma_i(j\omega)|$ are maximized at $\omega = 0$. □

Using the above observations, we now state a general result on the $\mathcal{H}_\infty$-norm of the edge agreement system.

Theorem 5.2.15. *The $\mathcal{H}_\infty$ norms for Σ_τ (4.22) and $\hat{\Sigma}_\tau$ (4.23), are, respectively,*

$$\|\Sigma_\tau\|^2_\infty = \sigma_w^2\left(\bar{\sigma}\left[R^T(RR^T)^{-1}(L_e(\mathcal{G}_\tau))^{-1}(RR^T)^{-1}R\right]\right) + \sigma_v^2 \quad (5.57)$$

and

$$\|\hat{\Sigma}_\tau\|^2_\infty = \bar{\sigma}\left[\sigma_w^2(RR^T)^{-1}(L_e(\mathcal{G}_\tau))^{-1}(RR^T)^{-1} + \sigma_v^2(RR^T)^{-1}\right]. \quad (5.58)$$

Proof. From Propositions 5.2.1 and 5.2.2, we can evaluate (5.49) at $s = 0$ and calculate the singular values of the corresponding matrix as

$$\Sigma_\tau(s)|_{s=0} = R^T(L_e(\mathcal{G}_\tau)RR^T)^{-1}\left[\begin{array}{cc} \sigma_w E(\mathcal{G}_\tau)^T & \sigma_v L_e(\mathcal{G}_\tau)R \end{array}\right].$$

In general, $\Sigma_\tau(s)$ is not square, so we determine the singular values by finding the eigenvalues of $\Sigma_\tau(s)\Sigma_\tau(s)^*$. In this direction, we observe that

$$\Sigma_\tau(s)\Sigma_\tau(s)^*|_{s=0} \;=\; \sigma_w^2 R^T \left(RR^T\right)^{-1} (L_e(\mathcal{G}_\tau))^{-1} \left(RR^T\right)^{-1} R + \sigma_v^2 R^T (RR^T)^{-1} R. \quad (5.59)$$

We note that the second term in (5.59) is a *projection matrix*. Moreover, the matrix $R^T(RR^T)^{-1}R$ has exactly $n-1$ eigenvalues at one, and the remaining eigenvalues at zero (with multiplicity equal to the number of independent cycles). As R has full row rank, and $L_e(\mathcal{G}_\tau)$ and RR^T are invertible matrices, we have that both terms in (5.59) have the same null space. Therefore, the eigenvalues of $\Sigma_\tau(s)\Sigma_\tau(s)^*|_{s=0}$ can be determined from the first term in (5.59) which yields the desired result. For the $\hat{\Sigma}_\tau$ system, an analogous proof can used by replacing the observation matrix R^T with identity. □

As in §5.2.2, we provide examples on how for certain classes of graphs the expression (5.57) can be simplified and interpreted.

(a) **Spanning Trees:** When the underlying graph is a spanning tree, we have that $R = I$, and (5.58) reduces to

$$\|\hat{\Sigma}_\mathcal{T}\|_\infty^2 \;=\; \sigma_w^2 \left(\overline{\sigma}\left[(L_e(\mathcal{G}_\mathcal{T}))^{-1}\right]\right) + \sigma_v^2. \quad (5.60)$$

In the context of $\mathcal{H}_\infty$, we see that the choice of spanning tree is important, as opposed to the corresponding scenario for the $\mathcal{H}_2$ norm. In [62] and [34] it was shown that the path graph has the smallest largest eigenvalue of the graph Laplacian, and the star graph has the greatest largest eigenvalue. As $\|\hat{\Sigma}_\mathcal{T}\|_\infty$ is determined by the inverse of the edge Laplacian, we conclude that the star graph corresponds to the tree topology with minimum $\mathcal{H}_\infty$ norm, and the path graph with largest norm. As in the $\mathcal{H}_2$-norm case, we have $\|\Sigma_\mathcal{T}\|_\infty = \|\hat{\Sigma}_\mathcal{T}\|_\infty$.

(b) ***k*-Regular Graphs:** As shown in §5.2.2, regular graphs admit certain algebraic simplifications that prove useful for system norm calculations for the corresponding agreement protocol. To maintain a parallel analysis with the $\mathcal{H}_2$ problem, we examine the cycle graph and complete graph as special cases here.

Corollary 5.2.16. *The $\mathcal{H}_\infty$-norm of the Σ_τ system (4.22) when the underlying graph is the cycle graph C_n is given as*

$$\|\Sigma_\tau\|_\infty^2 \;=\; \frac{\sigma_w^2}{\lambda_2(C_n)} + \sigma_v^2, \tag{5.61}$$

where $\lambda_2(C_n)$ denotes the second smallest eigenvalue of the cycle graph Laplacian.

Proof. The proof follows from Theorem 5.2.15 and Proposition 3.2.9. □

Corollary 5.2.17. *The $\mathcal{H}_\infty$ norm of the Σ_τ system when the underlying graph is the complete graph K_n is given as*

$$\|\Sigma_\tau\|_\infty^2 \;=\; \frac{\sigma_w^2}{n} + \sigma_v^2. \tag{5.62}$$

The $\mathcal{H}_\infty$ norm of the $\hat{\Sigma}_\tau$ system when the underlying graph is the complete graph K_n is given as

$$\|\tilde{\Sigma}_\tau\|_\infty^2 \;=\; \frac{\sigma_w^2}{n} + \sigma_v^2. \tag{5.63}$$

Proof. The proof follows from propositions 3.2.7, 3.2.8, and the fact that $RR^T = nI - \mathbf{J}$ for the complete graph. □

We conclude this section by noting that for the system $\tilde{\Sigma}_\tau$ (4.23), one has

$$\|\tilde{\Sigma}_\tau\|_\infty^2 \;=\; (n-1)\|\tilde{\Sigma}_\tau\|_2^2.$$

Chapter 6
SYNTHESIS OF NETWORKED DYNAMIC SYSTEMS

In this chapter we explore various scenarios for the synthesis of NDS using the results of §5.2 to motivate appropriate graph-centric objective functions. We consider three general types of synthesis problems:

1. Topology design
2. Inner-loop control design for each agent
3. Decentralized outer-loop control design

In each design scenario, we are primarily concerned with minimizing $\|T_{het}^{w \mapsto \mathcal{G}}\|_p$; each objective function will contain an element related to the sensed output $\mathbf{y}_{\mathcal{G}}(t)$.

We will assume for the remainder of this section that the relative output of the RSN corresponds to a relative position measurement between each agent as

$$\mathbf{y}_{\mathcal{G}}(t) = E(\mathcal{G})^T \otimes \begin{bmatrix} I_p & 0 \end{bmatrix} = E(\mathcal{G})^T \otimes C_p; \tag{6.1}$$

we have assumed the states corresponding to the position of each agent are the first p states of $x_i(t)$.

6.1 *Topology Design*

Here we consider how to design the underlying connection topology and where to place agents within that topology. The general synthesis problem can be written as

$$\begin{aligned} \min_{\mathcal{G}} \quad & \|T_{het}^{w \mapsto \mathcal{G}}\|_p \\ \text{s.t.} \quad & \mathcal{G} \text{ is connected.} \end{aligned} \tag{6.2}$$

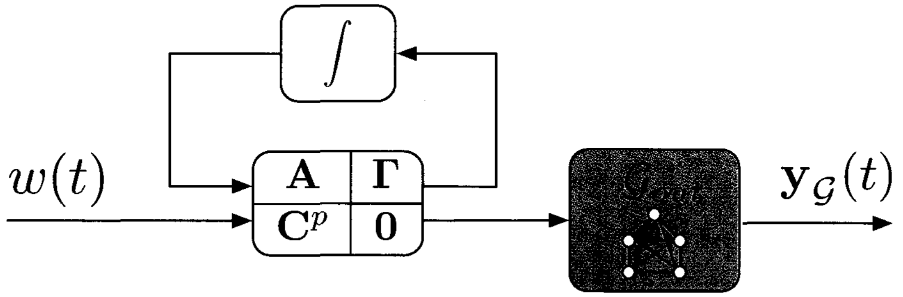

Figure 6.1: Topology design; the feedback connection represents an upper fractional transformation [24].

Note that the decision to include an edge or not is a combinatorial one. The challenge, therefore, is to find numerically tractable algorithms to solve (6.2). We explore in this section an optimal $\mathcal{H}_2$ topology design for NDS coupled at the output, a robust topology design with $\mathcal{H}_\infty$ performance for NDS coupled at the output, and an optimal $\mathcal{H}_2$ sensor selection problem for an NDS coupled at the state.

6.1.1 $\mathcal{H}_2$ Optimal Topology Design for NDS Coupled at the Output

In this section we consider (6.2) for a heterogeneous NDS coupled at the output (an RSN). As we are only considering the topology, we use the following heterogeneous state-space model for the RSN,

$$T_{het}^{w\mapsto\mathcal{G}} : \left\{ \begin{array}{rcl} \dot{\mathbf{x}}(t) & = & \mathbf{A}\mathbf{x}(t) + \mathbf{\Gamma}\mathbf{w}(t) \\ \mathbf{y}_{\mathcal{G}}(t) & = & \left(E(\mathcal{G})^T \otimes C_p\right)\mathbf{x}(t) \end{array} \right. . \qquad (6.3)$$

Given the RSN (6.3) as shown in Figure 6.1, we wish to design the topology $\mathcal{G}$ such that $\|T_{het}^{w\mapsto\mathcal{G}}\|_p$ is minimized. More generally, we aim to find topologies that minimize the effect of disturbances entering each agent on the relative sensed output of the entire system. This can be considered a problem in combinatorial optimization [47], as the decision to include an edge in the graph is binary. Recall from §5.2.1 that in terms of the $\mathcal{H}_2$ norm objective, an optimal topology should always correspond to a spanning tree. The design problem, therefore, is to determine which spanning tree will achieve the smallest $\mathcal{H}_2$ norm for the RSN (6.3). We assume in this case that each agent has already adopted a feedback controller for its local operation.

The design of the topology reduces to the design of the incidence matrix, $E(\mathcal{G})$. This problem is combinatorial in nature, as there are only a finite number of graphs that can be constructed from a set of n nodes. As the number of agents in the RSN becomes large, solving this problem becomes prohibitively hard [47]. However, we find that with an appropriate modification of the problem statement, results from combinatorial optimization can be used, leading to a polynomial-time algorithm.

Specifically, the *minimum spanning tree* (MST) problem can be adapted to solve (6.2). The MST can be efficiently solved using Kruskal's algorithm in $\mathcal{O}(|\mathcal{E}|\log(|\mathcal{V}|))$ time. The algorithm is given below and a proof of its correctness, for example, can be found in [47].

Algorithm 1: Kruskal's Algorithm

```
Data: A connected undirected graph $\mathcal{G}(\mathcal{V},\mathcal{E})$ and weights $w:\ \mathcal{E} \mapsto \mathbb{R}$.
Result: A spanning tree $\mathcal{G}_t$ of minimum weight.
begin
    Sort the edges such that $w(e_1) \leq w(e_2) \leq \cdots \leq w(e_{|\mathcal{E}|})$, where $e_i \in \mathcal{E}$
    Set $\mathcal{G}_t := \mathcal{G}_t(\mathcal{V},\emptyset)$
    for $i := 1$ to $|\mathcal{E}|$ do
        if $\mathcal{G}_t + e_i$ contains no cycle then
            set $\mathcal{G}_t := \mathcal{G}_t + e_i$
end
```

In order to apply the MST to the $\mathcal{H}_2$ synthesis problem we must reformulate the original problem statement. To begin, we first write the expression for the $\mathcal{H}_2$ norm of the system in (6.3).

$$\begin{aligned}\left\| T_{het}^{w\mapsto\mathcal{G}} \right\|_2^2 &= \sum_i^n d_i \mathbf{trace}\{C_p X_i C_p^T\} \\ &= \sum_i^n d_i \|T_i^{w\mapsto p}\|_2^2, \qquad (6.4)\end{aligned}$$

where $T_i^{w\mapsto p}$ is the map from the exogenous input entering agent i to its position, $C_p x_i(t)$, and d_i is the node degree of agent i (defined in §2.2). We reiterate here that the RSN norm description is related to the degree of each node in the network. Using the weighted incidence graph interpretation of the norm, as in (5.25), we see that the gain of each agent, $\|T_i^{w\mapsto p}\|_2^2$, acts as a weight on the nodes.

As each agent is assumed to have fixed dynamics, the problem of minimizing the RSN $\mathcal{H}_2$ norm reduces to finding the degree of each agent while ensuring the resulting topology is a spanning tree. This objective is related to properties of the nodes of the graph. To use the MST results, we must convert the objective from weights on the nodes to weights on the edges.

To develop this transformation, consider the graph $\mathcal{G} = (\mathcal{V}, \mathcal{E})$ with fixed weights q_i on each node ($i = 1, \ldots, n$). The node-weighted Frobenius norm of the incidence matrix is

$$\|QE(\mathcal{G})\|_F^2 \; = \; \sum_i d_i q_i^2 \, , \tag{6.5}$$

where $Q = \mathbf{diag}(q_1, \ldots, q_n)$.

Next, consider the effect of adding an edge $\hat{e} = (i,j)$ to $\mathcal{E}$ in terms of the Frobenius norm of the augmented incidence matrix,

$$\left\| Q \begin{bmatrix} E(\mathcal{G}) & \hat{e} \end{bmatrix} \right\|_F^2 = \left(\sum_k d_k q_k^2 \right) + q_i^2 + q_j^2 \, , \tag{6.6}$$

where d_k represents the degree of node k *before* adding the new edge $\hat{e}$. This shows that each edge $\hat{e} = (i,j)$ contributes $(q_i^2 + q_j^2)$ to the overall norm. Therefore, weights on the edges can be constructed by adding the node weights corresponding to the nodes adjacent to each edge as

$$\mathbf{w}_e = |E(\mathcal{G})^T| \mathbf{w}_n^2 \, . \tag{6.7}$$

This result can be used to generate an equivalent norm characterization to the one presented in (6.4)

$$\left\| T_{het}^{w\mapsto \mathcal{G}} \right\|_2^2 \; = \; \left\| |E(\mathcal{G})^T| \begin{bmatrix} \|T_1^{w\mapsto p}\|_2^2 \\ \vdots \\ \|T_n^{w\mapsto p}\|_2^2 \end{bmatrix} \right\|_1 \, , \tag{6.8}$$

where $\|x\|_1 = \sum_i |x_i|$.

Using the above transformation from node weights to edge weights, we arrive at the following result.

Theorem 6.1.1. *The connection topology that minimizes the $\mathcal{H}_2$ norm of (6.3), can be found using Kruskal's MST algorithm with input data $\mathcal{G}$, and edge weights*

$$w = |E(\mathcal{G})|^T \begin{bmatrix} \|T_1^{w\mapsto p}\|_2^2 \\ \vdots \\ \|T_n^{w\mapsto p}\|_2^2 \end{bmatrix}. \tag{6.9}$$

Proof. The proof follows from (6.4) and the transformation from node weights to edge weights described in (6.5)-(6.7). □

Remark 6.1.2. *The choice of the input graph $\mathcal{G}$ may be application specific, and can capture certain communication or sensing constraints between agents. For example, one may consider a scenario where agents are initially randomly distributed (a geometric random graph) upon deployment and can only sense neighboring agents within a specified range. The results of Theorem 6.1.1 can be used to determine the optimal spanning tree for that initial configuration.*

Remark 6.1.3. *There are many distributed algorithms that solve the MST problem [30, 6]. These could be used in place of the centralized version when the optimal spanning tree topology needs to be reconfigured. This scenario can arise due to the initialization problem discussed in Remark 6.1.2, or in situations when certain agents are disabled, lost, or reallocated for different mission purposes.*

If there are no initial constraints on the input graph for Theorem 6.1.1, then we arrive at the following result.

Corollary 6.1.4. *When the input graph in Theorem 6.1.1 is the complete graph, then the star graph with center node corresponding to the agent with minimum norm is the (non-unique) optimal topology.*

Proof. The degree of the center node in a star graph is $n-1$, and all other nodes have degree one. Assume the node weights are sorted as $q_1 \leq \cdots \leq q_n$, then the $\mathcal{H}_2$ norm of the RSN is $\|T_{het}^{w\mapsto\mathcal{G}}\|_2^2 = (n-1)q_1 + \sum_{i=2}^{n} q_i$. Any other tree can be obtained by removing and adding a single edge, while ensuring connectivity. With each such operation, the cost is non-decreasing, as any new edge will increase the degree of node $i > 1$ and by assumption $q_1 \leq q_i$. □

Lemma 6.1.4 shows that if there are no restrictions on the initial configuration, the optimal topology can be obtained without the MST algorithm. The computational effort required is only to determine the agent with smallest norm. The non-uniqueness of the star graph can occur if certain agents have identical norm, resulting in other possible configuration with an equivalent cost.

An Example: ANTS

We now consider an application of the above results to a mission scenario related to the *Autonomous NanoTechnology Swarm* project, or ANTS, currently under investigation by NASA [2]. One component of the ANTS mission involves the deployment of 1,000 pico-satellites to the asteroid belt for observational study. The spacecraft are deployed en-route to the asteroid belt, and then must organize into smaller teams which will coordinate to search for various resources and materials. We consider here one aspect of this mission.

When the pico-satellites are initially deployed they must be configured into teams. One scenario is to consider forming a team with a topology that minimizes the $\mathcal{H}_2$ performance of the team. Such a performance metric can be justified by considering the various physical interpretations of the system $\mathcal{H}_2$ norm. For example, the $\mathcal{H}_2$ norm can be viewed as the energy of the impulse-response function for the system under investigation. Solar wind gusts can be approximated as an impulse to the team of satellites, and the $\mathcal{H}_2$ norm would correspond to a measure of how that gust causes the formation to drift apart. For this example, we will consider a system comprised of 75 heterogeneous pico-satellites. Each agent's state-space was generated randomly using MATLAB, with a single input and a single output (corresponding to the position, as in C_p defined in (6.1). It is worth mentioning for this mission there may be certain pico-satellites that contain different sensors depending on their mission objectives. This variation would introduce heterogeneity, but for ease of presentation we use random models. Each of the agents are randomly distributed and the initial topology is determined by assigning an edge between two agents if their Euclidean

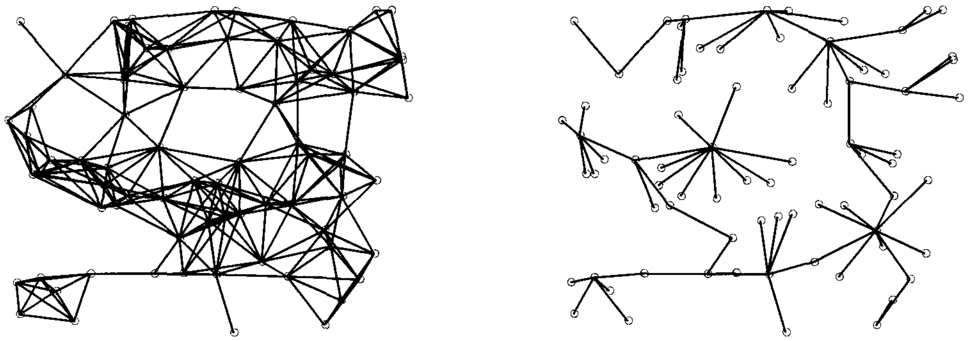

(a) Random Geometric Graph with $r = 0.20$

(b) Optimal spanning tree

Figure 6.2: Application example of Theorem 6.1.1.

distance is less than $r = 0.20$. This could correspond to the relative sensing capabilities available on each spacecraft. The initial connection graph is given in Figure 6.2(a), and the resulting MST is given in Figure 6.2(b). A key point in this example is to highlight the non-triviality of the resulting topology. When designing a topology based on heuristics, this result most likely would not be found, especially when dealing with large networks.

6.1.2 $\mathcal{H}_\infty$ Robust Topology Design for NDS Coupled at the Output

In this section we consider a variation of (6.2) whereas we design the nominal weights on the edges in the connection graph for an RSN that minimizes the robust performance of the system. Motivated by the results of §5.2.1, we find that (6.2) for $p = \infty$ reduces to the minimization of the spectral norm of the weighted incidence matrix, $\|QE(\mathcal{G})\|$, where Q was defined in Theorem 5.2.9. Minimization of this objective can be formulated as a mixed-integer semi-definite program. For reasonably sized problem instances this can be solved using, for example, branch-and-bound algorithms [47].

While topology design is an important application, the $\mathcal{H}_\infty$ framework allows us to consider the robustness of certain topologies. In this direction, we consider a variation of (6.2) that aims to minimize the *robust performance* of the RSN in (6.3). For such an analysis, we adjust the RSN model to allow for uncertainty in the sensing protocol. Specifically, we

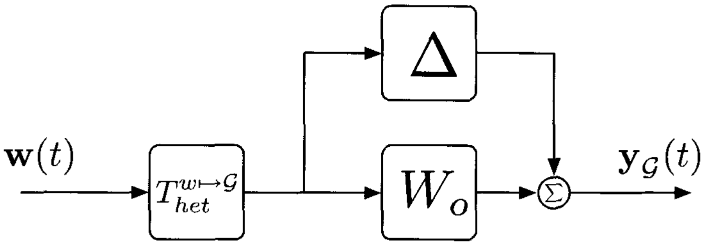
Δ
$\mathbf{w}(t)$
$T_{het}^{w\mapsto\mathcal{G}}$
W_o
Σ
$\mathbf{y}_{\mathcal{G}}(t)$

Figure 6.3: Multiplicative uncertainty for NDS coupled at the output.

introduce the notion of a weighted edge for the sensed output. This model might be used to capture the fidelity of a relative measurement.

$$T_{het}^{w\mapsto\mathcal{G}}(W_o) \;:\; \left\{ \begin{array}{rcl} \dot{\mathbf{x}}(t) & = & \mathbf{A}\mathbf{x}(t) + \mathbf{\Gamma}\mathbf{w}(t) \\ \mathbf{y}_{\mathcal{G}}(t) & = & \left(W_o E(\mathcal{G})^T \otimes C_p\right)\mathbf{x}(t) \end{array} \right. . \tag{6.10}$$

Here, $W_o = \mathbf{diag}\{w_1, \ldots, w_{|\mathcal{E}|}\}$ represents the nominal weights on each edge in the graph. A weight of zero corresponds to the edge not existing. We will also assume all the weights are non-negative ($w_i \geq 0$). The model (6.10) relates to (6.3) through the output as $T_{het}^{w\mapsto\mathcal{G}}(W_o) = (W_o \otimes I)T_{het}^{w\mapsto\mathcal{G}}$.

Using (6.10), we can introduce a structured uncertainty on each edge weight. The uncertainty set is defined as

$$\mathbf{\Delta} \;=\; \{\text{diag}\{\delta_1, \ldots, \delta_{|\mathcal{E}|}\} \;: \delta_i \in \mathbb{R},\; |\delta_i| \leq 1\}. \tag{6.11}$$

The true edge weight can thus be written as $W = W_o + \Delta$, for $\Delta \in \mathbf{\Delta}_w$. This can be considered as an output-multiplicative uncertainty, as shown in Figure 6.3.

The problem (6.2) can now be restated as the *robust optimization* problem [12],

$$\begin{array}{lll} \min\limits_{W_o} & \max_{\|\mathbf{\Delta}\|\leq 1} & \|QE(\mathcal{G})\,(W_o + \mathbf{\Delta})\,\| \\ \text{s.t.} & & \mathcal{G} \text{ is connected in the presence of edge weight uncertainty.} \end{array} \tag{6.12}$$

This problem can be solved as a semi-definite program, the procedure of which is outlined in [12]. To apply these results, we must express the objective and constraints of the system as a perturbed LMI,

$$F(x,\delta) \;=\; F_0(x) + \sum_{i=1}^{l} \delta_i F_i(x), \tag{6.13}$$

where each $F_i(x)$ is a symmetric matrix and affine in the variable x.

First, we scalarize the objective function by introducing a new variable γ and noting that $\|QE(\mathcal{G})\,(W_o + \mathbf{\Delta})\,\| \leq \gamma$ can be written (via the Schur complement) as the LMI

$$\begin{bmatrix} \gamma I & QE(\mathcal{G})(W_o + \mathbf{\Delta}) \\ (W_o + \mathbf{\Delta})E(\mathcal{G})^T Q & I \end{bmatrix} \;\geq\; 0. \tag{6.14}$$

Defining the matrices $S_i \in \mathbb{R}^{|\mathcal{E}| \times |\mathcal{E}|}$ and $V(\gamma)$ as

$$[S_i]_{kl} = \begin{cases} 1 & k = l = i \\ 0 & \text{otherwise} \end{cases}, \quad V(\gamma) = \begin{bmatrix} \gamma I & \mathbf{0} \\ \mathbf{0} & I \end{bmatrix}, \tag{6.15}$$

we can express (6.14) in the form (6.13) as

$$F_1(w,\delta) = V(\gamma) + \sum_{i=1}^{|\mathcal{E}|} (w_i + \delta_i) \begin{bmatrix} \mathbf{0} & QE(\mathcal{G})S_i \\ S_i E(\mathcal{G})^T Q & \mathbf{0} \end{bmatrix} \;\geq\; 0. \tag{6.16}$$

Similarly, the robust connectivity constraint can also be expressed in the form (6.13). Recall that for a connected graph, $\lambda_2(\mathcal{G}) > 0$, and the eigenvector associated with $\lambda_1(\mathcal{G}) = 0$ is the vector of all ones, $\mathbb{1}$. Defining the matrix P such that $\mathbf{IM}\{P\} \;=\; \mathbf{span}\{\mathbb{1}^{\perp}\}$, we obtain[1]

$$F_2(w,\delta) = \sum_{i=1}^{|\mathcal{E}|} (w_i + \delta_i) P^T (e_i e_i^T) P \;>\; 0. \tag{6.17}$$

Using (6.16) and (6.17) we define

$$F_0^1(w) = \begin{bmatrix} \gamma I & QE(\mathcal{G})W_o \\ W_o E(\mathcal{G})^T Q & I \end{bmatrix}, \quad F_0^2(w) = P^T E(\mathcal{G}) W_o E(\mathcal{G})^T P, \tag{6.18}$$

$$F_i^1 = \begin{bmatrix} \mathbf{0} & QE(\mathcal{G})S_i \\ S_i E(\mathcal{G})^T Q & \mathbf{0} \end{bmatrix}, \quad F_i^2 = P^T e_i e_i^T P. \tag{6.19}$$

[1] Here we note that $A > 0$ means there exists an ϵ such that $A - \epsilon I > 0$.

The expressions in (6.18) and (6.19) can now be applied to the results in [12] to obtain the following SDP,

$$
\begin{aligned}
\min_{w,S_i,T_i} \quad & \gamma \\
\text{s.t.} \quad & \begin{bmatrix} S_i & F_1^i & \cdots & F_{|\mathcal{E}|}^i \\ F_1^i & T_i & & \\ \vdots & & \ddots & \\ F_{|\mathcal{E}|}^i & & & T_i \end{bmatrix} \geq 0 \,, \; i = 1,2 \\
& S_i + T_i \leq 2F_0^i \,, \; i = 1,2 \\
& 0 \leq w_i \leq w_{max} \,, \; i = 1, \ldots, |\mathcal{E}| \\
& \sum_i w_i = \alpha,
\end{aligned}
\tag{6.20}
$$

where the last constraint constrains the aggregate edge weight sum.

An Example: Robust Edge Weights

To illustrate this procedure, we consider an RSN with $n = 10$ heterogeneous and SISO systems (generated randomly in MATLAB). The input graph is the complete graph, K_n, allowing the program in (6.20) to select the optimal weights on every possible edge combination. For $\alpha = n - 1$ and $w_{max} = 2$, (6.20) was solved using SeDuMi in Matlab. The resulting topology is shown in Figure 6.4. Note that every edge has a positive weight, however, only edges with $w_i > 0.1$ were drawn. The thickness of the line indicates a larger weight.

Remark 6.1.5. *While the problem formulation presented above is concerned with static edge weight uncertainty, the principle can be extended to include dynamic edge weights. For example, each relative sensor may be characterized by a frequency dependent weight, $w_i(s)$, and the corresponding uncertainty can be considered as an unstructured norm-bounded uncertainty.*

Remark 6.1.6. *The SDP (6.20) presents an analytic framework for solving the robust topology design problem. However, it should be noted that due to the auxiliary variables defined, the size of this problem can grow very large with the number of nodes (for the complete graph on n nodes,*

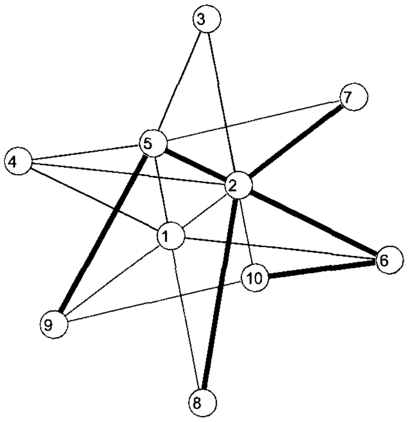

Figure 6.4: Optimal topology for robust edge weight design; edges with weights less than 0.1 are not drawn.

there are $n(n-1)/2$ edges). While interior-point methods offer polynomial-time algorithms, for excessively large problem instances (6.20) might lead to numerical problems. This points to the need to consider specialized solution methods or alternative problem formulations.

6.1.3 $\mathcal{H}_2$ Optimal Sensor Placement for NDS Coupled at the State

We now consider a variation of (6.2) for NDS coupled at the state whereas we would like to chose where to place sensors in a distributed system running a consensus algorithm. Encouraged by the graph-theoretic characterization of the $\mathcal{H}_2$ performance for consensus-type systems, in this section, we proceed to consider the problem of sensor selection and placement for consensus-type systems. Consider, for example, a scenario where there are two types of sensors available for the relative measurements in the open-loop consensus problem. One sensor is a high-fidelity and high cost, with associated noise covariance of $\overline{\sigma}_v^2$. The other sensor is a less expensive lower fidelity sensor with covariance of $\underline{\sigma}_v^2 > \overline{\sigma}_v^2$. When synthesizing the topology for the consensus problem, the designer must consider the tradeoff between the sensor costs and the overall system performance.

In this direction, consider the system in (4.22) in the form

$$\Sigma_\tau : \begin{cases} \dot{x}(t) & = & -L_e(\mathcal{G}_\tau)RR^T x_\tau(t) & + & \sigma_w E(\mathcal{G}_\tau)^T \hat{w}(t) - L_e(\mathcal{G}_\tau)^T R\Gamma\hat{v}(t) \\ z(t) & = & R^T x_\tau(t) & & \end{cases}, \quad (6.21)$$

where $\hat{w}(t)$ and $\hat{v}(t)$ are the normalized noise signals, and the matrix Γ is a diagonal matrix with elements σ_i corresponding to the variance of the sensor on edge i. We note that the most general version of this problem considers a finite set of p sensors each with an associated variance,

$$P = \{\sigma_1^2, \sigma_2^2, \ldots, \sigma_p^2\}, \quad (6.22)$$

where for each element $\sigma_i^2 \in P$ there is an associated cost $c(\sigma_i^2)$. The cost function has the property that $c(\sigma_i^2) > c(\sigma_j^2)$ if $\sigma_i^2 < \sigma_j^2$. Using (5.34)-(5.35), in order to find the optimal placement of these sensors, one can consider the mixed-integer program [47],

$$\begin{array}{lll} \mathcal{P}_1 : & \min\limits_{X,W} & \lambda \mathbf{trace}[R^T X R] + \sum\limits_{i=1}^{|\mathcal{E}|} c(w_i) \\ & \text{s.t.} & W = \mathbf{diag}\{w_1, \ldots, w_{|\mathcal{E}|}\},\ w_i \in P,\ \sum\limits_i w_i \leq \mu, \\ & & -L_e(\mathcal{G}_\tau)^T RR^T X - XRR^T L_e(\mathcal{G}_\tau)^T + \sigma_w^2 L_e(\mathcal{G}_\tau) + L_e(\mathcal{G}_\tau)^T RWR^T L_e(\mathcal{G}_\tau) = 0, \end{array}$$

where λ represents a weighting on the $\mathcal{H}_2$ performance of the solution, and μ represents the maximum aggregated noise covariance. Note that in general $|\mathcal{E}| \min_i \sigma_i^2 \leq \mu \leq |\mathcal{E}| \max_i \sigma_i^2$.

The problem $\mathcal{P}_1$ is combinatorial in nature, as a binary decision needs to be made as to which sensor to use and place in the network. Although $\mathcal{P}_1$ can certainly be solved by using a mixed-integer programming solvers [47], certain relaxations can be made to convexify the resulting problem. Most notably, one approach involves relaxing the discrete nature of the set P (6.22) into a box-type constraint as

$$\hat{P} = [\underline{\sigma}^2, \overline{\sigma}^2]. \quad (6.23)$$

The cost function can now be written as a continuous map $c : \hat{P} \mapsto \mathbb{R}$ which is convex and a strictly decreasing function. The simplest version of such a function would be the linear map

$$c(\sigma_i^2) = -\beta\sigma_i^2$$

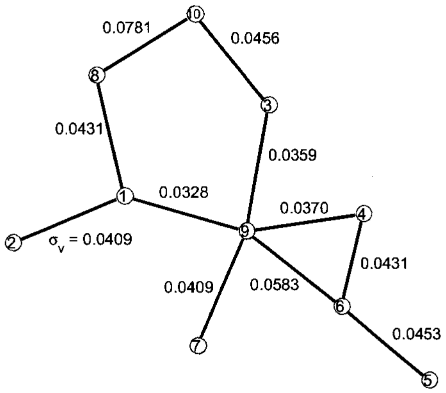

Figure 6.5: A graph on 10 nodes with optimal sensor selection; σ_v denotes the sensor variance.

for some $\beta > 0$. This relaxation leads to the following modified program,

$$
\begin{array}{lll}
\mathcal{P}_2: & \min\limits_{X,W} & \lambda\,\mathbf{trace}[R^T X R] - \beta\,\mathbf{trace}[W] \\
& \text{s.t.} & W = \mathbf{diag}\{w_1, \ldots, w_{|\mathcal{E}|}\},\ \underline{\sigma}^2 \le w_i \le \overline{\sigma}^2,\ \sum_i w_i \le \mu, \\
& & -L_e(\mathcal{G}_\mathcal{T})^T R R^T X - X R R^T L_e(\mathcal{G}_\mathcal{T})^T + \sigma_w^2 L_e(\mathcal{G}_\mathcal{T}) + L_e(\mathcal{G}_\mathcal{T})^T R W R^T L_e(\mathcal{G}_\mathcal{T}) = 0.
\end{array}
$$

An Example: Sensor Selection

As an example of the applicability of $\mathcal{P}_2$, we considered the sensor selection for the graph in Figure 6.5. A random graph on 10 nodes with an edge probability of 0.15 was generated. The resulting graph is connected and contains two independent cycles, resulting in a more general problem instance. The sensor constraints were $\hat{P} = [0.001 \quad 0.1]$ and $\mu^2 = 0.501$. Finally, the cost function weights were chosen as $\beta = 5$ and $\lambda = 1$. Solving $\mathcal{P}_2$ then resulted in a non-trivial selection of sensors for each edge. The sensor covariance for each edge is labeled in Figure 6.5; we observe that the highest fidelity sensors tend to be concentrated around the node of highest degree. Also, the edge with the lowest fidelity sensor is placed in "low traffic" areas.

6.2 Inner-loop Controller Design

We now consider the problem of designing a local control for each agent such that both local performance objectives are achieved in addition to the global objective, $\|T_{het}^{w \mapsto \mathcal{G}}\|_p$.

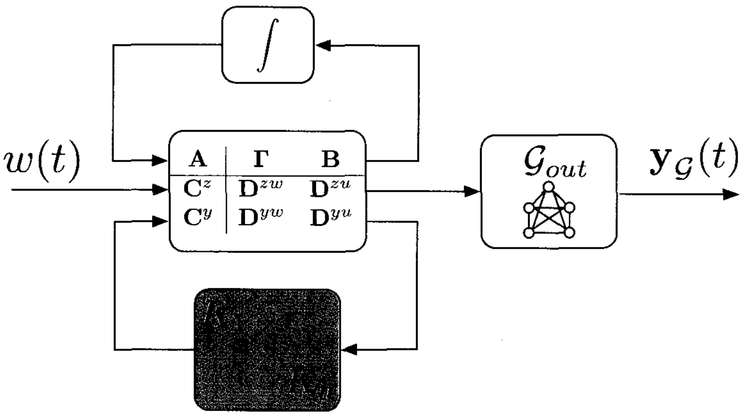

Figure 6.6: Inner-loop design; the feedback connections represents lower and upper fractional transformations [24].

Therefore, the general synthesis problem has the form

$$\begin{aligned} \min_{K_i} \quad & \|T_{het}^{w \mapsto \mathcal{G}}\|_p + \sum_{i}^{n} \|T_i^{w \mapsto z}\|_p \\ \text{s.t.} \quad & K_i \text{ stabilizes } \Sigma_i, \; i = 1, \ldots, n. \end{aligned} \tag{6.24}$$

We note that while $\|T_i^{w \mapsto z}\|_p$ represents a purely local objective for each agent, the term $\|T_{het}^{w \mapsto \mathcal{G}}\|_p$ introduces a coupling between all the agents. For $p = 2$, we present a semidefinite program that solves (6.24) for NDS coupled at the output with the additional feature of being solved in a decentralized way.

6.2.1 $\mathcal{H}_2$ Optimal Inner-loop Design for NDS Coupled at the Output

In this scenario, the connection topology is given and fixed. From a synthesis point of view, each agent behaves independently and does not use information from the RSN for its control; this can be considered an inner-loop type of control design, as shown in Figure 6.6. For the duration of this section, we will assume that each agent has full-state feedback available for its controller ($C_i^y = I$). The model we consider is (4.14), with $y_{\mathcal{G}}(t)$ replaced by (6.1). Note that $y_{\mathcal{G}}(t)$ will be treated as an additional controlled variable for the $\mathcal{H}_2$ synthesis problem. For technical reasons related to $\mathcal{H}_2$ synthesis we also have $\mathbf{D^{zw}} = 0$

and $\mathbf{D}^{\mathbf{yw}} = 0$.

The state-feedback optimal $\mathcal{H}_2$ control problem for a single agent without considering the global RSN objective can be formulated as an SDP [24], as shown in (2.33). From that SDP, we have that $\|T_i^{w\mapsto z}\|_2^2 = \mathbf{trace}(W_i)$. Here, we note that X_i corresponds to the controllability gramian of the closed-loop system for agent i. That is, it is the controllability gramian for a realization of the system $T_i^{w\mapsto z}$.

The SDP in (2.33), however, does not incorporate the global RSN performance objective into the problem. While each agent can generate a solution to (2.33) independently of each other, the addition of the global RSN layer couples the design of each agent's controller. The SDP (2.33) can be modified to incorporate the global performance objective, leading to the following result.

Theorem 6.2.1. *Given the RSN system described in (4.14), a local state-feedback controller of the form $u_i(t) = K_i x_i(t)$ that minimizes local performance objectives in addition to the global RSN performance objective can be found by solving*

$$\min_{W_i, X_i, Z_i, V_i} \sum_i^n \mathbf{trace}[W_i] + \mathbf{trace}[V_i] \tag{6.25}$$

s.t.

$$\begin{bmatrix} A_i & B_i \end{bmatrix} \begin{bmatrix} X_i \\ Z_i \end{bmatrix} + \begin{bmatrix} X_i & Z_i^T \end{bmatrix} \begin{bmatrix} A_i^T \\ B_i^T \end{bmatrix} + \Gamma_i \Gamma_i^T \leq 0 \tag{6.26}$$

$$\begin{bmatrix} X_i & (C_i^z X_i + D_i^{zu} Z_i)^T \\ (C_i^z X_i + D_i^{zu} Z_i) & W_i \end{bmatrix} > 0 \tag{6.27}$$

$$\begin{bmatrix} X_i & (C_p X_i)^T \\ C_p X_i & \frac{1}{d_i} V_i \end{bmatrix} > 0 \tag{6.28}$$

where

$$K_i = Z_i X_i^{-1}.$$

Proof. Consider the control $\mathbf{u}(t) = \mathbf{K}\mathbf{x}(t)$ implemented, where $\mathbf{K} = \mathbf{diag}(K_1, \ldots, K_n)$. The closed-loop system becomes

$$\Sigma_{cl}\left\{\begin{array}{rcl} \dot{\mathbf{x}}(t) & = & (\mathbf{A}+\mathbf{B}\mathbf{K})\mathbf{x}(t)+\mathbf{\Gamma}\mathbf{w}(t) \\ \begin{bmatrix} \mathbf{z}(t) \\ \mathbf{y}_{\mathcal{G}}(t) \end{bmatrix} & = & \begin{bmatrix} \mathbf{C}^z+\mathbf{D}^{zu}\mathbf{K} \\ E(\mathcal{G})^T\otimes C_p \end{bmatrix}\mathbf{x}(t). \end{array}\right. \tag{6.29}$$

To guarantee the stability of the closed loop system, we require that $(\mathbf{A}+\mathbf{B}\mathbf{K})$ be Hurwitz. This is guaranteed by the LMI given in (6.26) by noting the block diagonal structure of the matrix, and defining $Z_i = K_iX_i$. In fact, when the constraint (6.26) is satisfied at equality, we note that X_i is the controllability gramian for the system in (6.29).

The $\mathcal{H}_2$ norm of (6.29) can be calculated as

$$\begin{aligned} \|\Sigma_{cl}\|_2^2 &= \mathbf{trace}\left\{\begin{bmatrix} \mathbf{C}^z+\mathbf{D}^{zu}\mathbf{K} \\ E(\mathcal{G})^T\otimes C_p \end{bmatrix}\mathbf{X}\begin{bmatrix} \mathbf{C}^z+\mathbf{D}^{zu}\mathbf{K} \\ E(\mathcal{G})^T\otimes C_p \end{bmatrix}^T\right\} \\ &= \mathbf{trace}\left\{(\mathbf{C}^z+\mathbf{D}^{zu}\mathbf{K})\mathbf{X}(\mathbf{C}^z+\mathbf{D}^{zu}\mathbf{K})^T\right\}+\mathbf{trace}\left\{(E(\mathcal{G})^T\otimes C_p)\mathbf{X}(E(\mathcal{G})^T\otimes C_p)^T\right\}, \end{aligned} \tag{6.30}$$

where $\mathbf{X} = \mathbf{diag}(X_1,\ldots,X_n)$. The first term on the right hand side corresponds precisely to the $\mathcal{H}_2$ norm of the system in (4.4) with the feedback law $\mathbf{u}(t) = \mathbf{K}\mathbf{x}(t)$ implemented. The second term is the $\mathcal{H}_2$ norm of $T_{het}^{w\mapsto\mathcal{G}}$. Using the results from §5.2.1 we can express the performance as

$$\begin{aligned} \left\|T_{het}^{w\mapsto\mathcal{G}}\right\|_2^2 &= \mathbf{trace}\left\{(E(\mathcal{G})^T\otimes C_p)\mathbf{X}(E(\mathcal{G})\otimes C_p)\right\} \\ &= \sum_i^n d_i\mathbf{trace}\left\{C_pX_iC_p^T\right\}. \end{aligned} \tag{6.31}$$

The objective is to minimize $\|\Sigma_{cl}\|_2$, which can be accomplished by minimizing both terms in the right-hand side of (6.30). Using the matrix Schur-complement[36], we note that

$$d_iC_pX_iC_p^T \quad < \quad V_i \tag{6.32}$$

is equivalent to

$$\begin{bmatrix} X_i & (C_pX_i)^T \\ C_pX_i & \frac{1}{d_i}V_i \end{bmatrix} \quad > \quad 0. \tag{6.33}$$

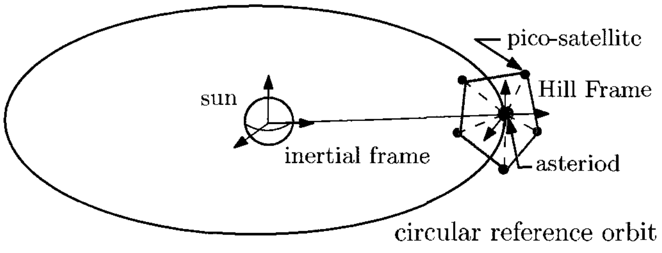

Figure 6.7: The Hill frame for a circular orbit.

We now note that if $d_i C_p X_i C_p^T < V_i$, then $d_i \mathbf{trace}\{C_p X_i C_p^T\} < \mathbf{trace}\{V_i\}$.

A similar derivation is used to arrive at the LMI in (6.27). □

Remark 6.2.2. *The full-state feedback assumption can be relaxed without loss of generality using an LMI formulation for the more general output-feedback problem (such as LQG) [71]. The LMI (6.27) will consequently be modified, but the LMI corresponding to the global RSN performance (6.28) remains the same.*

A striking feature of the SDP (6.25)-(6.28) is its structure. Although the global RSN layer couples each agent, we see that the coupling can be removed via the formulation of the $\mathcal{H}_2$ norm. The SDP is therefore separable across each of the agents which has implications for the parallelization of the computation and decision-making process.

An Example: ANTS

Returning to the ANTS mission scenario presented in §6.1.1, we consider a component of the mission that involves collecting data from an asteroid. To accomplish this the pico-satellite team must rendezvous with an asteroid. For this scenario, we first consider a rendezvous problem for each pico-satellite individually. Each satellite is assumed to have continuous actuation on each axis. We also introduce disturbances in the form of process noise for the actuators and measurement noise for the sensors. The noises are assumed to be white Gaussian with $\sigma_w^2 = 0.1$ for the process and $\sigma_v^2 = 0.01$ for the sensors. Contrary to the previous example, we will assume homogeneous agent dynamics generated

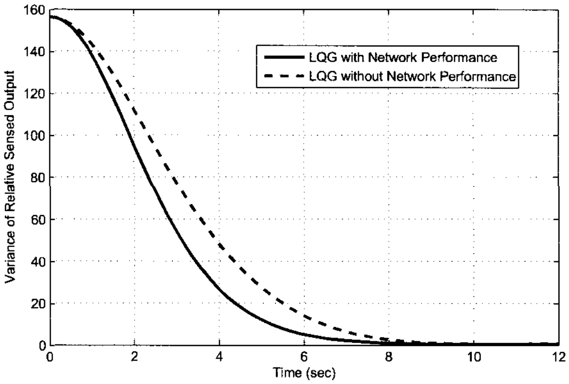

Figure 6.8: Variance of $y_{\mathcal{G}}(t)$ for a system with additional network performance constraints (solid) and without these constraints (dashed).

by the Hill's equations which is used to describe the linearized relative dynamics of the agents with respect to the circular orbit, visualized in Figure 6.7 [79]. The target asteroid is assumed to be in a circular orbit around the Sun with radius of $r_o = 3 \times 10^9$ km. We next generate a random spanning tree graph and the results of Theorem 6.2.1 are applied to generate a control for each pico-satellite to drive them to the asteroid. We also address the issue in Remark 6.2.2 regarding the full-state information. For this example we employ LQG for estimation and control while including the additional performance constraint for the network. Figure 7.1 depicts the variance of the RSN output $y_{\mathcal{G}}(t)$ for the system using the network performance constraint and the system without the constraint. This shows that the inclusion of the network performance constraint will tend to keep the agents closer together even in the presence of noise.

6.3 Outer-loop Controller Design

In this section we consider the design of decentralized controllers for networked dynamic systems, as represented in Figure 6.9. The structure of the NDS will determine the structure of the controller. In fact, the controller itself can be considered an NDS with the same underlying connection graph as the original plant. In this direction, we formulate the

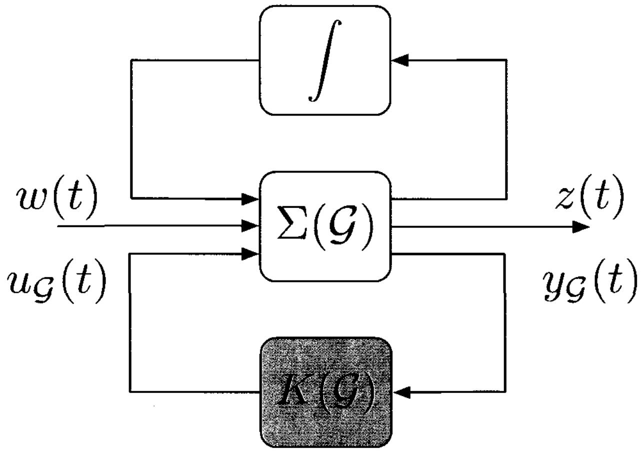

Figure 6.9: Outer-loop design; the feedback connections represent lower and upper fractional transformations [24].

control problem as

$$\begin{array}{ll} \min\limits_{K(\mathcal{G})} & \|T_{het}^{w \mapsto \mathcal{G}}\|_p \\ \text{s.t.} & K(\mathcal{G}) \text{ stabilizes } \Sigma(\mathcal{G}). \end{array} \tag{6.34}$$

Here, $K(\mathcal{G})$ is meant to specify that the underlying connection graph is fixed and the controller must embed that structure in its design.

In a broader context, the problem defined in (6.34) falls under the scope of decentralized control theory [69]. One of the main challenges in solving (6.34) is the underlying connection topology constraint makes the problem non-convex. There has been some work describing relaxations that lead to convex programs, in addition to conditions when the original problem may be solved via convex programming [61, 67].

Rather than focus directly on (6.34), this section highlights the intricate relationship between the different NDS models via the design of a decentralized stabilizing control law. In the context of (6.34), we are looking for a *feasible* solution $K(\mathcal{G})$ rather than the optimal one. This leads us to consider a simplified model for a decentralized formation control problem that emphasizes the dual nature of the NDS coupled at the input and output. At the same time we also show these dual systems become transformed into an NDS coupled at the state with an appropriate choice of a decentralized control.

6.3.1 *Decentralized Formation Control for NDS: Dual Systems*

The objective of this section is to highlight the intricate connection between the different NDS models via the design of decentralized controllers [88]. In this direction we define two complimentary homogeneous NDS models. To emphasize the role of the connection topology we restrict our analysis to agents with simple integrator dynamics.

The first system is comprised of n agents and each agent is able to sense the relative state of its neighbor based on a given connection topology; this is the relative sensing model presented in §4.2.

$$\Sigma_{out}(\mathcal{G}) \left\{ \begin{array}{rcl} \dot{x}(t) & = & u(t) \\ y_{\mathcal{G}}(t) & = & (E(\mathcal{G})^T \otimes I)x(t) \end{array} \right. , \tag{6.35}$$

where $x(t) \in \mathbb{R}^{3n}$ is the collection of all n agent states, $u(t) \in \mathbb{R}^{3n}$ is the collection of the agent's controls, and $y_{\mathcal{G}} \in \mathbb{R}^{3|\mathcal{E}|}$ is the sensed relative output of the system. Here we are assuming that the dynamics for each agent are with respect to a common reference frame in $\mathbb{R}^3$. For this system, we interpret a sensing edge to mean that the relative state between agent i and j (if $(i,j) \in \mathcal{E}$) is available to both the controls $u_i(t)$ and $u_j(t)$.

The second system we examine is an NDS coupled at the input with the same underlying connection topology as $\Sigma_{out}(\mathcal{G})$, and is given as

$$\Sigma_{in}(\mathcal{G}) \left\{ \begin{array}{rcl} \dot{x}(t) & = & (E(\mathcal{G}) \otimes I)u_{\mathcal{G}}(t) \\ y(t) & = & x(t) \end{array} \right. , \tag{6.36}$$

where, as in the previous model, $x(t) \in \mathbb{R}^{3n}$ is the collection of all the states, $u_{\mathcal{G}} \in \mathbb{R}^{3|\mathcal{E}|}$ is the networked input that is distributed to each agent via the incidence matrix, and $y(t) \in \mathbb{R}^{3n}$ is the collection of each agent's state. This represents a simplified version of the model presented in §4.3. A control edge in this scenario assumes that $[u_{\mathcal{G}}(t)]_{(i,j)}$ has access to both the state $x_i(t)$ and $x_j(t)$; we are using the same notation for $u_{\mathcal{G}}(t)$ described in §4.3.

For both models, we would like the NDS to move to a relative reference formation. For a fixed and given connection topology $\mathcal{G}$, we first note that arbitrary formations can not be achieved due to the physical position constraints imposed by the graph. In this direction, we define the notion of an *admissible relative formation* for a given connection topology.

Definition 6.3.1. *A relative reference formation $r(t) \in \mathbb{R}^{3|\mathcal{E}|}$ for a given connected graph $\mathcal{G}(\mathcal{V},\mathcal{E})$ is considered admissible if for any spanning tree subgraph $\mathcal{G}_\tau \subset \mathcal{G}$ one has*

$$r_c(t) \;=\; (T_\tau^c(\mathcal{G})^T \otimes I) r_\tau(t), \tag{6.37}$$

where $T_\tau^c(\mathcal{G})$ is defined in (2.24) and $r_\tau(t)$, $r_c(t)$ denote respectively, the component of $r(t)$ specifying the relative position for edges on the tree and cycles.

Using this definition, we can specify the controlled variable for both systems as the formation error,

$$\begin{aligned} e(t) &= -(E(\mathcal{G})^T \otimes I)x(t) + r(t) \\ &= -(R(\mathcal{G})^T E(\mathcal{G}_\tau)^T \otimes I)x(t) + (R(\mathcal{G})^T \otimes I) r_\tau(t), \end{aligned} \tag{6.38}$$

where $R(\mathcal{G})$ is defined in (2.26). The form derived in (6.55) is a direct consequence of Definition 6.3.1; it highlights the dependance of the formation error over the cycle edges on the error over a spanning tree.

For both systems we can define the corresponding error dynamics by differentiating (6.55) with respect to the dynamic models (6.35) and (6.36). We also assume that the reference formation is not time-varying, and can be considered a constant reference signal.

$$\Sigma_{out}(\mathcal{G}) \;:\; \dot{e}(t) \;=\; (-E(\mathcal{G})^T \otimes I)u(t) \tag{6.39}$$

$$\Sigma_{in}(\mathcal{G}) \;:\; \begin{aligned} \dot{e}(t) &= (-E(\mathcal{G})^T E(\mathcal{G}) \otimes I)u_{\mathcal{G}}(t) \\ &= (-L_e(\mathcal{G}) \otimes I)u_{\mathcal{G}}(t) \end{aligned} \;. \tag{6.40}$$

A stabilizing decentralized controller must drive the error to the origin. This can only be accomplished, however, if (6.39) and (6.40) are controllable systems. As in §5.1, we can derive a graph-theoretic description of each system's controllability properties.

Proposition 6.3.1. *The formation error dynamics (6.39) and (6.40) are controllable if and only if the underlying connection topology has no cycles.*

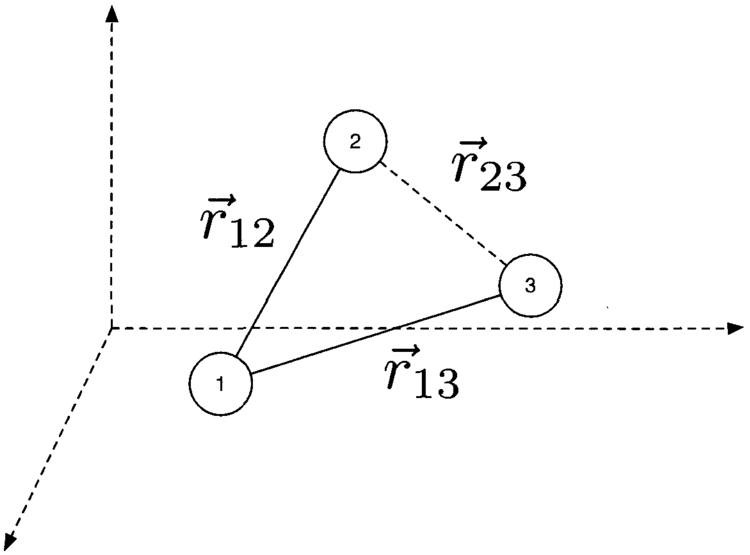

Figure 6.10: The relative position across a cycle edge ($\vec{r}_{23}$) is determined by the relative positions across the tree edges ($\vec{r}_{12}$ and $\vec{r}_{13}$).

Proof. The controllability matrix of (6.39) is recognized as $C = -E(\mathcal{G})^T \otimes I$. If (6.39) is controllable, than **rank**$[C] = 3|\mathcal{E}|$. From Theorem 2.2.1 the maximal rank $E(\mathcal{G})$ can obtain is $n-1$. Any graph with cycles, however, must have at least n edges, resulting in an uncontrollable system.

For (6.40), the controllability matrix is $C = -L_e(\mathcal{G}) \otimes I$. The results of §3 show that each independent cycle in $\mathcal{G}$ corresponds to an eigenvalue at the origin for the edge Laplacian. Consequently, $L_e(\mathcal{G})$ is full rank only when there are no cycles. □

Remark 6.3.1. *Note that the statement of Proposition 6.3.1 allows for disconnected graphs. If the relative reference formation is based on the underlying connection topology then this subtlety is acceptable; the formation problem can be addressed over each connected component of the graph.*

The interpretation of Proposition 6.3.1 follows the same idea used to define an admissible formation. The physical constraint imposed by the underlying connection topology does not permit the relative position of each agent to be controlled independently. Just as two sides of a triangle can be used to specify the third, the relative positions of the states across the tree edges must specify the relative position for the states across the cycle edges, visualized in Figure 6.10. While this might seem to be a limitation, we note that any admissible relative formation will always ensure that these constraints are respected. This concept is demonstrated by recognizing that

$$\begin{aligned} e(t) = \begin{bmatrix} e_\tau(t) \\ e_c(t) \end{bmatrix} &= (R(\mathcal{G})^T \otimes I)\left((-E(\mathcal{G}_\tau)^T \otimes I)x(t) + r_\tau(t)\right) \\ &= (R(\mathcal{G})^T \otimes I)(-x_\tau(t) + r_\tau(t)) \\ &= (R(\mathcal{G})^T \otimes I)e_\tau(t), \end{aligned} \tag{6.41}$$

where $x_\tau(t)$ corresponds to the relative states on the spanning tree $\mathcal{G}_\tau$.

As in our work on the analysis of the edge agreement problem in §5.2.2, we can consider minimal realizations for (6.39) and (6.40). We will show that for appropriate coordinate transformations, the minimal realization corresponds to the error dynamics specified for a tree sub-graph of the underlying connection topology.

Given a spanning tree $\mathcal{G}_\tau \subset \mathcal{G}$, and edge set $\mathcal{E} = \mathcal{E}_\tau \cup \mathcal{E}_c$ define the transformation matrix as

$$S = \begin{bmatrix} I_{n-1} & \mathbf{0} \\ (T_\tau^c(\mathcal{G}))^T & I_{|\mathcal{E}_c|} \end{bmatrix} \quad \text{and} \quad S^{-1} = \begin{bmatrix} I_{n-1} & \mathbf{0} \\ -(T_\tau^c(\mathcal{G}))^T & I_{|\mathcal{E}_c|} \end{bmatrix}. \tag{6.42}$$

Applying the transformation $(S \otimes I)\tilde{e}(t) = e(t)$ to both (6.39) and (6.40) leads to

$$\Sigma_{out}(\mathcal{G}) \ : \ \dot{\tilde{e}}(t) = \left(-\begin{bmatrix} E(\mathcal{G}_\tau)^T \\ \mathbf{0} \end{bmatrix} \otimes I\right) u(t) \tag{6.43}$$

$$\Sigma_{in}(\mathcal{G}) \ : \ \dot{\tilde{e}}(t) = \left(-\begin{bmatrix} L_e(\mathcal{G}_\tau)R(\mathcal{G}) \\ \mathbf{0} \end{bmatrix} \otimes I\right) u_{\mathcal{G}}(t) \ . \tag{6.44}$$

This transformation identifies the formation error corresponding to the spanning tree $\mathcal{G}_\tau$ as the controllable modes of the system. Furthermore, the first $|\mathcal{E}_c|$ columns of the transformation matrix S^{-1} form a basis for the null-space of $E(\mathcal{G})$; each column constitutes a signed path vector (Definition 2.2.1) for each independent cycle of the graph. This highlights again the intricate connection between cycles and system properties.

We can now consider finding stabilizing control laws for the minimal representations of (6.43) and (6.44). Results from §3 on the edge Laplacian motivate a particular form for the control. In this direction, define the control for (6.43) as

$$u(t) = (E(\mathcal{G}_\tau) \otimes I)\, \tilde{e}_\tau(t), \tag{6.45}$$

and for (6.44)

$$u_{\mathcal{G}}(t) = \left(R(\mathcal{G})^T \otimes I\right) \tilde{e}_\tau(t), \tag{6.46}$$

where $\tilde{e}_\tau(t)$ corresponds to the first $n-1$ states of the transformed formation error $\tilde{e}(t)$.

This leads to the closed-loop system for the transformed error dynamics as

$$\begin{aligned} \Sigma_{out}(\mathcal{G}) \;:\; \dot{\tilde{e}}_\tau(t) &= (-L_e(\mathcal{G}_\tau) \otimes I)\, \tilde{e}_\tau(t) & (6.47)\\ \Sigma_{in}(\mathcal{G}) \;:\; \dot{\tilde{e}}_\tau(t) &= (-L_e(\mathcal{G}_\tau)R(\mathcal{G})R(\mathcal{G})^T \otimes I)\, \tilde{e}_\tau(t)\ . & (6.48) \end{aligned}$$

The closed-loop systems in (6.47) and (6.48) correspond precisely to the edge agreement problem over a spanning tree and a graph with cycles respectively. Furthermore, the state matrices for both (6.47) and (6.48) are Hurwitz guaranteeing that $\tilde{e}(t)$ converges to the origin.

It remains to show that the control used on the minimal and transformed system translates to a decentralized control for the systems in (6.35) and (6.36), which we derive in the following theorem.

Theorem 6.3.2. *For the system (6.35) and a constant admissible relative reference formation $r(t)$, a decentralized control of the form*

$$u(t) = (-L(\mathcal{G}_\tau) \otimes I)x(t) + (E(\mathcal{G}_\tau) \otimes I)r_\tau(t) \tag{6.49}$$

drives the formation error $e(t) = -E(\mathcal{G})^T x(t) + r(t)$ to the origin.

Similarly, for the system (6.36) and a constant admissible relative reference formation $r(t)$, a decentralized control of the form

$$u_{\mathcal{G}}(t) = -(R(\mathcal{G})^T E(\mathcal{G}_\tau)^T \otimes I)x(t) + (R(\mathcal{G}) \otimes I)r_\tau(t), \tag{6.50}$$

drives the formation error to the origin.

Proof. First, we show that the controls (6.49) and (6.50) do in fact drive the formation error to the origin. Applying the control leads to the closed loop systems

$$\begin{aligned}\Sigma_{out}(\mathcal{G}) \;\; : \;\; \dot{x}(t) &= (-L(\mathcal{G}_\tau)\otimes I)x(t) + (E(\mathcal{G}_\tau)\otimes I)r_\tau(t), &(6.51)\\ \Sigma_{in}(\mathcal{G}) \;\; : \;\; \dot{x}(t) &= (-L(\mathcal{G})\otimes I)x(t) + (E(\mathcal{G})R(\mathcal{G})^T\otimes I)r_\tau(t) \; \cdot &(6.52)\end{aligned}$$

The remainder of this proof will focus on (6.52) noting that the same procedure can be used for (6.51). Denote the modal decomposition of the graph Laplacian as $L(\mathcal{G}) = U\Lambda(\mathcal{G})U^T$, with u_i corresponding to the ith column of U. Recall that the eigenvector for $\lambda_1(\mathcal{G}) = 0$ is the all ones vector, $u_1 = \mathbb{1}$. Using results from linear systems theory, we can express the state-response for (6.52) as

$$x(t) = \left(\sum_{i=1}^{n}\phi_i(t)\right)x(t_0) + \left(\sum_{i=2}^{n}\frac{1}{\lambda_i(\mathcal{G})}(U_i - \phi_i(t)) + \frac{1}{n}(J\otimes I)t\right)(E(\mathcal{G})R(\mathcal{G})^T\otimes I)r_\tau(t), \tag{6.53}$$

where

$$\phi_i(t) = U_i e^{-\lambda_i(\mathcal{G})t}\otimes I \quad \text{and} \quad U_i = u_i u_i^T \otimes I. \tag{6.54}$$

Using (6.53) we can examine the steady-state solution of the formation error,

$$\lim_{t\longrightarrow\infty} e(t) \;\; = \;\; (-E(\mathcal{G})^T\otimes I)x(t) + (R(\mathcal{G})^T\otimes I)r_\tau(t). \tag{6.55}$$

Since $\lambda_i(\mathcal{G}) > 0$ for $i = 2,\dots,n$ we have

$$\lim_{t\longrightarrow\infty}\phi_i(t) \;\; = \;\; \mathbf{0},\; i = 2,\dots,n. \tag{6.56}$$

Using (6.56) and recalling that $E(\mathcal{G})^T J = \mathbf{0}$ results in

$$\lim_{t\longrightarrow\infty}(E(\mathcal{G})^T\otimes I)\left(\sum_{i=1}^{n}\phi_i(t)\right)x(t_0) \;\; = \;\; \tfrac{1}{n}(E(\mathcal{G})^T\otimes I)(J\otimes I)x(t_0) \;\; = \;\; \mathbf{0}. \tag{6.57}$$

Next, observe that the incidence matrix has a singular value decomposition $E(\mathcal{G}) = UMV^T$, where $MM^T = \Lambda$. This, in turn, can be used to show that

$$E(\mathcal{G})^T\left(\sum_{i=2}^{n}\frac{1}{\lambda_i(\mathcal{G})}u_i u_i^T\right)E(\mathcal{G}) \;\; = \;\; I. \tag{6.58}$$

Finally, using (6.56)-(6.58) we conclude that

$$\lim_{t\rightarrow\infty} e(t) \quad = \quad \mathbf{0}.$$

To conclude the proof we must show that the form of (6.49) and (6.50) indeed correspond to a decentralized solution. This is immediately verified by noting the structure graph Laplacian and incidence matrices. □

Remark 6.3.3. *The choice of the control law in (6.45) is not unique. In fact, choosing the control* $u(t) = \left(E(\mathcal{G}_\tau)R(\mathcal{G})R(\mathcal{G})^T \otimes I\right)\tilde{e}_\tau(t)$ *would be equally valid, and the resulting closed-loop system would be identical to (6.45). While both control laws are stabilizing, we note the latter will result in a faster convergence to the formation due to the inclusion of cycles in the control. More generally, this suggests that cycles not explicitly defined in the connection graph can be artificially constructed through the control, resulting in a faster closed-loop response.*

Perhaps the most striking feature of this analysis is the relationship between the different NDS models. Via an appropriate choice of a decentralized control law, both an NDS coupled at the output and at the input can be transformed into an NDS coupled at the state. More revealing is the observation that the closed loop systems in (6.51) and (6.52) are examples of the consensus model derived in §4.4. The analysis results derived for NDS models coupled at the state can now be applied to the decentralized relative formation control problem to address notions of optimality and performance. The synthesis results of this chapter can also lead to insight on topologies that yield good performance in the context of reference tracking, in addition to notions of robustness and sensor placement for these systems.

An Example: Formation in the Plane

We illustrate the results of this section with a simple example. Consider the NDS coupled at the output (6.35) with 4 agents and $\mathcal{G} = S_4$. The agents are initially oriented in a horizontal line in $\mathbb{R}^2$, and the desired formation is a diamond shape. Using the control law defined in (6.49), the NDS achieves the desired formation. The trajectories of each agent are shown in

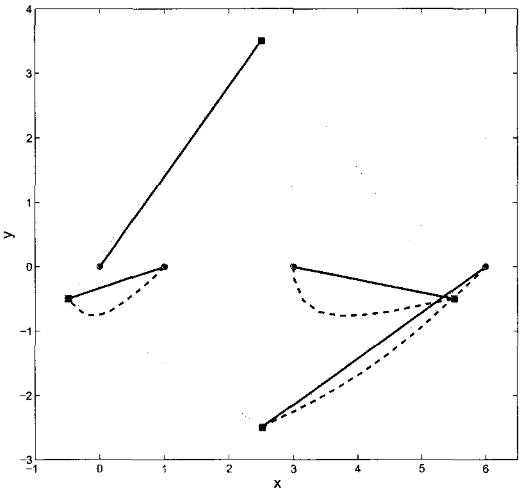

Figure 6.11: State trajectory of agents in an NDS forming a diamond; the dashed lines are the trajectories from the control (6.49) and the solid lines from the control (6.59).

Figure 6.11 (dashed lines). We also explore the ramifications of Remark 6.3.3 and consider the modified control law

$$u(t) \quad = \quad (L(K_n) \otimes I)x(t) + (E(\mathcal{G}_\tau) \otimes I)r_\tau. \tag{6.59}$$

To obtain this variation, we replace (6.45) with

$$u(t) \quad = \quad (E(\mathcal{G}_\tau)R(K_n)R(K_n)^T \otimes I)\tilde{e}_\tau(t), \tag{6.60}$$

and follow the procedure outlined in this section. Note that for a star topology, every independent cycle can be constructed via 3 connected nodes (see, for example, the proof for Proposition 3.2.2). Thus the virtual cycle edges created still respect the sensing constraints imposed by the given connection graph. The resulting trajectories (also plotted in Figure 6.11) exhibit a more direct route to the final state. Figure 6.12 plots the maximum formation error for both controllers highlighting the faster convergence due to the inclusion of the virtual cycle edges in (6.59).

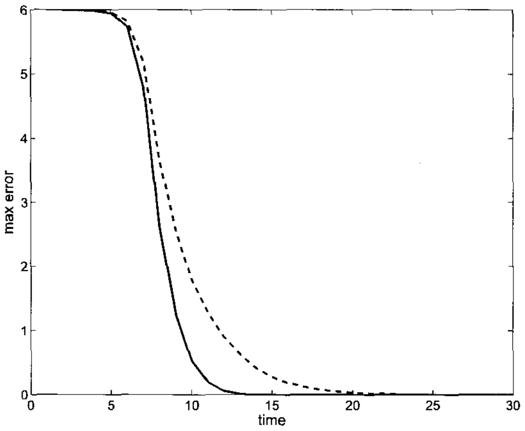

Figure 6.12: Maximum formation error for the control (6.49) (dashed) and (6.59) (solid).

Chapter 7

CONCLUDING REMARKS

The complexity of large-scale systems requires a systematic approach for their analysis and synthesis that blends constructs from system theory on one hand, and graph theory on the other. The goal of this work, therefore, was to present a viable framework for studying these systems. By defining four canonical models of networked dynamic systems, we proceeded to explicitly describe how the underlying interconnections affect some of the system-theoretic properties of the overall system. Furthermore, the generality of the models developed allowed for a further specification of system complexity via the notion of heterogeneity of the agent dynamics.

One of the recurring themes that arose in the analysis of these systems is the importance of the node degree of each agent in an NDS. The relative degree of observability and controllability of NDS were shown to be intimately related to the degree of the agents through the description of the gramians. The $\mathcal{H}_2$ performance of these systems was shown to be closely related to the number of edges in the system; a property directly attributed to the degree of each node. On the other hand, the structure of the graph itself played a more central role in the $\mathcal{H}_\infty$ performance analysis. While the second smallest eigenvalue of the graph Laplacian is recognized as an important parameter in consensus systems, our analysis pointed to the significance of the largest eigenvalue.

Perhaps a more subtle point of this work is the implicit relationship between the different NDS models. For certain NDS models, as in NDS coupled at the input and output, a natural duality arose in their description. More generally, we noted that via appropriate transformations and the inclusion of structured decentralized control laws, distinct types of NDS models can be transformed to one another. This suggests, for example, that certain models might be more advantageous to use than others when considering analysis and synthesis for a particular networked system. This was most clearly demonstrated in the consensus model with exogenous inputs.

The various synthesis results highlighted an important connection between combinatorial optimization and topology design for NDS. One of the more salient features of this work pertains to the application of the celebrated MST algorithm from combinatorial optimization for designing the interconnection topology for overall optimal $\mathcal{H}_2$ performance of NDS coupled at the output. While the other synthesis procedures for topology design involved some form of a relaxation that led to numerically tractable algorithms, the common theme revolved around optimization of the edge weights of the graph. This points to an interesting observation whereas we find the analysis of these systems to be facilitated by considering node weights, and synthesis by considering edge weights. More importantly, the synthesis results emphasize the need to explore more connections between methods in combinatorial optimization and systems theory.

7.1 Future Directions

The breadth of work presented here represents only an initial attempt to completely characterize and define networked dynamic systems for both analysis and synthesis purposes. Certainly, each chapter of this work can lead to further investigation, both from a theoretical and practical standpoint. In this section, we would like to highlight some potentially interesting extensions of this work.

7.1.1 Duality in NDS

Perhaps one of the most elegant and powerful constructs that arises in both optimization theory and control theory is the concept of duality [7, 18, 19, 33, 66]. For example, in control theory the notions of controllability and observability can be considered dual properties. Given an LTI system with state-space representation

$$\Sigma_{\mathcal{P}} \; : \; \left\{ \begin{array}{rcl} \dot{x}(t) & = & Ax(t) + Bu(t) \\ y(t) & = & Cx(t) \end{array} \right. ,$$

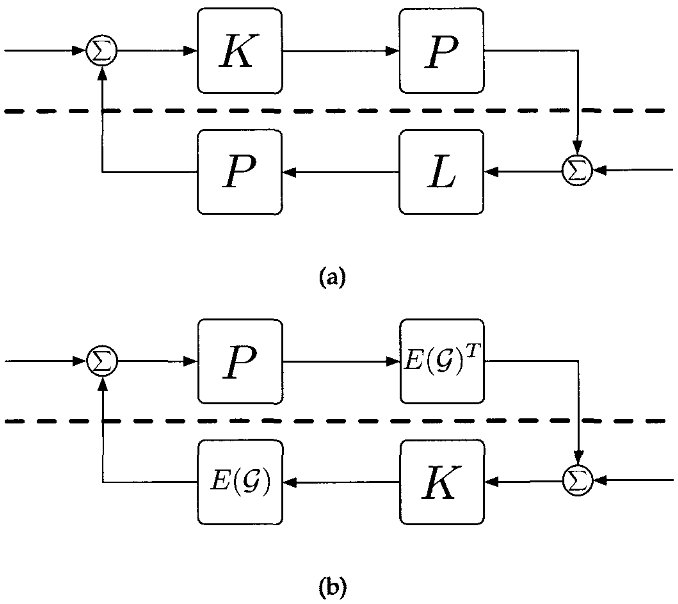

Figure 7.1: Duality in control systems and NDS.

one can construct the corresponding dual system as

$$\Sigma_{\mathcal{D}} \; : \; \left\{ \begin{array}{rcl} \dot{x}(t) & = & A^T x(t) + C^T u(t) \\ y(t) & = & B^T x(t) \end{array} \right. .$$

It can be verified that $\Sigma_{\mathcal{P}}$ is controllable if and only if $\Sigma_{\mathcal{D}}$ is observable (and similarly, $\Sigma_{\mathcal{P}}$ is observable if and only if $\Sigma_{\mathcal{D}}$ is controllable). This notion is further extended to the synthesis of controllers and estimators for linear systems via the celebrated *separation principle*, which states that the design of an optimal output feedback controller for a stochastic system can be designed by considering separately the optimal state-estimator and the optimal state-feedback control problems [4]. This is abstractly represented in Figure 7.1(a); the design of the controller gain K and observer gain L are performed independently, yet their feedback interconnection guarantees stability of the entire system.

Duality is even more prevalent in optimization theory and is elegantly illustrated in problems defined in network optimization[66]. For example, the linear optimal flow problem is a linear program used to determine how much flow can be pushed across a network defined by a graph $\mathcal{G}(\mathcal{V},\mathcal{E})$, with linear costs and box constraints specified for each edge[1],

$$\begin{aligned}\mathcal{P}\ :\ \min_{x} \quad & \sum_{j\in\mathcal{E}} d_j x_j + p_j \\ \text{s.t.} \quad & E(\mathcal{G})x = y \\ & x_j \geq c_j,\ \forall j \in \mathcal{E}.\end{aligned} \tag{7.1}$$

This problem has a corresponding dual problem, which is known as the linear optimal potential problem, and is defined as

$$\begin{aligned}\mathcal{D}\ :\ \max_{u,v} \quad & -\sum_{j\in\mathcal{E}}(c_j v_j + q_j) - \sum_{i\in\mathcal{V}} b_i u_i \\ \text{s.t.} \quad & v = -E(\mathcal{G})^T u \\ & v_j \leq d_j, \forall j \in \mathcal{E}\end{aligned} \tag{7.2}$$

Under mild assumptions ($p_j + q_j = -c_j d_j$) the solution of $\mathcal{P}$ and $\mathcal{D}$ coincide as a result of linear programming duality.

The interpretation of these dual problems, however, lead to insights on the role that the network plays in the optimization. In the optimal flow problem, the optimization variables are the flows across each edge. These flows must satisfy a kind of network conservation principle, which states that the net flow entering and leaving node i must equal the value y_i (referred to as the *divergence* at node i). When examining the dual problem, we can interpret the values at each node, u_i, to represent a *potential*; the potential difference between two nodes induces a *tension* across each edge[2]. The relationship between network flows and potentials can concisely be stated as

$$v^T x = -u^T y = -u^T E(\mathcal{G})x.$$

It seems tempting, therefore, to interpret the notions of duality found in linear systems and network optimization in the context of an NDS. Consider an NDS coupled at the output connected in a feedback configuration with a decentralized controller, as shown in

[1] This problem, for example, can be used to determine how to optimally transport goods from a warehouse to retailer over a transportation network.

[2] In electrical networks, for example, the current flowing through a resistor is induced by the voltage potential across the resistor.

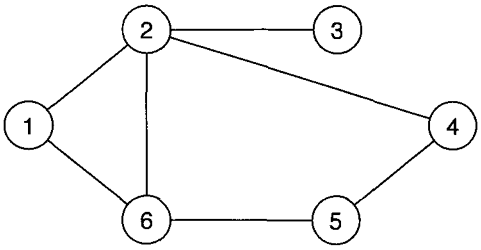

Figure 7.2: Undirected graph on 6 nodes.

Figure 7.1(b). By associating the interpretation of the incidence matrix as a mapping from flows to divergences, and potentials to tensions, we are able to assign similar terminology to the signals in the block diagram of Figure 7.1(b). For example, the state of each agent in an NDS coupled at the output can be viewed as a potential which induces a tension over the network, described by the relative measurements $y_{\mathcal{G}}(t)$. Similarly, the control signal of each agent in the NDS is a result of a flow distributed over the network. In this direction, the plant P can be viewed abstractly as a transformation from network divergences to network potentials, and the controller K as a transformation from network tensions to network flows.

Although this discussion remains abstract, it offers a compelling framework to explore deeper connections between network optimization and control theory. One conjecture is that the solution of the decentralized control problem for NDS should be intimately related to the solution of an associated optimal flow problem. Further investigation of this relationship will hopefully result in efficient algorithms for the design of decentralized controllers in addition to a new description of duality for NDS.

7.1.2 Centralized and Decentralized NDS

An important issue that must be addressed within the framework presented here is the notion of a centralized versus decentralized view of the NDS. In an NDS coupled at the output, for example, the measurement $y_{\mathcal{G}}(t)$ can be considered a centralized description of the system. Any controller or estimator designed based on the global measurement vector

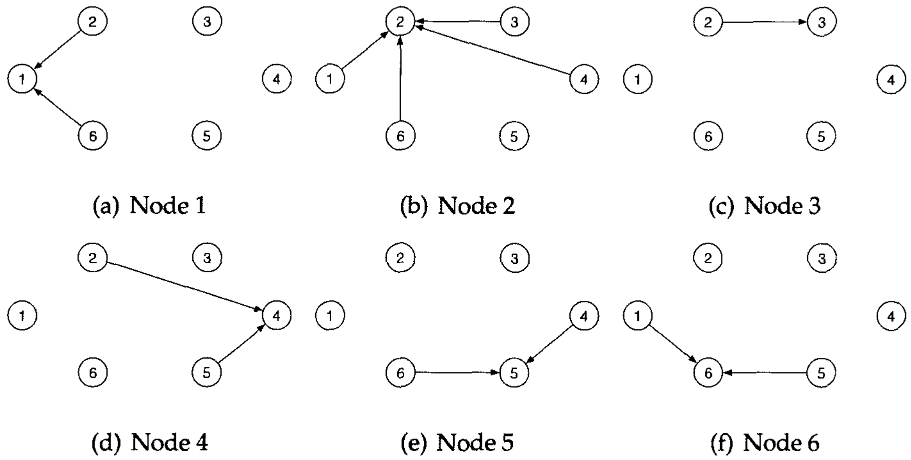

(a) Node 1 (b) Node 2 (c) Node 3

(d) Node 4 (e) Node 5 (f) Node 6

Figure 7.3: Local views of a graph.

predicates the existence of a central fusion or command center. Although the decentralized controller synthesis results of §6.3 are compelling in their unifying description of NDS models, they lack the rigor of optimality.

One approach to this problem is to define the notion of a *local graph view* for each agent in an NDS. Consider the undirected graph in Figure 7.2 representing a communication topology for a 6-agent NDS where each agent is permitted to transmit state information to its neighbors (a bi-directional communication link). The view of the network from the perspective of each agent, therefore, is only the set of edges incident to itself; the agent might not be aware of the size or connectivity of the entire system. In this direction, we define the $|\mathcal{V}| \times |\mathcal{N}_i|$ *local undirected incidence matrix*, $\overline{E}_i(\mathcal{G})$, where $|\mathcal{N}_i|$ is the cardinality of the set of nodes adjacent to node i, i.e.,

$$[\overline{E}_i(\mathcal{G})]_{jk} = \begin{cases} +1 & \text{if } (j,i) = e_k \in \mathcal{E} \\ 0 & \text{otherwise} \end{cases} . \tag{7.3}$$

As an example, using the graph in Figure 7.2 we can construct 6 local graphs, and their corresponding incidence matrices, as in Figure 7.3. Equation (7.4) gives the local undirected incidence matrices for the first three nodes,

$$\overline{E}_1(\mathcal{G}) = \begin{bmatrix} 0 & 0 \\ 1 & 0 \\ 0 & 0 \\ 0 & 0 \\ 0 & 0 \\ 0 & 1 \end{bmatrix}, \quad \overline{E}_2(\mathcal{G}) = \begin{bmatrix} 1 & 0 & 0 & 0 \\ 0 & 0 & 0 & 0 \\ 0 & 1 & 0 & 0 \\ 0 & 0 & 1 & 0 \\ 0 & 0 & 0 & 0 \\ 0 & 0 & 0 & 1 \end{bmatrix}, \quad \overline{E}_3(\mathcal{G}) = \begin{bmatrix} 0 \\ 1 \\ 0 \\ 0 \\ 0 \\ 0 \end{bmatrix}. \tag{7.4}$$

This description can be used to describe the measurement available to a particular agent in the network. For example, consider the following state-space model,

$$\Sigma_i : \left\{ \begin{array}{rcll} \dot{x}_i(t) & = & A_i x_i(t) & + \; B_i u_i(t) \\ y_i(t) & = & C_i^y x_i(t) & \\ y_i^{\mathcal{G}}(t) & = & (\overline{E}_i(\mathcal{G})^T \otimes I)\mathbf{C}^y \mathbf{x}(t) & \end{array} \right. , \tag{7.5}$$

where $y_i^{\mathcal{G}}(t)$ represents the information available to agent i from its neighbors, and $\mathbf{x}(t)$ is the concatenated state vector for the entire NDS.

A modification of this system reveals a model that is very similar to the relative sensing network developed in §4.2. The outputs $y_i(t)$ and $y_i^{\mathcal{G}}(t)$ can be combined as

$$y_i^{\mathcal{G}}(t) \;=\; (\begin{bmatrix} P_i & E_i(\mathcal{G}) \end{bmatrix}^T \otimes I)\mathbf{C}^y \mathbf{x}(t) \tag{7.6}$$

where $P_i = \begin{bmatrix} \mathbf{0} & \cdots & I & \mathbf{0} & \cdots \end{bmatrix}^T$ with the identity matrix in the ith block position, and $E_i(\mathcal{G})$ is the standard incidence matrix for the local directed graph from the view of agent i. Although (7.6) includes relative state information, the knowledge of the agent's own state can be used to construct the true transmitted state of its neighbors.

Using this system description for each agent for analysis leads to extensions of the results presented earlier. For example, the $\mathcal{H}_2$ norm of (7.5) with the output (7.6) has the form

$$\|\Sigma_i\|_2 \;=\; \left((d_i + 1)\|\Sigma_i\|_2^2 + \sum_{j \in \mathcal{N}_i} \|\Sigma_j\|_2^2 \right)^{1/2}. \tag{7.7}$$

This kind of analysis can lead to synthesis procedures that operate on *centralized clusters*. A centralized cluster can be thought of as a sub-network in the NDS that can be treated in a centralized manner. Rather than having one large fusion center in the NDS, the above expression suggests that we may be able to use multiple fusion centers across different clusters of agents in the NDS. The additive nature of the norm expression suggests that synthesis procedures for control and estimation would decouple cleanly across these clusters, resulting in potentially optimal decentralized solutions.

The results of §6.2 highlighted how the structure of the system performance can lead to a naturally separable optimization problem for the design of inner-loop controllers. The expression in (7.7) suggests that the design of a decentralized outer-loop control might be facilitated by considering sub-problems over centralized clusters. Extensions of the work in §6.3, therefore, depends on a continuation of this type of analysis.

7.1.3 Random, Switching, and State-Dependant Graphs

The work presented thus far has dealt with deterministic systems. A natural progression is to examine NDS where the underlying connection topology is random, switching, or state-dependant. These extensions are motivated by scenarios where the connection topology is itself dynamic. For example, a relative sensing network using a camera-based sensor might encounter a different set of agents within its sensing range during the horizon of a particular mission. The evolution of the connection graph can therefore be considered state-dependent [52].

While state-dependant interpretations of NDS seem natural for modeling, it can potentially lead to non-linear representations. One means to approximate this concept is via random or switching graphs. For example, if the topology for an NDS coupled at the output is unknown, but each edge has a probability p of being present, how would the analysis and synthesis results change? Studying such a scenario would lead to stochastic versions of all the results presented here.

7.1.4 Node and Edge Impact and Robustness

A natural question to consider for a heterogeneous NDS is which group of agents contribute the greatest to the overall performance of the system. Similarly, one might consider which set of communication or sensing links are most important for the entire NDS. The implications of these questions relate to problems in network security, infiltration, and robustness. In fact, the robustness results of §6.1.2 provide a general framework for considering these kinds of problems. Robustness measures for linear systems, such as the gain and phase margin, provide methods for describing how much uncertainty a system can tolerate before performance requirements or stability is lost. A compelling extension is to consider a similar measure that focuses on the interconnections and nodes in an NDS. Extending the robustness analysis of this work to include dynamic uncertainty in both the agent's system representation and the connection graph will invariably lead to a richer description and intuition of these systems.

BIBLIOGRAPHY

[1] [Online]. Available: http://en.wikipedia.org/wiki/File:Konigsberg_bridges.png

[2] "Autonomous nanotechnology swarms." [Online]. Available: http://ants.gsfc.nasa.gov

[3] I. Akyildiz, W. Su, Y. Sankarasubramaniam, and E. Cayirci, "A survey on sensor networks," *IEEE Communications Magazine*, vol. 40, pp. 102–114, 2002.

[4] P. J. Antsaklis and A. N. Michel, *A Linear Systems Primer*. Boston: Birkhäuser Boston, December 2007.

[5] M. Arcak, "Passivity as a design tool for group coordination," *IEEE Transactions on Automatic Control*, vol. 52, pp. 1380–1390, August 2007.

[6] B. Awerbuch, "Optimal distributed algorithms for minimum weight spanning tree, counting, leader election, and related problems," in *Proceedings of the nineteenth annual ACM conference on Theory of computing - STOC '87*, pp. 230–240.

[7] V. Balakrishnan and L. Vandenberghe, "Semidefinite programming duality and linear time-invariant systems," *IEEE Transactions on Automatic Control*, vol. 48, pp. 30–41, January 2003.

[8] T. Balch and R. Arkin, "Behavior-based formation control for multirobot teams," *IEEE Transactions on Robotics and Automation*, vol. 14, pp. 926–939.

[9] B. Bamieh, F. Paganini, and M. A. Dahleh, "Distributed control of spatially invariant systems," *IEEE Transactions on Automatic Control*, vol. 47, pp. 1091–1107, 2002.

[10] P. Barooah and J. P. Hespanha, "Estimation on graphs from relative measurements," *IEEE Control Systems Magazine*, vol. 45, pp. 57–74, July.

[11] A. Behar, J. Matthews, F. Carsey, and J. Jones, "Nasa/jpl tumbleweed polar rover," in *2004 IEEE Aerospace Conference Proceedings (IEEE Cat. No.04TH8720)*, pp. 388–395.

[12] A. Ben-Tal, L. El Ghaoui, and A. Nemirovski, *Robust semidefinite programming*. New York: Springer-Verlag, 2000, ch. 6.

[13] D. P. Bertsekas and J. Tsitsiklis, *Parallel and distributed computation*. Old Tappan, NJ: Prentice Hall Inc., 1989.

[14] G. Blackwood, O. Lay, B. Deininger, M. Gudim, A. Ahmed, R. Duren, C. Noecker, and B. Barden, "The starlight mission: a formation-flying stellar interferometer," Waikoloa, HI, 2002.

[15] B. Bollobas, *Graph theory: an introductory course.* New York, NY: Springer Verlag, 1979.

[16] S. Boyd, "Convex optimization of graph laplacian eigenvalues," in *International Congress of Mathematicians*, vol. 3, pp. 1311–1310.

[17] S. Boyd, L. El Ghaoui, E. Feron, and V. Balakrishnan, *Linear matrix inequalities in system and control theory.* Philidelphia, PA: SIAM, 1994.

[18] S. Boyd and L. Vandenberghe, *Convex optimization.* Cambridge: Cambridge University Press, 2004.

[19] J. B. Burl, *Linear Optimal Control: $\mathcal{H}_2$ and $\mathcal{H}_\infty$ Methods.* Boston, MA: Addison-Wesley Longman Publishing Co., Inc., 1998.

[20] R. D'Andrea and G. Dullerud, "Distributed control design for spatially interconnected systems," *IEEE Transactions on Automatic Control*, vol. 48, pp. 1478–1495, September 2003.

[21] K. Danzmann and L. S. Team, "Lisa: Laser interferometer space antenna for the detection and observation of gravitational waves," Garching, Germany, 1998.

[22] R. Diestel, *Graph Theory.* Springer-Verlag, Heidelberg, 2005, vol. 173.

[23] D. Dimarogonas and K. Johansson, "On the stability of distance-based formation control," *...Conference on Decision and Control, 2008. CDC 2008*, 2008.

[24] G. Dullerud and F. Paganini, *A course in robust control theory: a convex approach.* New York: Springer-Verlag, 2000.

[25] E. Estrada, "Edge adjacency relationships and a novel topological index related to molecular volume," *Journal of Chemical Information and Modeling*, vol. 35, pp. 31–33, January 1995.

[26] J. A. Fax and R. M. Murray, "Information flow and cooperative control of vehicle formations," *IEEE Transactions on Automatic Control*, vol. 49, pp. 1465–1476, September 2004.

[27] M. Fiedler, "Algebraic connectivity of graphs," *Czechoslovak Mathematical Journal*, vol. 23, pp. 298 – 305, 1973.

[28] ——, "A property of eigenvectors of nonnegative symmetric matrices and its application to graph theory," *Czechoslovak Mathematical Journal*, vol. 25, pp. 619–633, 1975.

[29] C. Fridlund, "Infrared space interferometry the darwin mission," *Advances in Space Research*, vol. 30, pp. 2135–2145, 2002.

[30] R. G. Gallager, P. A. Humblet, and P. M. Spira, "A distributed algorithm for minimum-weight spanning trees," *ACM Transactions on Programming Languages and Systems*, vol. 5, pp. 66–77, 1983.

[31] A. Ghosh and S. Boyd, "Growing well-connected graphs," in *Proceedings of the 45th IEEE Conference on Decision & Control*, pp. 6605–6611.

[32] C. Godsil and G. Royle, *Algebraic graph theory.* Springer, 2001.

[33] C. J. Goh and X. Q. Yang, *Duality in optimization and variational inequalities.* New York, NY: Taylor & Francis, 2002.

[34] I. Gutman, "The star is the tree with greatest greatest laplacian eigenvalue," *Kragujevac J. Math*, vol. 24, pp. 61–65, 2002.

[35] Y. Hatano and M. Mesbahi, "Agreement over random networks," *IEEE Transactions on Automatic Control*, vol. 50, pp. 1867–1872, 2005.

[36] R. A. Horn and C. R. Johnson, *Matrix Analysis.* New York, NY: Cambridge University Press, 1991.

[37] ——, *Topics in Matrix Analysis.* New York, NY: Cambridge University Press, 1991.

[38] A. Jadbabaie, J. Lin, and A. Morse, "Coordination of groups of mobile autonomous agents using nearest neighbor rules," *IEEE Transactions on Automatic Control*, vol. 48, pp. 988–1001, 2003.

[39] A. Jadbabaie, N. Motee, and M. Barahona, "On the stability of the kuramoto model of coupled nonlinear oscillators," in *2004 American Control Conference.*

[40] M. Ji and M. Egerstedt, "Observability and estimation in distributed sensor networks," in *2007 46th IEEE Conference on Decision and Control*, pp. 4221–4226.

[41] C. R. Johnson, Ed., *Matrix Theory and Applications.* Phoenix, AZ: American Mathematical Society, 1990.

[42] T. Kailath, *Linear Systems.* Englewood Cliffs, NJ: Prentice Hall, 1980.

[43] S. Kar and J. M. F. Moura, "Ramanujan topologies for decision making in sensor networks," in *44th Annual Allerton Conference on Communications, Control, and Computing*, pp. 145–150.

[44] H. K. Khalil, *Nonlinear systems*, 3rd ed. Upper Saddle River, NJ: Prentice Hall Inc., 1996.

[45] S. Kim and Y. Moon, "Structurally constrained $\mathcal{H}_2$ and $\mathcal{H}_\infty$ control: A rank-constrained lmi approach?" *Automatica*, vol. 42, pp. 1583–1588, September 2006.

[46] E. Klavins, R. Ghrist, and D. Lipsky, "A grammatical approach to self-organizing robotic systems," *IEEE Transactions on Automatic Control*, vol. 51, pp. 949–962, 2006.

[47] B. H. Korte and J. Vygen, *Combinatorial optimization: theory and algorithms*. Berlin: Springer-Verlag, 2000.

[48] P. Lawson, "The terrestrial planet finder," in *2001 IEEE Aerospace Conference Proceedings*, pp. 4/2005–4/2011.

[49] P. LIN, Y. JIA, and L. LI, "Distributed robust h8-consensus control in directed networks of agents with time-delay," *Systems & Control Letters*, vol. 57, pp. 643–653, August 2008.

[50] L. Lovász, "On the shannon capacity of a graph," *Information Theory, IEEE Transactions on*, vol. 25, pp. 1–7, 1979.

[51] L. Lovász and A. Schrijver, "Cones of matrices and set-functions and 0-1 optimization," *SIAM Journal on Optimization*, vol. 1, pp. 166–190, 1991.

[52] M. Mesbahi, "State-dependent graphs," *42nd IEEE Conference on Decision and Control, 2003. . . .* , 2003.

[53] ——, "On state-dependent dynamic graphs and their controllability properties," *IEEE Transactions on Automatic Control*, vol. 50, pp. 387–392, 2005.

[54] M. Mesbahi and M. Egerstedt, *Graph-theoretic Methods in Multi-agent Networks*. Princeton University Press (forthcoming).

[55] M. Mesbahi and F. Y. Hadaegh, "Graphs, matrix inequalities, and switching for the formation flying control of multiple spacecraft," *Proceedings of the 1999 American Control Conference (Cat. No. 99CH36251)*, pp. 4148–4152, 1999.

[56] A. Muhammad and M. Egerstedt, "Control using higher order laplacians in network topologies," in *Mathematical Theory of Networks and Systems*, pp. 1024–1038.

[57] R. Olfati-Saber, "Distributed kalman filter with embedded consensus filters," in *Proceedings of the 44th IEEE Conference on Decision and Control*, pp. 8179–8184.

[58] R. Olfati-Saber, J. A. Fax, and R. M. Murray, "Consensus and cooperation in networked multi-agent systems," *Proceedings of the IEEE*, vol. 95, pp. 215–233, January 2007.

[59] R. Olfati-Saber and R. M. Murray, "Agreement problems in networks with directed graphs and switching topology," in *Proceedings of the 42nd IEEE Conference on Decision and Control, 2003.*

[60] ——, "Consensus problems in networks of agents with switching topology and time-delays," *IEEE Transactions on Automatic Control*, vol. 49, pp. 1520–1533, 2004.

[61] M. C. D. Oliveira, J. C. Geromel, and L. Hsu, "Lmi characterization of structural and robust stability: the discrete-time case," *Linear Algebra and its Applications*, vol. 296, pp. 27–38, 1999.

[62] M. Petrovic and I. Gutman, "The path is the tree with smallest greatest laplacian eigenvalue," *Kragujevac J. Math*, vol. 24, pp. 67–70, 2002.

[63] A. Rahmani, M. Ji, M. Mesbahi, and M. Egerstedt, "Controllability of multiagent systems: from a graph-theoretic perspective," *SIAM Journal on Control and Optimization*, vol. 48, p. 162, 2008.

[64] W. Ren, "Consensus based formation control strategies for multi-vehicle systems," in *2006 American Control Conference.*

[65] W. Ren, R. Beard, and E. Atkins, "A survey of consensus problems in multi-agent coordination," in *Proceedings of the 2005, American Control Conference*, pp. 1859–1864.

[66] R. T. Rockafellar, *Network flows and monotropic optimization.* New York, NY: John Wiley, 1984.

[67] M. Rotkowitz and S. Lall, "A characterization of convex problems in decentralized control," *IEEE Transactions on Automatic Control*, vol. 50, pp. 1984–1996, December 2005.

[68] A. Saberi, P. Sannuti, and B. M. Chen, $\mathcal{H}_2$ *optimal control.* Upper Saddle River, NJ: Prentice-Hall, Inc., 1996.

[69] N. R. J. Sandell, "Survey of decentralized control methods for large scale systems," *IEEE Transactions on Automatic Control*, vol. AC-23, pp. 108–128, 1978.

[70] J. Sandhu, M. Mesbahi, and T. Tsukamaki, "Relative sensing networks: observability, estimation, and the control structure," in *Decision and Control, 2005 and 2005 European Control Conference. CDC-ECC '05*, vol. 05, pp. 6400–6405.

[71] C. Scherer and P. Gahinet, "Multiobjective output-feedback control via lmi optimization," *IEEE Transactions on Automatic Control*, vol. 42, pp. 896–911, April 1997.

[72] A. Schrijver, *Theory of linear and integer programming.* West Sussex, England: John Wiley & Sons Ltd., 1986.

[73] R. S. Smith and F. Y. Hadaegh, "Control of deep-space formation-flying spacecraft; relative sensing and switched information," *Journal of Guidance, Control, and Dynamics*, vol. 28, pp. 106–114, January 2005.

[74] ——, "Closed-loop dynamics of cooperative vehicle formations with parallel estimators and communication," *IEEE Transactions on Automatic Control*, vol. 52, pp. 1404–1414, August 2007.

[75] A. Tahbaz-Salehi and A. Jadbabaie, "Distributed coverage verification in sensor networks without location information," *Proc. IEEE Conf. Decis. Control*, 2008.

[76] ——, "A necessary and sufficient condition for consensus over random networks," *IEEE Transactions on Automatic Control*, vol. 53, pp. 791–795, 2008.

[77] T. Vicsek, A. Czirok, E. Ben-Jacob, I. Cohen, and O. Shochet, "Novel type of phase transition in a system of self-driven particles," *Physical Review Letters*, vol. 75, pp. 1226–1229, 1995.

[78] D. Watts and S. Strogatz, "Collective dynamics of small-world networks," *Nature*, vol. 393, 1998.

[79] B. Wie, *Space Vehicle Dynamics and Control.* Reston, VA: American Institute of Aeronautics and Astronautics, Inc., 1998.

[80] L. Xiao, S. Boyd, and S. Kim, "Distributed average consensus with least-mean-square deviation," *Journal of Parallel and Distributed Computing*, vol. 67, pp. 33–46, January 2007.

[81] D. Zelazo and M. Mesbahi, *Graph-theoretic Methods for Networked Dynamic Systems: Heterogeneity and $\mathcal{H}_2$ Performance.* Springer-Verlag (forthcoming).

[82] ——, "On the observability properties of homogeneous and heterogeneous networked dynamic systems," in *2008 47th IEEE Conference on Decision and Control*, pp. 2997–3002.

[83] ——, "Edge agreement: Graph-theoretic performance bounds and passivity analysis," *IEEE Transactions on Automatic Control (submitted)*, 2009.

[84] ——, "Graph-theoretic analysis and synthesis of relative sensing networks," *IEEE Transactions on Automatic Control (to be submitted)*, 2009.

[85] ——, "$\mathcal{H}_2$ performance of agreement protocol with noise: An edge based approach," in *2009 48th IEEE Conference on Decision and Control (to appear)*.

[86] ——, "$\mathcal{H}_2$ performance of relative sensing networks: Analysis and synthesis," in *AIAA Infotech@Aerospace Conference and AIAA Unmanned...Unlimited Conference*, vol. 21, pp. C3–C3.

[87] D. Zelazo, A. Rahmani, and M. Mesbahi, "Agreement via the edge laplacian," in *2007 46th IEEE Conference on Decision and Control*, pp. 2309–2314.

[88] D. Zelazo, A. Rahmani, J. Sandhu, and M. Mesbahi, "Decentralized formation control via the edge laplacian," in *2008 American Control Conference*, pp. 783–788.

[89] F. Zhang, *Matrix Theory: Basic Results and Techniques*. New York, NY: Springer-Verlag, 1999.